

A redescription of the Triassic kannemeyeriiform dicynodont *Sangusaurus* (Therapsida, Anomodontia), with an analysis of its feeding system

Kenneth D. Angielczyk, P. John Hancox & Ali Nabavizadeh

To cite this article: Kenneth D. Angielczyk, P. John Hancox & Ali Nabavizadeh (2017) A redescription of the Triassic kannemeyeriiform dicynodont *Sangusaurus* (Therapsida, Anomodontia), with an analysis of its feeding system, *Journal of Vertebrate Paleontology*, 37:sup1, 189-227, DOI: [10.1080/02724634.2017.1395885](https://doi.org/10.1080/02724634.2017.1395885)

To link to this article: <https://doi.org/10.1080/02724634.2017.1395885>



[View supplementary material](#)



Published online: 27 Mar 2018.



[Submit your article to this journal](#)



Article views: 545



[View related articles](#)



[View Crossmark data](#)



Citing articles: 6 [View citing articles](#)

A REDESCRIPTION OF THE TRIASSIC KANNEMEYERIIFORM DICYNODONT *SANGUSAURUS* (THERAPSIDA, ANOMODONTIA), WITH AN ANALYSIS OF ITS FEEDING SYSTEM

KENNETH D. ANGIELCZYK,^{*,1,2} P. JOHN HANCOX,² and ALI NABAVIZADEH³

¹Integrative Research Center, Field Museum of Natural History, 1400 South Lake Shore Drive, Chicago, Illinois 60605, U.S.A., kanielczyk@fieldmuseum.org;

²Evolutionary Studies Institute, University of the Witwatersrand, P.O. Wits 2050, Johannesburg, South Africa, jhancox@cciconline.com;

³Department of Biomedical Sciences, Cooper Medical School of Rowan University, 401 South Broadway, Camden, New Jersey 08103, U.S.A., alinabav@gmail.com

ABSTRACT—The Triassic dicynodont *Sangusaurus* is poorly known because the holotype of the first species to be described (*S. edentatus* from Zambia) is fragmentary, and the description of the second species (*S. parringtonii* from Tanzania) is extremely brief. Nevertheless, the genus has played a role in Triassic biostratigraphy by linking the Ntawere Formation and the Manda Beds. Here, we redescribe *Sangusaurus*, including a new, nearly complete skull from Tanzania. The incomplete holotype of *S. edentatus* results in few characters diagnosing the genus. The skull of *S. parringtonii*, however, is highly autapomorphic. The snout is telescoped, with only a thin strip of frontals separating the nasals and the parietals. The external surfaces of the premaxilla, the maxillae, the nasals, and the prefrontals are extremely rugose; a sharp median crest extends from the premaxilla to the frontals, terminating in a thickened boss. The occiput is broader than the skull is long, and the adductor fossa on the squamosal is nearly vertical. Our phylogenetic analysis shows that *Sangusaurus* is not a kannemeyeriid but instead is a stahleckeriid. The feeding system of *Sangusaurus* emphasizes an orthal jaw motion. The articular surfaces of the jaw joint form a single posteroventrally sloping surface; translating the quadrate and the articular results in a primarily orthal movement of the jaw symphysis. The internal and external jaw adductors provide a strong, dorsally-directed component to the power stroke. Adductor mechanical advantage is similar to *Stahleckeria*, but *Sangusaurus* likely had a stronger transverse component of jaw movement because of the very lateral placement of *M. adductor mandibulae externus lateralis*.

SUPPLEMENTAL DATA—Supplemental materials are available for this article for free at www.tandfonline.com/UJVP

Citation for this article: Angielczyk, K. D., P. J. Hancox, and A. Nabavizadeh. 2018. A redescription of the Triassic kannemeyeriiform dicynodont *Sangusaurus* (Therapsida, Anomodontia), with an analysis of its feeding system; pp. 189–227 in C. A. Sidor and S. J. Nesbitt (eds.), Vertebrate and Climatic Evolution in the Triassic Rift Basins of Tanzania and Zambia. Society of Vertebrate Paleontology Memoir 17. Journal of Vertebrate Paleontology 37(6, Supplement).

INTRODUCTION

Sangusaurus is one of the most enigmatic Triassic dicynodonts. Cox (1969) named the type species, *S. edentatus*, based on a series of skull fragments presumed to represent a single individual that were collected in the Ntawere Formation of Zambia by the 1963 British Museum (Natural History)–University of London Joint Palaeontological Expedition to Northern Rhodesia and Tanganyika. No additional material from Zambia or elsewhere has been referred to *S. edentatus* since its original description (Angielczyk et al., 2014). Cruickshank (1986a) named a second species of *Sangusaurus*, *S. parringtonii*, based on a more complete skull and partial jaw collected in the Manda Beds (K8 of Stockley, 1932; now the Lifua Member of the Manda Beds; see Markwort, 1991) of the Ruhuhu Basin, Tanzania, by Ernst Nowack during his work there in the late 1930s (Nowack, 1937). Although Cruickshank (1986a) provided a reconstruction of the skull of *S. parringtonii*, his description was extremely brief and included little information about the species' anatomy beyond the characters that differentiated it from *S. edentatus*. An additional specimen of *S. parringtonii* collected by Nowack was subsequently discovered in the Ruhuhu Basin collection of the

University of Cambridge Museum of Zoology, and a third specimen was collected in Tanzania in 2007 by a team including one of us (K.D.A.), but neither specimen has been formally described.

Given the small amount of information about *Sangusaurus* available in the literature, its phylogenetic relationships have remained unclear. Cox (1965) divided Triassic dicynodonts into four families (Lystrosauridae, Shansiodontidae, Kannemeyeriidae, and Stahleckeriidae), and within this framework he considered *Sangusaurus* to be a kannemeyeriid, positing a particularly close relationship to *Ischigualastia* (Cox, 1969). Cruickshank (1986a) agreed with the kannemeyeriid status of *Sangusaurus* when he described *S. parringtonii*, and his reconstruction of the specimen reflects this idea in bearing a strong resemblance to *Kannemeyeria lophorhinus* (e.g., compare Cruickshank, 1986a: fig. 1 with Renaut, 2000:fig. 70). Some subsequent workers followed the assignment of *Sangusaurus* to Kannemeyeriidae (Roy-Chowdhury, 1970; Keyser and Cruickshank, 1979; Keyser and Brink in Brink, 1982; Cox, 1991, 1998), but Cooper (1980) considered *Sangusaurus* to be more closely related to *Stahleckeria* than *Kannemeyeria* (i.e., a member of his Stahleckeriinae). Cox and Li (1983), King (1988), and Bandyopadhyay (1989) listed it as incertae sedis within the main clade of Triassic dicynodonts (i.e., Kannemeyeriinae of King, 1988; Kannemeyeriiformes of Maisch, 2001). More recently, *Sangusaurus* has been included in several phylogenetic analyses (Maisch, 2001; Surkov and Benton, 2004; Kammerer et al., 2011, 2013, 2015a; Castanhinha et al.,

*Corresponding author.

Color versions of one or more of the figures in the article can be found online at www.tandfonline.com/UJVP.

2013; Angielczyk and Cox, 2015; Cox and Angielczyk, 2015; Angielczyk et al., 2016; Boos et al., 2016). Maisch (2001) recovered it as the sister taxon of *Rechnisaurus* within his Dinodontosauridae, which also included *Dinodontosaurus*, *Parakanemeyeria*, *Sinokannemeyeria*, and *Rhadiodromus*. Surkov and Benton's (2004) analysis also suggested a close relationship to *Rechnisaurus* but reflected the more traditional position of *Sangusaurus* within Kannemeyeriformes, with it being reconstructed as the sister taxon of *Kannemeyeria* + *Rechnisaurus*. In contrast, *Sangusaurus* falls within Stahleckeriidae in the analyses stemming from modifications of Kammerer et al.'s (2011) data set (Castaninha et al., 2013; Kammerer et al., 2013, 2015a; Angielczyk and Cox, 2015; Cox and Angielczyk, 2015; Angielczyk et al., 2016; Boos et al., 2016), usually as the sister taxon of *Eubrachiosaurus*.

Despite being poorly known, *Sangusaurus* has played a role in Middle Triassic tetrapod biostratigraphy. The presence of *Sangusaurus* and *Zambiasaurus* in the upper Ntawere Formation and *Kannemeyeria lophorhinus* and 'K.' *latirostris* in the lower Ntawere of the Luangwa Basin, Zambia, has been used to support the hypothesis that these stratigraphic levels sample temporally distinct faunal assemblages (e.g., Cox, 1969, 1991; Cruickshank, 1986a; Battail, 1993; Fröbisch, 2009; Angielczyk et al., 2014). The occurrence of *Sangusaurus* in the Manda Beds of Tanzania also provides a direct correlation between the upper Ntawere and the Lifua Member of the Manda Beds (Cruickshank, 1986a; Cox, 1991; Battail, 1993; Angielczyk et al., 2014). Because

Sangusaurus is known only from the Luangwa and Ruhuhu basins, it generally has not been used in long-distance biostratigraphic correlations, although Jain and Roy-Chowdhury (1987) and Jain (1996) used comparisons of *Sangusaurus* and *Wadiasaurus* in their argument for a correlation between the Yerrapalli Formation of India and the Manda Beds.

Here, we present a detailed redescription of *Sangusaurus* (Fig. 1), with special attention paid to the relatively complete material of *S. parringtonii* from Tanzania that has not been considered previously. These specimens show that the highly autapomorphic skull morphology of *Sangusaurus* was not fully appreciated by previous researchers. We also investigate the implications of this unusual morphology for the function of its feeding system and reassess the phylogenetic relationships of the genus.

Institutional Abbreviations—**BP**, Evolutionary Studies Institute, University of the Witwatersrand, Johannesburg, South Africa; **GPIT**, Paläontologische Sammlung, Eberhard Karls Universität Tübingen, Tübingen, Germany; **NHCC**, National Heritage Conservation Commission, Lusaka, Zambia; **NHMUK**, Natural History Museum, London, U.K.; **NMT**, National Museum of Tanzania, Dar es Salaam, Tanzania; **PIN**, Paleontological Institute, Moscow, Russia; **SAM**, Iziko Museums of South Africa, Cape Town, South Africa; **UCMP**, University of California Museum of Paleontology, Berkeley, California, U.S.A.; **UMZC**, University Museum of Zoology, Cambridge, U.K.; **ZLS**, Livingstone Museum, Livingstone, Zambia.



FIGURE 1. The archosaur *Nundasuchus songaeensis* (left) attacks *Sangusaurus parringtonii* (right).

SYSTEMATIC PALEONTOLOGY

THERAPSIDA Broom, 1905

ANOMODONTIA Owen, 1860

DICYNODONTIA Owen, 1860

KANNEMEYERIIFORMES Maisch, 2001

STAHLCKERIIDAE (Lehman, 1961)

SANGUSAURUS Cox, 1969

Type Species—*Sangusaurus edentatus* Cox, 1969.

Revised Diagnosis—A large kannemeyeriiform dicynodont (basal skull length about 330 mm) characterized by the following unique combination of character states: longitudinal median ridge on anterior surface of premaxilla; caniniform tusks absent; low boss on skull roof posterior to the pineal foramen; parietals exposed on dorsal surface of intertemporal bar; intertemporal bar concave dorsally in cross-section; and interparietal makes large contribution to posterior portion of intertemporal bar. Can be differentiated from *Dinodontosaurus*, *Dolichuranus*, *Kannemeyeria*, *Moghreberia*, *Parakannemeyeria*, *Placerias*, *Rabidosaurus*, *Rechnisaurus*, *Rhadiodromus*, *Rhinodicynodon*, *Shaanbeikannemeyeria*, *Shansiodon*, *Sinokannemeyeria*, *Tetragonias*, *Uralokannemeyeria*, *Vinceria*, and *Xiyukannemeyeria* by the absence of caniniform tusks. Can be differentiated from *Ischigualastia* and *Jachaleria* by wider exposure of parietals on dorsal surface of intertemporal bar, presence of a boss posterior to the pineal foramen, and postorbitals that extend posteriorly for the entire length of the intertemporal bar. Can be differentiated from *Angonisaurus*, *Stahleckeria*, *Wadiasaurus*, and *Zambiasaurus* by the presence of a boss posterior to the pineal foramen. *Sangusaurus* likely can be differentiated from *Eubrachiosaurus* by the expanded, ventrally facing capitulum of the

humerus, and the straight ventral edge of the anterior iliac process, but these elements are only known in *S. parringtonii*.

Remarks—The extremely fragmentary nature of the only specimen of *Sangusaurus edentatus* makes it uncertain whether distinctive features of the skull seen in specimens of *S. parringtonii*, such as the prominent median crest on the nasals and the telescoping of the skull such that the nasals nearly reach the pineal foramen, are diagnostic of that species or of the genus as a whole.

SANGUSAURUS EDENTATUS Cox, 1969

(Figs. 3, 4)

Holotype—ZLS 9/1, skull fragments including premaxilla, portions of the right and left maxillae, right prefrontal, squamosal fragments, temporal bar preserving the parietals and the interparietal, and left and right quadrates.

Type Locality and Horizon—Locality 15 of Drysdall and Kitching (1963), about 3.5 miles [sic] west of the village of Sitwe, upper Luangwa Basin (*sensu* Barbolini et al., 2016), Eastern Province, Zambia (Cox, 1969) (Fig. 2). Drysdall and Kitching (1963) described and mapped this locality as including parts of the upper Ntawere Formation and the lower part of the overlying Red Marl. The distance from Sitwe noted by Cox (1969) would place the locality near the contact between the Ntawere Formation and the Red Marl in Locality 15 on Drysdall and Kitching's (1963) map, where they noted the presence of fossil vertebrates. Cox (1969) stated that the specimen originated in the upper fossiliferous horizon of the Ntawere Formation but noted that the exact stratigraphic level of the fossil within this unit could not be determined at the time of collection.



FIGURE 2. Geographic positions of localities that have produced specimens of *Sangusaurus*. Locality 1 is the type locality of *S. edentatus* in the upper Luangwa Basin. Locality 2 is the type locality of *S. parringtonii* in the Ngaka sub-basin of the Ruhuhu Basin. The referred specimens UMZC T1225 and UMZC T1340 were found within 100 m of this locality. Locality 3 is in the Ketewaka-Mchuchuma sub-basin of the Ruhuhu Basin and produced NMT RB42, a referred specimen of *S. parringtonii*.

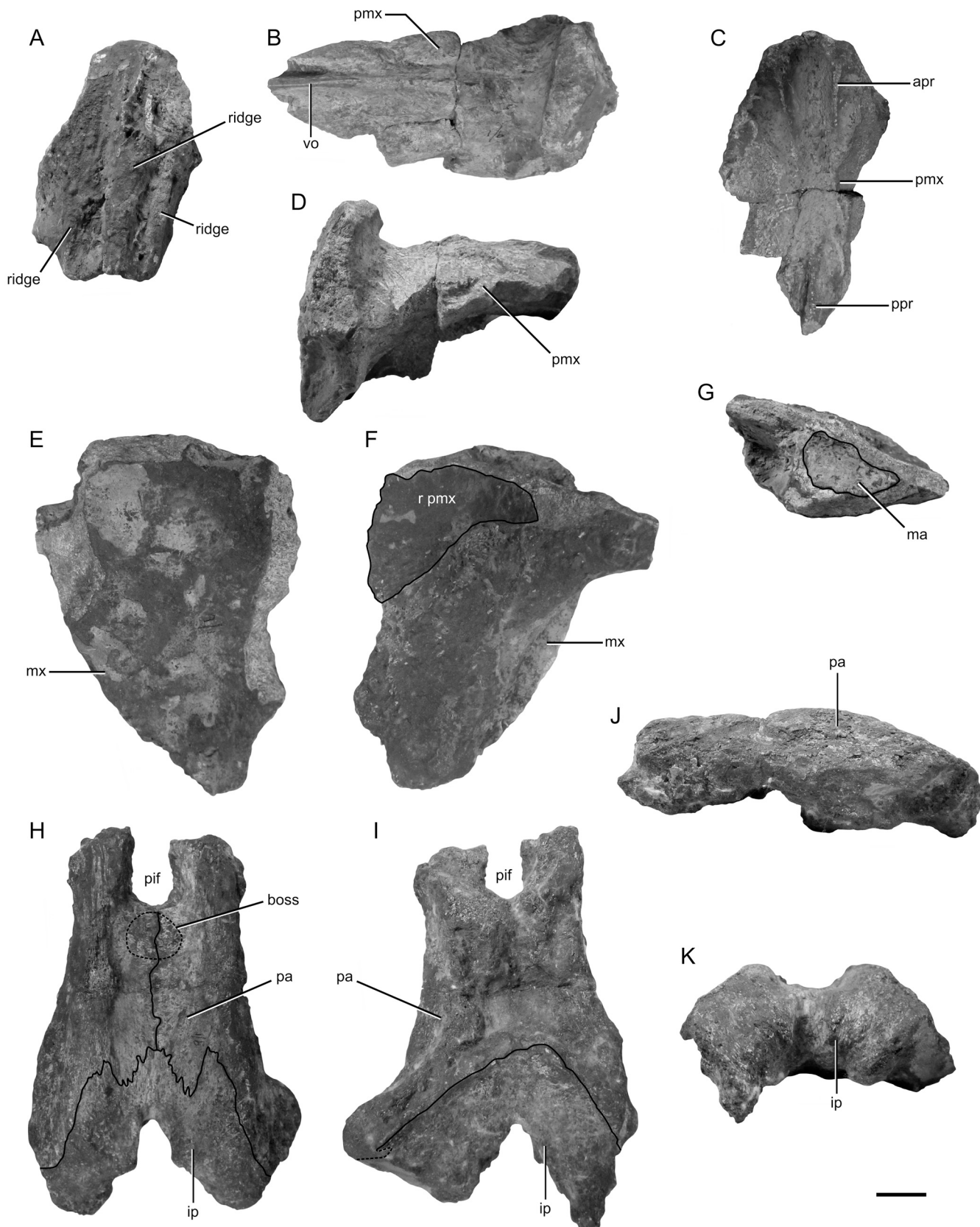


FIGURE 3. Photographs of the holotype of *Sangusaurus edentatus* (ZLS 9/1). Snout fragment in **A**, anterior, **B**, dorsal, **C**, ventral, and **D**, left lateral views. Right maxilla in **E**, lateral, **F**, medial, and **G**, proximal views. Intertemporal bar in **H**, dorsal, **I**, ventral, **J**, left lateral, and **K**, posterior views. Abbreviations: **apr**, anterior palatal ridge; **ip**, interparietal; **ma**, maxillary antrum; **mx**, maxilla; **pa**, parietal; **pif**, pineal foramen; **pmx**, premaxilla; **ppr**, posterior palatal ridge; **r pmx**, recess for premaxilla; **vo**, vomer. Scale bar equals 2 cm.

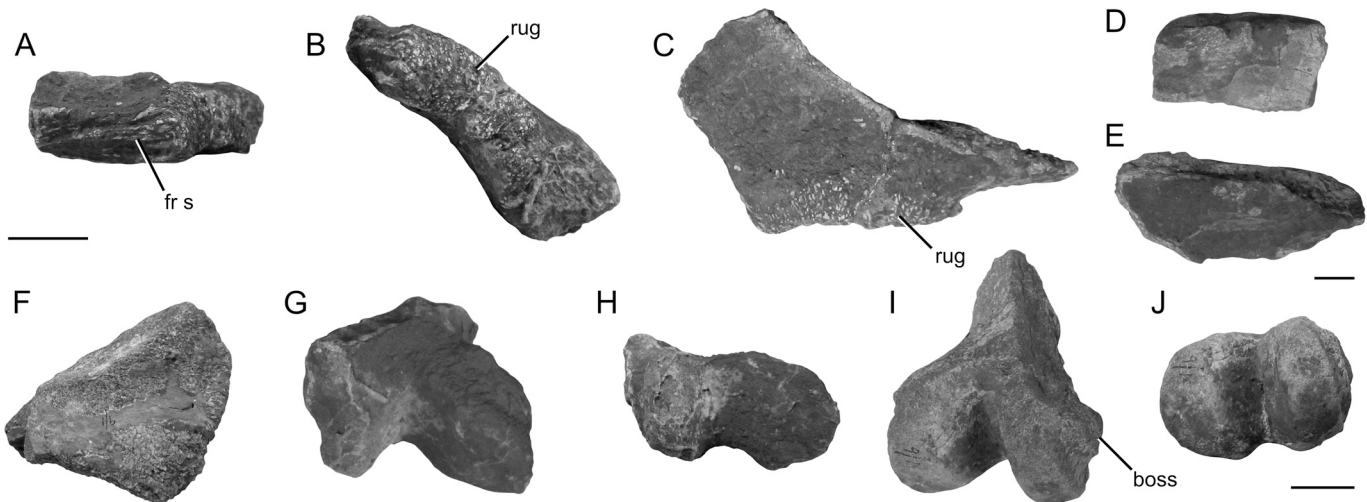


FIGURE 4. Additional photographs of the holotype of *Sangusaurus edentatus* (ZLS 9/1). Right prefrontal in **A**, posterior, **B**, lateral, and **C**, dorsal views. **D**, possible fragment of zygomatic arch (exact view uncertain). **E**, possible fragment of zygomatic arch (exact view uncertain). **F**, possible fragment of squamosal (exact view uncertain). Left quadrate in **G**, anterior, and **H**, ventral views. Right quadrate in **I**, anterior, and **J**, ventral views. Abbreviations: **fr s**, articular surface for the frontal; **rug**, rugosity. Scale bars equal 2 cm. Upper left scale bar applies to **A–C**. Upper right scale bar applies to **D–E**. Lower right scale bar applies to **F–J**.

Referred Material—None.

Revised Diagnosis—Can be differentiated from *Sangusaurus parringtonii* by presence of low longitudinal ridges flanking the median ridge on the anterior surface of the premaxilla, absence of a strong lateral caniniform buttress, approximately circular postspineal boss; minimum dorsal width of parietals about 58% of length of the intertemporal bar; and parietal-interparietal suture ‘W’-shaped in dorsal view.

Remarks—Cox (1969) reported that the material belonging to the specimen was collected over an area of about 50 square yards [sic], but due to the comparable size of the parts of the specimen and the non-duplication of elements, he considered it to belong to a single individual. We follow this assumption here.

DESCRIPTION

The holotype of *S. edentatus* consists of several broken and weathered skull fragments that appear to have undergone little if any preparation. Many areas of the bones are covered by a thin, dark red hematitic crust, and in places this is overlain by tan matrix. Most of the clean areas of the bone appear to have been exposed by natural weathering processes.

The premaxilla is a single fused element, and as preserved it includes a portion of the anterior surface of the snout and the median part of the secondary palate (Fig. 3A–D). The anterior face of the premaxilla meets the lateral surfaces of the bone at fairly distinct corners, suggesting a squared-off profile to the snout. A low, rounded median ridge extends up the ascending process of the premaxilla and is flanked by smaller lateral ridges that do not extend far up the snout and may originally have demarcated the junction between the lateral and anterior surfaces of the snout. The alveolar margin is weakly notched along the midline, suggesting that the anterior median palatal ridges originally extended ventrally past the rim of the palate. There is a suggestion of some rugose texturing on the external surfaces of the premaxilla, but it is difficult to determine the degree to which this is a real feature because of the poor exposure of the original bone surface.

The anterior median palatal ridges are well developed on the palatal surface of the premaxilla (Fig. 3C), and they do not

converge posteriorly. Their anterior tips are somewhat weathered, but it appears likely that they originally extended ventrally past the surrounding alveolar margin. A midline groove is present between the anterior ridges and is partially filled with matrix. There are no lateral anterior palatal ridges. The single posterior median palatal ridge is incompletely preserved. It is lowest anteriorly and becomes more prominent posteriorly. The posterior portion of the ridge curves anteroventrally so that it would have formed a cutting blade along the midline of the oral cavity. Premaxillary teeth are absent.

The dorsal surface of the secondary palate forms the floor of the nasal cavity (Fig. 3B). This surface is convex dorsally, with a midline ridge that extends along most of its length. The posterior section of this ridge is overlapped by an anterior process of the vomer. The anterior portion of the dorsal surface of the secondary palate, near its junction with the ascending process of the premaxilla, is covered by a thin layer of matrix. Because of this, we cannot determine if the pair of rounded depressions present in *S. parringtonii* (see below) were also present in *S. edentatus*.

Parts of the right and left maxillae are preserved in ZLS 9/1 (Fig. 3E–G), but there is a discrepancy in Cox’s (1969) description that makes the interpretation of these fragments somewhat confusing. In his written description, Cox (1969) states that the right maxilla is more complete and notes that a recess for articulation with the premaxilla is present near its preserved antero-dorsal end. This recess is typically found on the medial surface of the maxilla in other dicynodonts, but the drawing of the specimen that shows the recess (Cox, 1969:fig. 23a) is labeled as a lateral view. Because having a large recess for the premaxilla on the lateral surface of the maxilla would be very unusual for a dicynodont, and because it is not consistent with the morphology found in the more complete and articulated specimens of *S. parringtonii* known from Tanzania, we consider the caption of Cox’s (1969) figure 23 to contain a typographical error and to show a medial view of the right maxilla. This reinterpretation has important implications for Cruickshank’s (1986a) comparisons of the shapes of the caniniform processes in *S. edentatus* and *S. parringtonii* (see below). Our description focuses on the more complete right maxilla except where otherwise noted.

The caniniform process forms the majority of the preserved portion of the right maxilla (Fig. 3E, F). The lateral surface of

the element is still covered by matrix and is rather nondescript. It is fairly flat and is not strongly ornamented. A strong lateral caniniform buttress is not present, although the maxilla is thicker posteriorly near the body of the caniniform process. The caniniform process tapers distally to a blunt tip that is angled antero-medially relative to the apparent midline of the skull. The alveolar margin anterior to the caniniform process slopes antero-dorsally, giving the ventral edge of the maxilla a somewhat stepped appearance in lateral and medial views.

In medial view, the preserved anterodorsal portion of the maxilla is flat and forms a large articular surface for the premaxilla (Fig. 3F). This area is separated from the caniniform process by a low ridge that is subhorizontal posteriorly but slopes antero-ventrally near the anterior edge of the element. As Cox (1969) noted, when the posterior section of this ridge is held horizontally, the long axis of the caniniform process is angled anteroventrally. The medial surface of the caniniform process is convex medially, such that most of the thickness of the process is developed on its medial side. The bone surface of the medial side of the caniniform process is still covered by matrix, but there are a few areas where the bone is nearly exposed that suggest that the surface texture was rugose. A wide, shallow groove is present on the posterior surface of the caniniform process, which is bordered laterally by a flange of the facial surface of the maxilla that extends posteriorly past the level of the caniniform process.

The broken dorsal edge of the right maxilla exposes the matrix-filled maxillary antrum, and the exposed portion should be close to the proximal end of this sinus (Fig. 3G). The matrix infilling is trapezoidal, and it seems likely that this is a close approximation to the actual shape of the space at this level. The left maxilla fragment appears to expose a portion of the maxillary antrum that is closer to the apex of the caniniform process, which is round in cross-section. There is no evidence of a tusk in either maxilla, and there are no ‘postcanine’ teeth.

Cox (1969:287) noted the presence of an isolated right prefrontal among the material he assigned to *S. edentatus*, but he only stated that it showed “no features of significance.” As preserved, the bone is crescent-shaped, with a pointed anterior end and a squared-off posterior surface (Fig. 4A–C). The lateral margin of the bone is rugose and likely had an original appearance similar to the rugose prefrontals of *S. parringtonii* (see below). The posterior surface of the bone bears a number of straight, transverse ridges and grooves that presumably interlocked with similar features on the frontal. The medial and ventral surfaces are gently concave.

A relatively complete intertemporal bar is preserved in ZLS 9/1. It consists of the parietals and the interparietal (Fig. 3H–K). In dorsal view, the anterior end of the bar bears a ‘U’-shaped notch that is surrounded by the parietals and represents the posterior portion of the pineal foramen (Fig. 3H). A low, circular boss is located just posterior to the foramen. Its surface texture is slightly more rugose than that of the surrounding dorsal surface of the parietals. This boss is similar in position to that reported in *Rechnisaurus cristarhynchus* (Roy-Chowdhury, 1970; Bandyopadhyay, 1989), although it is more circular. It also shows some resemblance to the postpineal boss present in at least some specimens of *S. parringtonii* (e.g., NMT RB42), although in the latter species the boss is located further posteriorly on the skull roof and is more oval (see below). A prominent midline suture between the parietals is present. Cox (1969) noted that the dorsal surface of the temporal bar is concave in cross-section, with the lateral edges of the parietals forming raised ridges that flank a median trough. The median trough is relatively wide and more closely resembles that preserved in NMT RB42 than the very narrow, deep trough present in UMZC T1226 (both *S. parringtonii*). Cox (1969) speculated that the postorbitals likely overlapped at least part of the lateral ridges, and this is borne out by

the more complete temporal bars in NMT RB42 and UMZC T1226. However, the lateral surfaces of the ridges (Fig. 3J) are not prepared well enough to determine whether they bore the corrugations found in this area in *S. parringtonii* (see below). There also does not seem to be evidence of the deep depression at the anteroventral corner of the lateral surface of the parietal, which articulates with a rounded convexity on the medial surface of the postorbital in *S. parringtonii*.

The interparietal forms the posterior end of the temporal bar (Fig. 3H, I, K). The element is anteroposteriorly shorter at the midline than it is at the lateral margins of the skull, giving the posterior edge a ‘V’-shaped profile in dorsal view. About halfway along their length, the angle between the arms of the ‘V’ becomes more acute, forming a central notch along the posterior border of the skull roof. The interparietal meets the parietals along a highly interdigitated, ‘W’-shaped suture. Near the lateral edges of the skull roof, the parietal-interparietal suture turns posteriorly, such that the interparietal also contacts the parietals laterally. The posterolateral corners of the temporal bar are damaged, making it uncertain whether the interparietal contacted the squamosals. Cox (1969) stated that the occipital surface of the interparietal sloped strongly anteriorly, meeting the dorsal surface of the bone at an angle of about 25°. This caused him to hypothesize that the temporal bar was angled posterodorsally, and that it overhung the occipital plate. Comparison with more complete specimens of *S. parringtonii* (especially NMT RB42) confirms that Cox was partially correct and provides additional insight into the probable original morphology of the temporal bar and occiput. In *S. parringtonii*, the posterior processes of the parietal extend posteriorly past the level of the occipital plate, contributing to the ‘V’-shaped appearance of the posterior edge of the skull roof. To accommodate this emargination, the posterior end of the temporal bar extends posteriorly past the level of the occipital plate as well. As a result, the posterior surfaces of the parietals and interparietal slope anteriorly to meet the occipital plate, which is oriented vertically. The angle between the dorsal and occipital surfaces of the interparietal is steeper in *S. edentatus* than in *S. parringtonii*, suggesting that the overhang of the temporal bar over the occiput was greater in *S. edentatus*. Alternatively, the anterior slope of the interparietal in *S. edentatus* could have been exaggerated by dorsoventral flattening, although the other parts of the skull do not show strong evidence of such deformation.

Two fairly large fragments of bone that have complexly curved surfaces may represent parts of the squamosal of ZLS 9/1 (Fig. 4F). The finished edges of these fragments are quite thick and rugose, which contrasts strongly with the generally thin, smooth edges of the squamosal of *S. parringtonii* (see below) but is somewhat reminiscent of the condition seen in *Angonisaurus* (Hancox et al., 2013; Sidor et al., 2014). Two elongate, flattened to subrounded fragments of bone may represent portions of the zygomatic arch, but this is uncertain (Fig. 4D, E).

Specimen ZLS 9/1 includes isolated left and right quadrate (Fig. 4G–J). As is typical of dicynodonts, the articular portion of the quadrate is expanded and consists of two articular surfaces separated by a groove. The lateral condyle is wider than the medial one, but they have close to the same antero-posterior length. Differences in size and shape of the articular surfaces of the quadrates (Fig. 4H, J) raise the possibility that the elements represent two individuals, but this cannot be stated with complete certainty. A short, triangular process projects dorsally from the articular portion of the quadrate and would have articulated with the squamosal in life. Its posterior surface is rugose and gently convex. A prominent raised boss is present on the medial surface of the medial condyle of the right quadrate (Fig. 4I), perhaps representing an articular surface for the stapes.

SANGUSAURUS PARRINGTONII Cruickshank, 1986a
(Figs. 5–13)

Holotype—UMZC T1226, partial skull and partial mandible.
Type Locality and Horizon—Locality 328 of Nowack (1937), Ngaka sub-basin (sensu Kaaya, 1992), Ruhuhu Basin, Tanzania (Fig. 2). Nowack's (1937) map places this locality about 1.7 km southwest of the closest approach of the Ndatira River (Kiteho of Cox, 1991) and about 2.1 km northwest of the base of the highlands that form the southeast margin of this section of the basin. Nowack (1937) considered this locality to fall in his middle horizon of the Manda Beds (K8) of Stockley and Oates (1931) and Stockley (1932) (now the Lifua Member of the Manda Beds; Markwort, 1991). Based on the geographic location of this site, we agree that it is most likely in the middle to upper portion of the Lifua Member (see Smith et al., 2018, for discussion of fossil-bearing horizons in the Lifua Member).

Referred Material—UMZC T1225, complete right femur and left femur missing its proximal end, from Locality 328 of Nowack (1937). These specimens were collected in association with the holotype of *S. parringtonii* and are of the correct size to belong to that individual. The right femur includes a series of tooth impressions that constitute the holotype of the ichnofossil *Mandaodonites coxi* Cruickshank, 1986b. UMZC T1340, partial skull and partial mandible, from Locality 329 of Nowack (1937). Nowack's (1937) map places this locality about 100 m due north of the type locality, and he considered it to sample the same stratigraphic horizon of the Lifua Member of the Manda Beds. NMT RB42, nearly complete skull, associated with two isolated dorsal vertebrae, nearly complete pelvis, distal humerus fragment (Fig. 5). This specimen was discovered at a locality in the Kete-waka-Mchuchuma sub-basin (sensu Kaaya, 1992), west of the other occurrences of *S. parringtonii* in the Ruhuhu Basin (Fig. 2). The locality is about 4.6 km northeast of the village school in Litumba Ndyosi and about 1.4 km from the closest approach of the Ruhuhu River. Detailed locality information is available to qualified researchers from the National Museum of Tanzania or from K.D.A. Smith et al. (2018) place fossil occurrences in this area in the mid Lifua Member, and they discuss the sedimentology and taphonomy of nearby localities, which they consider to represent distal floodplain pond deposits.

A skull of the traversodontid cynodont *Scalenodon angustifrons* (NMT RB31) was found within the skull during collection. Four edentulous cynodont jaws tentatively referred to *S. angustifrons* (NMT RB32, RB33, RB34, RB35), and an indeterminate cynodont femur (NMT RB353) were found nearby at the same locality.

Revised Diagnosis—Can be differentiated from *Sangusaurus edentatus* by absence of low longitudinal ridges flanking the median ridge on the anterior surface of the premaxilla, strong lateral caniniform buttress, oval postpineal boss (absent in UMZC T1226), minimum dorsal width of parietals less than about 37% of length of intertemporal bar, and parietal-interparietal suture 'U'-shaped to 'V'-shaped in dorsal view.

Remarks—The skull of *S. parringtonii* presents several highly distinctive features, including extremely rugose ornamentation of the premaxilla, the maxillae, the nasals, and the frontals; strongly developed midline crest on the premaxilla and the nasals; nasals that extend nearly to the pineal foramen, such that the frontals are exposed as a narrow strip on the dorsal surface of the snout; and strongly developed boss on the frontals anterior to the pineal foramen. Of these, the telescoping of the skull that results in the nasals nearly reaching the pineal foramen is unique among dicynodonts and therefore a useful autapomorphy. However, the highly fragmentary nature of the only known specimen of *S. edentatus* prevents most of these characters from being assessed in that species. Therefore, it is unclear whether they are diagnostic of *S. parringtonii* or the genus *Sangusaurus*.

DESCRIPTION

Skull

The premaxillae (Figs. 6–8) are indistinguishably fused, and the resulting single element forms the anterior portion of the snout. Anteriorly, the premaxilla is strongly squared-off (Figs. 6A, B, 8C), with its anterior surface meeting the lateral surfaces at nearly right angles, and it is heavily sculptured by large vascular foramina and rugose texturing of the bone. A low midline ridge begins near the alveolar margin and extends up the anterior face of the premaxilla, becoming more prominent until it merges with the midline crest on the nasals. The smaller ridges

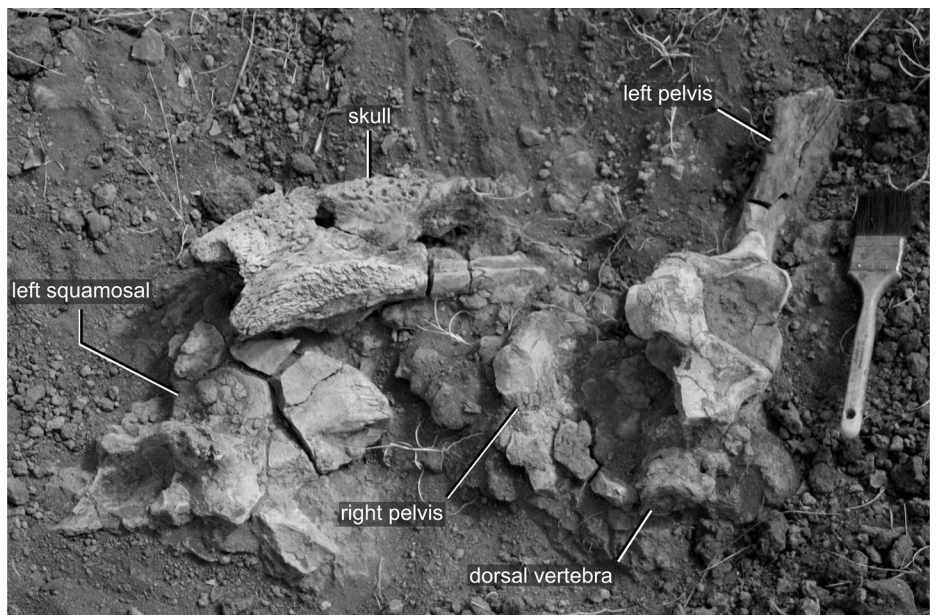


FIGURE 5. NMT RB42 shortly after discovery in the Lifua Member (Manda Beds, Ruhuhu Basin, Tanzania).

near the edges of the anterior surface of the premaxilla observed in the holotype of *S. edentatus* are not apparent in either of the *S. parringtonii* specimens in which this area is preserved (NMT RB42, UMZC T1226). The anterior median palatal ridges project below the level of the alveolar margin in anterior view, and this likely resulted in a morphology similar to the tomiodonts of extant turtles (Moldowan et al., 2015) when the keratinous beak was present. Dorsally, the premaxilla tapers to a pointed process that is clasped between the nasals, and this ascending process is well separated from the frontals by the long internasal suture (Figs. 6A, B, 8C). The lateral expression of the premaxilla-nasal suture is difficult to differentiate, but preserved morphology in NMT RB42 suggests that the nasal might have formed more of the anterior margin of the external naris than is the case in most dicynodonts (Figs. 7A, B, 8A). In the more complete specimens (NMT RB42 and UMZC T1226), the premaxilla is overlapped by the maxilla on the lateral surface of the skull, forming a long, straight suture that extends subvertically from the ventral edge of the external naris to the alveolar margin (Figs. 7A, B, 8A). The broken surface on the right side of UMZC T1340 shows that this overlap results from the premaxilla slotting into a recess on the medial surface of the maxilla, similar to the recess that is visible in the holotype of *S. edentatus*. The anteroventral corner of the septomaxilla rests on the premaxilla (Figs. 7A, B, 8A).

On the ventral surface of the skull, the premaxilla forms the majority of the secondary palate (Figs. 6C, D, 8D, E). The anterior median palatal ridges are strongly developed, separated by a median groove, and do not converge posteriorly. Their ventral surfaces are visible in lateral view, in contrast to most Permian dicynodonts, where the ridges are hidden in lateral view by the rim of the palate (Fig. 7A, B). There are no lateral anterior ridges. The single posterior median palatal ridge is relatively low and rounded anteroventrally, but it becomes much more prominent posteriorly, extending some 32 mm beyond the surrounding surface of secondary palate at its highest point in NMT RB42. The posterior section of the ridge curves anteroventrally, such that it forms a near-vertical cutting blade located along the midline of the oral cavity. There are no distinct grooves or vascular channels lateral to the posterior median ridge. The suture between the premaxilla and maxilla is primarily located on the lateral wall of the palate and is relatively straight. The palatine contacts the posterior edge of the premaxilla laterally, and the vomer contacts the posterior median palatal ridge. There is no premaxillary dentition.

The snout of UMZC T1226 is broken in such a way that the dorsal surface of the premaxillary secondary palate, which forms the floor of the nasal cavity, can be examined. Most of the anterior portion of this surface is broad and flat. There is a small, round depression on either side of the midline near the anterior wall of the nasal cavity, and the depressions are separated by a low, rounded ridge. Posteriorly, the floor of the nasal cavity slopes posteroventrally on either side of a raised midline ridge formed by an anterior process of the vomer. Lateral to the anterior process of the vomer, a blind, rounded pocket is formed between the premaxilla (floor) and the septomaxilla, the nasal, and the maxilla (lateral wall).

The septomaxilla is triangular in lateral view, with the apex of the triangle oriented posterodorsally (Figs. 7A, B, 8A). In contrast to other dicynodonts, in which the septomaxilla is recessed within the nostril, the septomaxilla of *S. parringtonii* has a prominent facial exposure that is wedged between the nasal and maxilla, forming the posterior border of the external naris. The anteroventral corner of the septomaxilla contacts the premaxilla, but the septomaxilla does not contact the lacrimal. As preserved,

neither UMZC T1226 nor NMT RB42 shows strong evidence of a septomaxillary canal or foramen, although we cannot completely rule out incomplete preservation as the cause of this absence.

Given the relatively large size of *S. parringtonii*, the external naris is surprisingly small (about 27 mm along its greatest dimension in NMT RB42, a skull with a basal length of 335 mm) (Figs. 7A, B, 8A). The dorsal edge of the naris in UMZC T1226 is straight and nearly horizontal, but this appears to be an artifact of dorsoventral flattening. Specimen NMT RB42 preserves the three-dimensional shape of the snout more faithfully, and there the dorsal edge of the external naris has a saddle shape that is somewhat reminiscent of that seen in *Dinanomodon* (Kammerer et al., 2011).

The maxilla is a large element that forms the majority of the lateral surface of the snout (Figs. 7A, B, 8A, B). Anteriorly, the premaxilla slots into a recess in the maxilla, such that the lateral surface of the maxilla overlaps the premaxilla. The external manifestation of this contact is a relatively straight suture that extends anteroventrally from the ventral edge of the external naris to the alveolar margin. The septomaxilla contacts the maxilla near the dorsal end of the premaxilla-maxilla suture, and together the septomaxilla and premaxilla exclude the maxilla from the margin of the external naris. Posterior to the contact with the septomaxilla, the maxilla presents a thin, sharp ridge that trends in the same direction as the premaxilla-maxilla suture and nearly reaches the suture between the maxilla and the nasal. This ridge is best preserved in NMT RB42, and it forms the anterior margin of a rounded fossa on the lateral surface of the maxilla that is located between the external naris, the margin of the orbit, and the lateral caniniform buttress. This is somewhat similar to the postnarial excavation reported in some dicynodonts, such as *Parakannemeyeria* and *Sinokannemeyeria* (e.g., Vega-Dias et al., 2004), although it differs in not being contiguous with the external naris itself. Above the fossa, the maxilla contacts the nasal along a straight suture.

Posterior to the fossa, the maxilla extends to the anterior margin of the orbit. Oddly, there is essentially no exposure of the prefrontal and the lacrimal on the lateral side of the snout in front of the anterior margin of the orbit (Figs. 7A, B, 8A, B). Instead, these bones articulate with the posterior surface of the maxilla to form the inner surface of the anterior wall of the orbit. The size of the contact between maxilla and prefrontal is difficult to assess due to poor preservation of sutures in the available specimens. Both UMZC T1226 and NMT RB42 suggest a very small contact, whereas the left side of UMZC T1340 shows a somewhat larger contact. Broken surfaces in this area in UMZC T1340 and NMT RB42 show that the interior surface of the maxilla bears a series of ridges and grooves that interlock with similar structures on the lacrimal, implying a very rigid connection between the bones. More posteriorly, the jugal contacts the maxilla to form the floor of the orbit and the base of the zygomatic arch, and the maxilla bears a small zygomatic process that meets the anterior tip of the squamosal along a straight contact. The lateral surface of the zygomatic process bears a weak ornamentation of fine longitudinal striations.

Most of the lateral surface of the maxilla, including the caniniform process, is highly rugose and heavily pitted, although the fossa anterior to the orbit has a smoother texture (Figs. 7A, B, 8A, B). The areas of the snout inferred to be covered by the keratinous beak of dicynodonts typically present a somewhat rugose texture and numerous small vascular foramina, but the extreme degree to which this ornamentation is developed in *S. parringtonii* suggests that the keratin covering was unusually thick and possibly more ornamented than in other dicynodonts.

The caniniform process is well developed, but no tusk is present (Figs. 7A, B, 8A, B). The process tapers distally to a bluntly

pointed tip. As in *S. edentatus*, the tip of the caniniform process is angled anteromedially relative to the rest of the skull, although the caniniform process is contiguous with the rest of the alveolar margin (i.e., it is not set off by a notch as in ptylaecephalids). When the pterygoids are positioned horizontally, the caniniform process is strongly anteroventrally angled, so that the apex is close to the level of the external naris, well anterior of the anterior margin of the orbit. A very strong lateral caniniform buttress is present, which contrasts with the much flatter lateral surface of the maxilla in *S. edentatus*. Cruickshank (1986a) noted the difference in the cross-sectional shape of the caniniform process in *S. edentatus* and *S. parringtonii* and used this feature to differentiate the species, although this is complicated by the fact that he reversed the lateral and medial surfaces of the process in *S. edentatus*, likely as a result of the incorrect label in Cox's (1969) figure (see above). Despite the strong lateral caniniform buttress, the posterior surface of the caniniform process is relatively flat. A low ridge extending from the alveolar margin near the tip of the process to near the base of the zygomatic arch separates the areas with highly rugose bone texturing from a smoother area closer to the contact with the pterygoid. This may correspond to the posterior edge of the keratinous beak in life. There is no postcaniniform crest or keel comparable to the structures seen in cryptodonts and emydopoids, respectively, although the alveolar margin posterior to the caniniform process does come to a fairly sharp edge (Fig. 6C, D).

A labial fossa surrounded by the maxilla, the jugal, and the palatine is present, and its structure is best preserved in UMZC T1226 (Fig. 8E). The labial fossa opens into the maxillary antrum, portions of which are exposed through breakage in all three skulls. As in *S. edentatus*, the antrum appears to have extended through most of the caniniform process and was relatively narrow and tubular. There is no evidence of an unerupted tusk in any of the specimens, and there are no maxillary 'postcanine' teeth.

The maxilla makes little contribution to the secondary palate, but it does form much of the lateral wall of the oral cavity (Figs. 6C, D, 7D, E). The palatal suture between maxilla and premaxilla is relatively straight for most of its length. Posteriorly, the palatine and pterygoid contact the maxilla on the ventral surface of the skull.

Together, the nasals form almost the entire dorsal surface of the snout, with only a narrow exposure of the frontals separating them from the pineal foramen (Figs. 6A, B, 8C). This morphology is unique among dicynodonts and gives the skull a distinctly telescoped appearance.

The most striking feature of the nasals is the tall crest that runs along the midline of the snout and includes the internasal suture (Figs. 6A, B, 7A, B, 8C). The anterior end of the crest bifurcates to clasp the ascending process of the premaxilla, and it forms a continuation of the midline ridge on the anterior surface of the premaxilla. Moving posteriorly, the crest becomes increasingly prominent, and it reaches its tallest point at the nasal-frontal suture, where it stands about 40 mm above the surrounding surface of the snout in NMT RB42. The surface of the nasals lateral to the midline crest is relatively flat anteriorly, but the postero-lateral and posterior edges of the bone are raised, such that a rounded fossa is present on each side of the ridge near its posterior end. The nasal crest of *S. parringtonii* is superficially similar to those of *Rechnisaurus cristarhynchus* (Roy-Chowdhury, 1970; Bandyopadhyay, 1989) and *Kannemeyeria lophorhinus* (Crozier, 1970; Keyser and Cruickshank, 1979; Renault, 2000; see Renault et al., 2003, for information on the taxonomy of this species) but differs in important ways from the morphologies present in each of those species. In *R. cristarhynchus*, the nasal crest is flanked by much more prominent depressions for its entire length (Bandyopadhyay, 1989) and the frontals have a large exposure on the skull roof that prevents the crest from closely approaching the

pineal foramen. The crest is wider and has a more rounded dorsal edge in *K. lophorhinus*, and it extends onto the frontals, although it does not approach the pineal foramen as closely as the crest of *S. parringtonii*.

Lateral to the midline crest, each nasal bears an anteroposteriorly elongate nasal boss (Figs. 6A, B, 7A, B, 8A, C). The bosses are not strongly raised relative to the surrounding dorsal surface of the skull roof, but they overhang the external naris and post-narial fossa of the maxilla. As such, they are more strongly defined in lateral view than in anterior or dorsal view. The bone surface of the nasal bosses is highly rugose and bears numerous, deep vascular channels. This ornamentation is similar to that of the premaxilla and maxilla and suggests that the nasal bosses were likely covered by the same thick, keratinous covering. The medial portions of the nasals and the nasal crest are less rugose and pitted, although some presumed vascular channels are visible on the left side of the crest in NMT RB42, suggesting that these areas also were covered by extensions of the keratinous beak. Posteriorly, the nasals contact the prefrontals and frontals along a prominent 'W'-shaped suture.

In lateral view, the nasal forms the dorsal border of the snout (Figs. 7A, B, 8A). It forms the dorsal margin of the external naris, and the nasal boss overhangs the naris and contacts the septomaxilla and the maxilla along a relatively straight, subhorizontal suture. The heavy ornamentation of the nasal bosses continues onto the lateral surface of the nasals but ends abruptly at the nasal-maxilla suture. The posterior edge of the lateral surface of the nasal contacts the prefrontal. Much like the case with the lacrimal and the maxilla, the prefrontal articulates with the posterior surface of the nasal, as opposed to having a distinct facial portion that contacts the nasal on the lateral surface of the snout as in most dicynodonts. Unusually, the nasal does not contact the lacrimal. Lack of contact between the lacrimal and the nasal has been reported in *Kannemeyeria* (Renaut, 2000) but otherwise is unknown in dicynodonts.

The prefrontal is a relatively small, crescent-shaped element, but it makes important contributions to the margins of the orbit (Figs. 6A, B, 7A, B, 8A–C). In lateral view, the prefrontal forms parts of the anterior and dorsal margins of the orbit. The bone surface in these areas is rugose and pitted, and the prefrontal essentially forms a continuation of the nasal boss. However, the dorsal margin of the orbit is not strongly raised above the surrounding surface of the skull roof. As noted above, the prefrontal lacks a distinct facial exposure but instead articulates with the posterior surface of the nasal within the orbit. A small contact with the maxilla also appears to be present, although sutures in this area are somewhat poorly preserved in the available specimens (the contact is most apparent on the left side of UMZC T1340). The prefrontal contacts the lacrimal ventrally, just below the level of the nasal-maxilla suture. Posteriorly, the prefrontal contacts the small frontal contribution to the orbit. The prefrontal forms much of the anterior and dorsal portions of the interior surface of the orbit, and its bone texture in this region is very smooth. The anterior margins of the orbit extend relatively far medially to partially close off the nasal cavity, but not as extensively as is the case in *Myosaurus* (Cluver, 1974a).

The lacrimal is a plate-like element that forms parts of the anterior and ventral margins of the orbit (Figs. 7A, B, 8A–C). Like the prefrontal, the lacrimal has no real facial exposure, instead articulating with the posterior surface of the maxilla. As noted above, UMZC T1340 and NMT RB42 demonstrate that a series of ridges and grooves on the lacrimal and the maxilla interlocked, providing a firm joint between the bones. The posterior surface of the lacrimal, which contributes to the interior surface of the orbit, is best preserved in NMT RB42. This surface is deeply concave, with its lowest point being a depression on the anterior wall of the orbit. Presumably this depression terminated in the lacrimal foramen, although the opening of the foramen

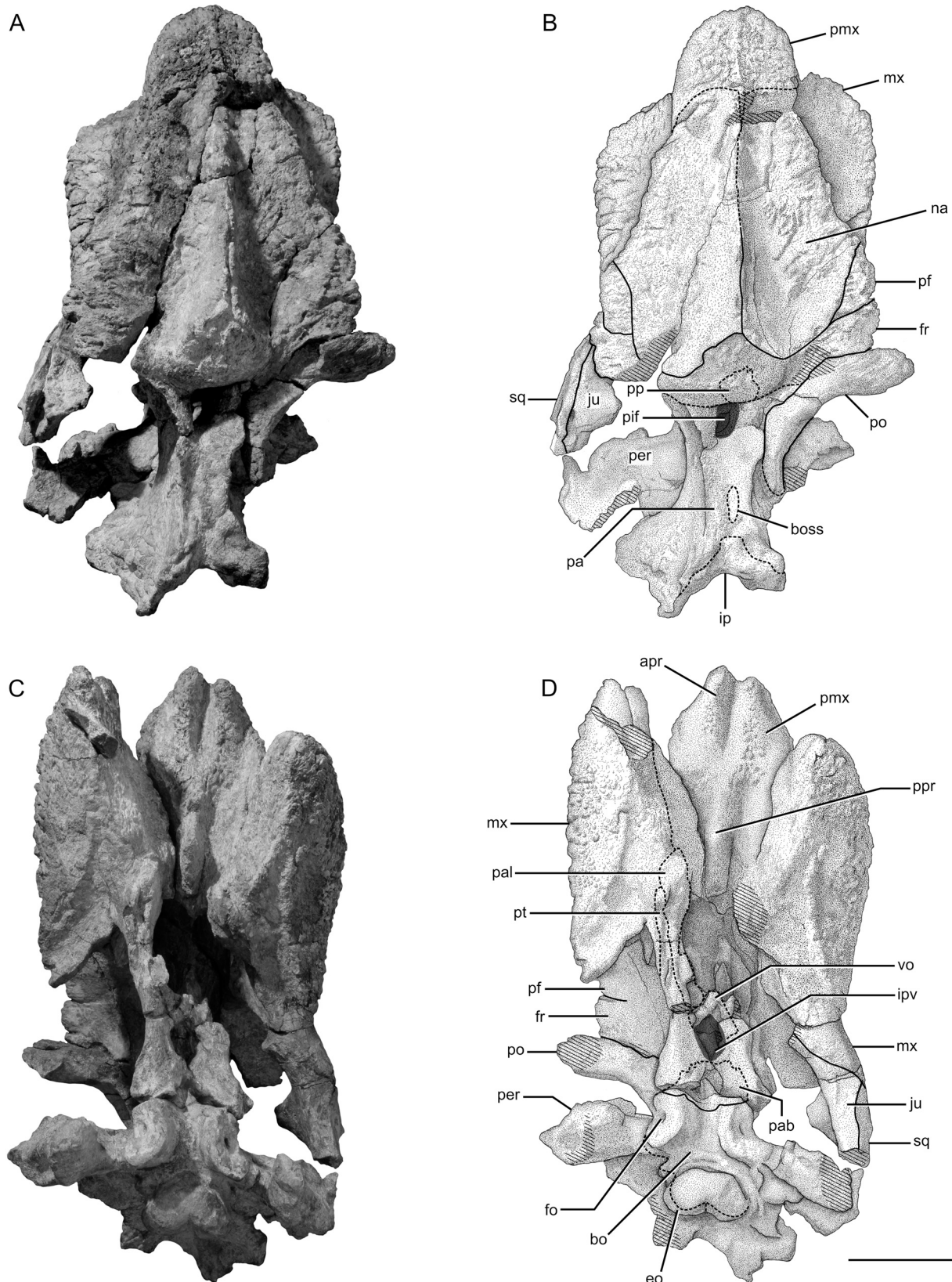


FIGURE 6. Referred skull of *Sangusaurus parringtonii* (NMT RB42). **A**, photograph and **B**, interpretive drawing in dorsal view. **C**, photograph and **D**, interpretive drawing in ventral view. **Abbreviations:** apr, anterior palatal ridge; bo, basioccipital; eo, exoccipital; fo, fenestra ovalis; fr, frontal; ip, interparietal; ipv, interpterygoid vacuity; ju, jugal; mx, maxilla; na, nasal; pa, parietal; pab, parabasisphenoid; pal, palatine; per, periotic; pf, prefrontal; pif, pineal foramen; pmx, premaxilla; po, postorbital; pp, preparietal; ppr, posterior palatal ridge; pt, pterygoid; sq, squamosal; vo, vomer. Scale bar equals 6 cm.

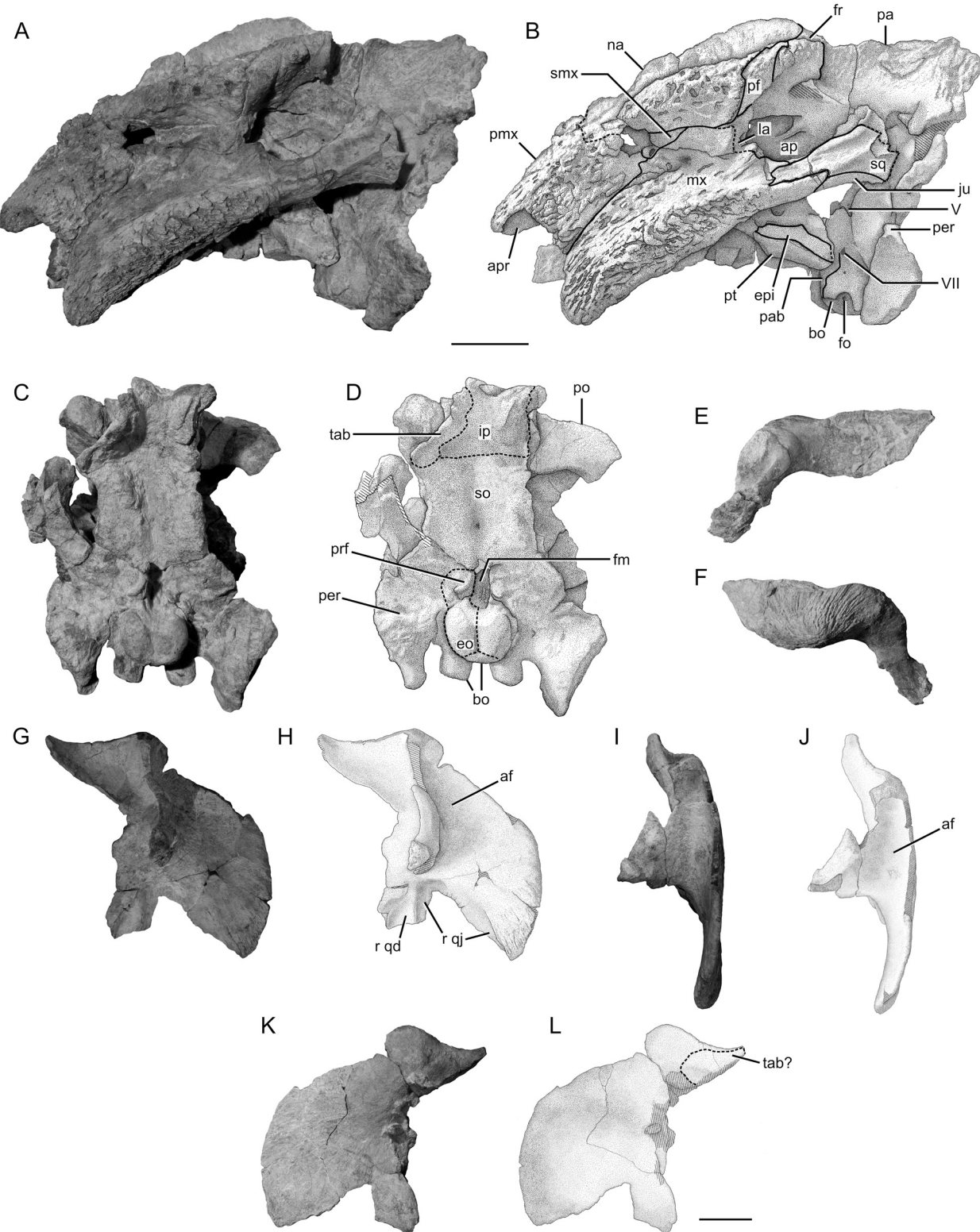


FIGURE 7. Referred specimen of *Sangusaurus parringtonii* (NMT RB42). **A**, photograph and **B**, interpretive drawing of skull in left lateral view. **C**, photograph and **D**, interpretive drawing of skull in posterior view. Left postorbital in **E**, lateral and **F**, medial views. **G**, photograph and **H**, interpretive drawing of left squamosal in anterior view. **I**, photograph and **J**, interpretive drawing of left squamosal in lateral view. **K**, photograph and **L**, interpretive drawing of left squamosal in posterior view. **Abbreviations:** **af**, fossa for *M. adductor mandibulae externus lateralis*; **ap**, anterior plate; **apr**, anterior palatal ridge; **bo**, basioccipital; **eo**, exoccipital; **epi**, epipterygoid; **fm**, foramen magnum; **fo**, fenestra ovalis; **fr**, frontal; **ip**, interparietal; **ju**, jugal; **la**, lacrimal; **mx**, maxilla; **na**, nasal; **pa**, parietal; **pab**, parabasisphenoid; **per**, periotic; **pf**, prefrontal; **pmx**, premaxilla; **po**, postorbital; **prf**, facet for proatlas; **pt**, pterygoid; **r qd**, recess for quadrate; **r qj**, recess for quadratojugal; **smx**, septomaxilla; **so**, supraoccipital; **sq**, squamosal; **tab**, tabular; **V**, trigeminal notch; **VII**, facial nerve foramen. Scale bars equal 6 cm. Upper scale bar applies to **A–F**. Lower scale bar applies to **G–L**.

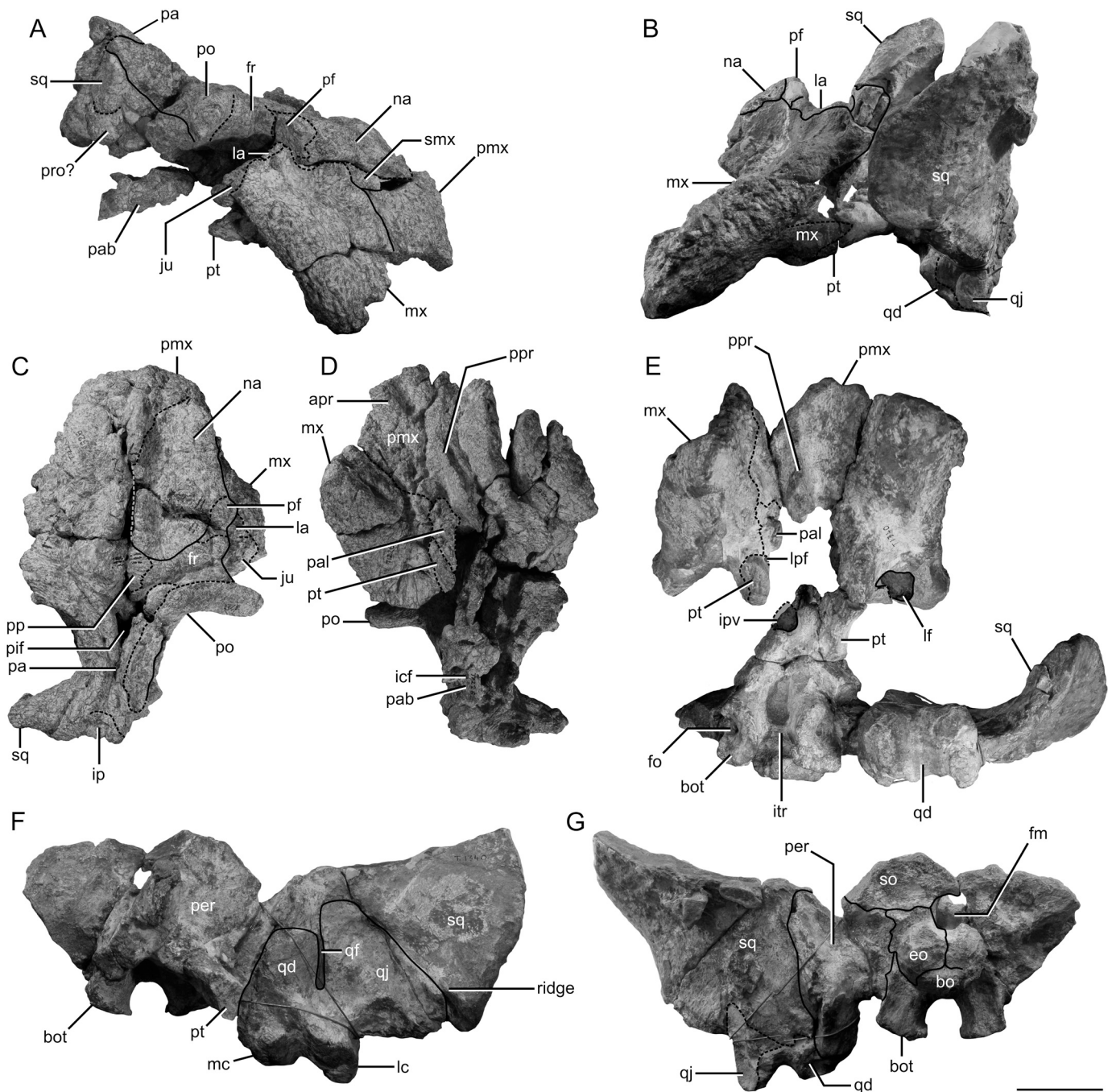


FIGURE 8. Holotype (UMZC T1226) and referred (UMZC T1340) skulls of *Sangusaurus parringtonii*. **A**, UMZC T1226 in right lateral view. **B**, UMZC T1340 in left lateral view. **C**, UMZC T1226 in dorsal view. **D**, UMZC T1226 in ventral view. **E**, UMZC T1340 in ventral view. **F**, occipital plate of UMZC T1340 in anterior view. **G**, occipital plate of UMZC T1340 in posterior view. Abbreviations: **apr**, anterior palatal ridge; **bo**, basioccipital; **bot**, basioccipital tuber; **eo**, exoccipital; **fm**, foramen magnum; **fo**, fenestra ovalis; **fr**, frontal; **icf**, internal carotid foramen; **ip**, interparietal; **itr**, intertuberal ridge; **ju**, jugal; **la**, lacrimal; **lc**, lateral articular condyle of quadrate; **lf**, labial fossa; **lpf**, lateral palatal foramen; **mx**, maxilla; **na**, nasal; **pa**, parietal; **pab**, parabasisphenoid; **per**, periotic; **pf**, prefrontal; **pif**, pineal foramen; **pmx**, premaxilla; **po**, postorbital; **pp**, prefrontal; **ppr**, posterior palatal ridge; **pro**, prootic; **pt**, pterygoid; **qd**, quadrate; **qf**, quadrate foramen; **qj**, quadratojugal; **smx**, septomaxilla; **so**, supraoccipital; **sq**, squamosal. Scale bar equals 6 cm.

itself cannot be clearly seen in the specimen. Dorsally, the lacrimal contacts the prefrontal. Posteriorly, it contacts the jugal, and breakage on the right side of UMZC T1226 suggests that the elements overlapped along a scarf joint.

A complete jugal is not preserved in any of the three specimens, but together they offer a nearly complete picture of the morphology of this element (Figs. 6C, D, 7A, B, 8A, C).

As is typical for dicynodonts, the jugal contributes to the floor of the orbit, the zygomatic arch, and the postorbital bar. A small piece of the jugal is preserved on the posterior surface of the maxilla in UMZC T1226, and this shows that the element contributed to the dorsal margin of the labial fossa. In UMZC T1340, a portion of the jugal is preserved on a fragment of the left zygomatic arch. Here, the jugal forms

the medial and much of the ventral surfaces of this part of the zygoma. It bears a dorsal facet for articulation with the base of the postorbital bar as well as a lateral groove that articulates with the anterior end of the zygomatic process of the squamosal. When this fragment is articulated with the left maxilla, the lacrimal-jugal suture is located on the floor of the orbit at the level of the anterior end of the zygomatic arch. The morphology of NMT RB42 confirms these observations and shows that the facet for the postorbital was somewhat raised above the zygoma, forming the ventral section of the postorbital bar. However, there is no evidence of a long dorsal process that extends up the posterior surface of the postorbital bar, such as that which Cluver and King (1983) noted for *Pelanomodon* and *Aulacephalodon*. The articular facet bears several low ridges that interlock with similar ridges on the postorbital. The right jugal has been lost in NMT RB42, and the exposed articular surface of the maxilla also is ridged, especially near the base of the zygomatic arch. The posterior end of the jugal appears to have nearly reached the fossa for *M. adductor mandibulae externus lateralis* on the squamosal and may have had a more extensive lateral exposure near the posterior end of the zygomatic arch than is typical for dicynodonts (see below).

The frontals of *S. parringtonii* are well preserved in UMZC T1226 and NMT RB42, and they present a highly distinctive morphology (Figs. 6A, B, 7A, B, 8A, C). Typically, the frontals are broadly exposed on the skull roof in kannemeyeriiforms, although in some cases they make only a small contribution to the margins of the orbits (e.g., see Cox, 1965:fig. 29). In contrast, the frontals of *S. parringtonii* are narrowly exposed on the skull roof, giving the skull a telescoped appearance in dorsal view. Anteriorly, the frontals contact the nasals and the prefrontals along a curved 'W'-shaped suture. The appearance of this contact suggests that the nasal overlaps the frontal to some degree, but the available specimens do not provide much information about the extent of this overlap. The anteroposteriorly narrow lateral process of the frontal is wedged between the prefrontal and the postorbital and makes a minor contribution to the dorsal margin of the orbit. The lateral and dorsal surfaces of the lateral process bear the same rugose, pitted ornamentation that is found on the prefrontal and nasal. The frontal widens near the midline of the skull, where it forms a triangular, dorsally convex boss that is clasped anteriorly by the posterior edge of the nasal crest. The bone surface in this area is weakly rugose but not highly ornamented. Near the midline of the skull, the prefrontal articulates with the frontal on the dorsal and posterior surfaces of this boss. Plate-like processes extend posteriorly from the frontals and contribute to the temporal bar. These processes nearly completely enclose the pineal foramen and contact the parietals in UMZC T1226, but poor preservation of sutures in this area does not allow this to be confirmed in NMT RB42.

The appearance of UMZC T1226 is suggestive of retaining a distinct postfrontal (Fig. 8C), an element that is otherwise consistently absent among kannemeyeriiforms. However, this area of the skull has suffered several large breaks, and the bone surface is highly cracked, making it difficult to definitively trace sutures. In NMT RB42, a slight break in the contour of the orbital margin and a subtle change in ornamentation between the frontal and postorbital is suggestive of an additional element (i.e., the postfrontal) having been present (Fig. 6A, B), although clear sutures are no longer visible. We interpret this as evidence that a distinct postfrontal center of ossification was likely present at some point in ontogeny, but that it has become indistinguishably fused with the frontal. A similar morphology can occasionally be seen in other dicynodonts that lack postfrontals (e.g., NHCC LB117, an extremely well-preserved specimen of *Dicynodontoides*).

The sutures for the prefrontal are difficult to trace, but they seem best preserved in UMZC T1226 (Fig. 8C). In that specimen, the prefrontal has the shape of an asymmetrical diamond, with the posterior half of the diamond being longer than the anterior half. The frontal-prefrontal suture arises near the midline of the skull just posterior to the nasal-frontal suture. From there, the suture sweeps laterally to a point that is at about the same level anteroposteriorly as the suture between the postorbital and the frontal on the dorsal margin of the orbit. The suture then curves medially so that it is roughly parallel to the long axis of the skull and becomes highly interdigitated. As such, the prefrontal forms the central portion of the skull roof on the frontal boss and also contributes to the anterior wall of the pineal foramen as the frontal surface of the skull slopes ventrally towards that opening. The surface of the prefrontal is flush with the surrounding bones and bears the same weakly rugose texture as the frontals where it contributes to the surface of the frontal boss. It is difficult to assess whether the prefrontal was a plate-like element that sat atop the frontals or if it is thicker and has a more extensive contact.

In dorsal view, the pineal foramen is triangular, with its apex directed posteriorly (Figs. 6A, B, 8C). The walls of the foramen are nearly vertical, and there is no significant change in diameter between the foramen and the pineal tube that extends through the skull roof down into the braincase. The pineal foramen is not surrounded by a boss or collar, and it is oriented nearly vertically, as opposed to the more anterodorsal orientation seen in taxa such as *Rhachiocephalus* (e.g., Maisch, 2005). Specimen UMZC T1226 indicates that the pineal foramen is nearly completely surrounded by the frontal on the dorsal surface of the skull, although the prefrontal contributes to the anterior wall of the foramen and the parietal contributes to its posterior wall.

The morphology of the parietals on the dorsal surface of the skull differs in UMZC T1226 and NMT RB42. In the former specimen, the parietals contribute to the posterior wall of the pineal foramen and present a deep, narrow groove along the midline of the skull (Fig. 8C). A relatively straight suture between the parietals is visible, but there is no evidence of a boss similar to that in *S. edentatus* posterior to the pineal foramen. Lateral to the groove, the parietals slope dorsolaterally to meet the postorbitals, which overlap the parietals on the lateral sides of the skull roof and contribute to the raised lateral edges of the temporal bar. Posteriorly, the parietals diverge to surround the centrally located interparietal. A short posterior process of the parietal is wedged between the interparietal, postorbital, and squamosal at the posterolateral corner of the skull roof.

The lateral edges of the dorsal surface of the parietals slope dorsolaterally in NMT RB42, giving the temporal bar a concave appearance (Fig. 6A, B), but this concavity is much gentler than in UMZC T1226 and does not form a very distinct midline groove. A boss is present posterior to the pineal foramen, but it differs from that in *S. edentatus* in two important ways. First, it is located towards the anteroposterior midpoint of the temporal bar, as opposed to just behind the pineal foramen in *S. edentatus*. Second, the boss of *S. parringtonii* is anteroposteriorly elongate and oval instead of being roughly circular. The boss also differs from that reported in *Rechnisaurus cristarhynchus* (Roy-Chowdhury, 1970; Bandyopadhyay, 1989) in being mediolaterally narrower and located near the midpoint of the temporal bar, as opposed to arising just behind the pineal foramen. The parietal-interparietal suture is not clear in NMT RB42, but the specimen appears to be similar in having the parietals diverge around the interparietal to form short posterior processes. A midline suture between the parietals is not apparent in NMT RB42.

The lateral surface of the parietal is best seen on the left side of NMT RB42 (Fig. 7A, B). Anteriorly, this surface presents a

well-defined fossa that has a highly striated surface texture. This fossa receives a rounded, convex surface on the postorbital that is located near the junction of the postorbital bar and the temporal portion of the postorbital. The surface of this convexity is similarly highly striated, and the orientation of the striations closely matches on both elements, with the anterior striations curving anterodorsally and the posterior ones curving postero-dorsally. Posteriorly, the articular surface for the postorbital becomes flatter and less strongly striated, reflecting the weaker striations of the medial surface of the postorbital in this region. The size and shape of the isolated left postorbital of NMT RB42, and the extent of the articular surface for the postorbital on the parietal, shows that the temporal portion of the postorbital extended the entire length of the postorbital bar. Ventral to the articular surface for the postorbital, the lateral surface of the parietal is relatively flat, and it contacts the dorsal surfaces of the prootic and epipterygoid. Unlike the case in most Permian dicynodonts (e.g., Angielczyk and Kurkin, 2003; Maisch, 2003), there is no distinct fossa for muscle attachment between the ventral surface of the postorbital and the descending flange of the parietal.

The postorbital is preserved in UMZC T1226 and NMT RB42. Perhaps the most informative example of this element is the complete left postorbital of NMT RB42 (Fig. 7E, F), which is detached from the skull, although the element has been plastically deformed such that the former lateral surface of the postorbital bar now faces anteriorly. As is typical of dicynodonts, the postorbital consists of two main parts, the postorbital bar and a posteriorly directed process that contributes to the intertemporal skull roof, that are separated by a transitional zone that articulates with the frontal. In NMT RB42, the postorbital bar is flattened such that the original lateral and medial surfaces are quite broad. The ventral end of the postorbital bar is moderately expanded, and its medial surface is ridged to interlock with the jugal. As preserved, the jugal shows no evidence of a dorsally directed process that extended up the posterior surface of the postorbital. However, there is a groove on the posteromedial surface of the postorbital bar in NMT RB42 that is contiguous with the articular surface for the jugal, suggesting that such a process might have been present. Anterior to this groove, the postorbital bar is thickened and somewhat rugose. Near where the postorbital bar meets the skull roof, this rugosity takes on a more striated appearance and is contiguous with the ornamented portions of the prefrontal and frontal contributions of the orbital margin.

Where the bone transitions from the postorbital bar to the posterior process, the dorsal surface of the postorbital is flat and seems to have been flush with the surface of the frontals. Moving posteriorly, the lateral edge becomes raised as a thin ridge, which continues as the thin dorsal edge of the posterior process. When the postorbital is articulated with the temporal bar (i.e., the right side of NMT RB42, both sides of UMZC T1226), this thin edge is slightly taller than the corresponding surface on the parietals, contributing to the dorsally concave shape of the temporal bar in cross-section (Figs. 6A, B, 8C). The posterior process is oriented vertically and attaches to the lateral surface of the temporal bar, in contrast to the situation in taxa such as *Oudenodon*, where part of the posterior process is oriented horizontally and contributes to the dorsal surface of the skull roof. The process is tallest at its anterior end, near the transition to the postorbital bar, and it tapers to a sharp posterior point. The dorsal edge of the process is relatively straight, so most of this tapering is accomplished by the ventral edge of the process sloping postero-dorsally. The lateral surface of the posterior process is weakly concave. The posterior tip of posterior process contacts the squamosal but is separated from the interparietal by the short posterolateral process of the parietal.

The morphology of the medial surface of the temporal portion of the postorbital is shown well by the left postorbital of NMT RB42 (Fig. 7F). The whole medial surface of this area is gently convex anteroposteriorly and dorsoventrally. Where the posterior process arises, the ventral half of the medial surface is thickened to form a convex eminence. This articulates with a fossa located at the anteroventral corner of the lateral surface of the parietals. The entire medial surface of the postorbital is covered by an elaborate system of curving ridges and grooves, which interlock with similar features on the lateral surface of the parietals. These striations are most prominent on the medial surface of the transitional zone and the anterior end of the posterior process and become weaker moving posteriorly from there. The ridges near the transition to the postorbital bar curve anteromedially, whereas those on the posterior process curve posterodorsally.

The temporal bar of UMZC T1226 appears to be angled postero-dorsally relative to the dorsal surface of the snout, with the break in slope occurring at the level of the pineal foramen (Fig. 8A). This morphology is similar to that seen in *Kannemeyeria*, and it is reflected in Cruickshank's (1986a) reconstruction of the skull of *S. parringtonii*. As noted above, though, comparison of UMZC T1226 with NMT RB42 suggests that the snout of the former specimen was dorsoventrally compressed during preservation. The temporal bar of NMT RB42 also is angled dorsoventrally, but there is no distinct break in slope apparent at the level of the pineal foramen. Instead, the angulation of the temporal bar is a smooth continuation of the sloping profile of the snout. Because NMT RB42 experienced only a minor amount of lateral compression, we consider it to better represent the original orientation of the temporal bar relative to the snout.

The squamosal can be subdivided into three processes: a temporal process, a quadrate process, and a zygomatic process. This basic morphology is common to all dicynodonts, but the squamosal of *S. parringtonii* also presents a number of unusual features that contribute to the distinctive appearance and proportions of the skull in this species (Figs. 7G–L, 8B, E–G). Particularly striking is the transverse breadth of the squamosal, and the fact that it does not flare posteriorly past the level of the occipital plate. In NMT RB42, the nearly complete left squamosal is about 204 mm wide; for comparison, the basal length of the skull is 335 mm. Combined with the width of the occipital plate, we estimate the posterior breadth of NMT RB42 originally to have been slightly over 500 mm.

The temporal process of the squamosal meets the posterior end of the temporal bar at a ca. 90° angle. It does not curve anteriorly as seen in most Permian dicynodonts and some kannemeyeriforms such as *Kannemeyeria* (Renaut, 2000) (Fig. 7G–L). It forms the posterior wall of the temporal fenestra but does not contribute to the medial border of the fenestra. The dorsal edge of the process is near vertical at the contact with the parietal, but it curves ventrolaterally such that the edge is near horizontal at its junction with the zygomatic process. For most of its length, the dorsal edge of the temporal process is quite thin, but it widens slightly as it merges with the zygomatic process. The temporal process contacts the parietal and the postorbital on the lateral surface of the temporal bar. A contact with the supraoccipital on the occipital surface of the skull seems likely, but it is not well preserved in any of the specimens.

The posterior portion of the zygomatic process of the squamosal forms a natural partition that separates the temporal and quadrate portions of the bone (Fig. 7G–J). The posterior end of the process, where it joins the rest of the squamosal, is tall, robust, concave medially, and convex laterally. The ventral portion of the zygomatic process in this area is thick and rounded in cross-section, but it becomes thinner and more plate-like dorsally. The lateral surface of the zygomatic process forms much of the medial wall of the fossa for the attachment of *M. adductor*

mandibulae externus lateralis (e.g., Watson, 1948; Crompton and Hotton, 1967; Barghusen, 1976; Angielczyk, 2004). The fossa is oriented vertically, similar to those of *Ischigualastia* and *Jachaleria* (Cox, 1965; Araújo and Gonzaga, 1980; Vega-Dias and Schultz, 2004), and contrasts with the more horizontal orientation reconstructed by Cruickshank (1986a). Where it meets the temporal and quadrate processes, the dorsal edge of the zygomatic process is thickened and contributes to the convex dorsal edge of the squamosal: the squamosal is not ‘notched’ in posterior view, in contrast to most Permian dicynodonts (Fig. 7K, L). In NMT RB42, there is a distinct lateral facet on the anterior end of the portion of the zygomatic process that is still attached to the body of the squamosal (Fig. 7I, J). The facet is tallest at its posterior edge and is contiguous with an extremely rugose surface on the medial side of the process. The position of these features suggests that they are articular surfaces for the posterior end of the zygomatic process of the jugal, although the lateral facet implies that the jugal process had a larger lateral exposure than is usually the case in dicynodonts.

The anterior end of the zygomatic process of the squamosal is preserved in UMZC T1340 and NMT RB42 (Figs. 7A, B, 8B), although the latter specimen has undergone less weathering in this area and seems to preserve the original morphology better. This part of the squamosal is mediolaterally flattened, and it slots into a groove in the jugal such that the jugal cradled it medially and ventrally. The process tapers to a squared-off anterior tip. The ventral edge of the tip meets the zygomatic process of the maxilla along a straight contact on the lateral surface of the suborbital bar. The posterior corner of this articular surface on the squamosal curves ventrally to form a small fossa that receives the pointed tip of the zygomatic process of the maxilla. The lateral side of the zygomatic process of the squamosal is divided into two surfaces by a sharp ridge that extends posterodorsally from the fossa for the posterior tip of the maxilla. Dorsal to the ridge, the lateral surface is weakly concave laterally and bears an ornamentation of fine striations and small vascular foramina. This ornamentation is similar to that seen on the beak-bearing portions of the skull in other dicynodonts, raising the possibility that a thin, keratinized covering was present below the orbit that was perhaps contiguous with that covering the more heavily ornamented dorsal margins of the orbit. Ventral to the ridge, the lateral surface is smooth, unornamented, and flatter. The dorsal surface of the squamosal forms the lateral edge of the articular facet for the footplate of the postorbital bar.

The quadrate process of the squamosal forms the largest part of the bone. The lateral portion of the process forms a nearly vertical plate that faces anteriorly and extends laterally from the root of the zygomatic arch (Figs. 7G–L, 8B, E–G). It forms most of the fossa for the attachment of *M. adductor mandibulae externus lateralis*. In UMZC T1340, the lateral portion of the plate curls strongly anteriorly and almost no part of the adductor fossa is visible in lateral view (Fig. 8B, E). In NMT RB42 there is a much weaker anterior curvature (Fig. 7I, J). It is unclear how much this represents individual variation, differential taphonomic deformation of the specimens, or a combination of these factors. The lateral edge of the squamosal in this area is relatively thin, in contrast to the heavily thickened edge seen in *Angonisaurus* (Hancox et al., 2013; Sidor et al., 2014), although the ventrolateral corner of the plate, lateral to the facet for the quadratejugal, bears a striated ornamentation.

Ventral to the root of the zygomatic arch, the quadrate process has a large area for the articulation for the quadrate-quadratojugal complex (Fig. 7G, H). This articular surface can be divided into two main areas. Laterally, there is a large, shallow triangular facet that receives the quadratojugal. The lateral portion of this fossa is delimited by a rounded, ventrolaterally trending ridge that abuts the dorsolateral

edge of the quadratojugal, but most of the central portion of the fossa merges smoothly with the rest of the squamosal. Medially, the fossa for the quadratojugal is separated from the articular surface of the quadrate by a sharp subvertical ridge. This surface is much smaller than that for the quadratojugal and is suboval. Its lateral and medial margins are well defined, but dorsally it merges smoothly with the rest of the squamosal. The ventral edge of the quadrate process of the squamosal is slightly damaged in NMT RB42, but UMZC T1340 shows that it extensively overlapped the quadratoquadratojugal complex such that only the articular surfaces of the quadrate were visible in posterior view (Fig. 8B).

The posterior (occipital) surface of the squamosal is smooth and fairly nondescript, although the bone is weakly striated near its lateral edge (Figs. 7K, L, 8G). A medially facing groove is present on the medial surface of the bone, which receives the lateral edge of the paroccipital process of the periotic. There is no evidence for a strong ‘tympanic process’ (sensu Cox, 1959:326) in this area, but a weak dorsally trending ridge is present at the contact between the squamosal and paroccipital process (best seen in UMZC T1340). Above this contact, the squamosal should contribute to the posttemporal fenestra, but this feature is not preserved in either NMT RB42 or UMZC T1340.

None of the specimens of *S. parringtonii* preserve a complete vomer. Anteriorly, the vomer overlaps the dorsal surface of the premaxilla along the midline of the skull, forming part of the floor of the nasal cavity. In UMZC T1226, the dorsal surface of the vomer in this area bears a weak groove, but this may represent damage because the vomer in NMT RB42 has a sharp dorsal edge in this region. The anterior-most end of the mid-ventral vomerine plate is preserved in UMZC T1226. There it meets the posterior end of the posterior median palatal ridge. Breakage reveals that the vomer was dorsoventrally quite tall, spanning most of the interior height of the posterior median ridge. It is not possible to determine whether the mid-ventral vomerine plate was narrow and blade-like or wider with a central trough. The posterior end of the vomer is preserved in articulation with the anterior end of the median pterygoid plate in NMT RB42 (Fig. 6C, D). Its ventral surface bears a pair of rounded, posteriorly diverging ridges that form the anterior walls of the interpterygoid vacuity. There is no evidence of a midline suture on any of the preserved portions of the vomer, so we assume that it was a single fused element as in most dicynodonts.

The palatines also are poorly preserved in all of the specimens, but it is clear that their morphology resembled that of other dicynodonts in consisting of an anterior palatine pad that contacted the maxilla and premaxilla, and a more plate-like posterior portion that contributed to the choana (Figs. 6C, D, 8D, E). The right palatine pad of UMZC T1340 shows that the palatine pad was relatively small and that its ventral surface was somewhat rugose. Anteriorly, the pad twists so that it slopes dorsomedially where it meets the near-vertical posterior edge of the secondary palate. Near the posterolateral corner of the palatine pad, the palatine forms most of the margins of the oval lateral palatal foramen, although the pterygoid makes a small contribution to its lateral wall. A small part of the choanal portion of the palatine is preserved in UMZC T1226, showing that the bone contributed to the margins of the labial fossa.

A distinct ectopterygoid bone appears to be absent. The anterior end of the anterior pterygoid ramus meets a short posterior process of the maxilla (Fig. 8B), which may have included a center of ossification corresponding to the ectopterygoid at some stage in ontogeny. However, no suture between this posterior process and the rest of the maxilla is apparent in any of the three specimens.

The pterygoids are not completely preserved in any of the three specimens of *S. parringtonii*, but it is clear that they had the ‘X’ shape in ventral view that is typical of dicynodonts (Figs.

6C, D, 8E). The anterior pterygoid ramus is mediolaterally flattened and relatively straight, forming a strut of bone that extends between the maxilla and the median pterygoid plate (Figs. 8B, 9). There is no transverse process of the pterygoid. There are somewhat different morphologies in NMT RB42 and UMZC T1340 regarding a ventral keel on the anterior ramus. In NMT RB42, the ventral edge of the anterior-most tip of the right anterior ramus is quite narrow and keel-like, but it is truncated posteriorly by a broken surface (Fig. 6C, D), so it is uncertain how far posteriorly this narrow ventral edge continued. The ventral edge of the anterior ramus is more completely preserved in UMZC T1340 (Fig. 8E), and there it is also fairly narrow but somewhat more rounded and rugose than the preserved section of NMT RB42. This rugose edge continues posteriorly to the level of the median pterygoid plate, where it becomes smoother and thinner as it merges with the ventral surface of the plate. Anteriorly, the anterior ramus contacts the maxilla and it is flanked medially by the palatine. The medial surface of the anterior ramus makes a small contribution to the lateral wall of the lateral palatal foramen.

The median pterygoid plate is anteroposteriorly short but transversely wide, and a sharp edge separates its lateral and ventral surfaces (Figs. 6C, D, 8E). The left and right sides of the ventral surface slope dorsomedially, giving it a somewhat concave appearance in ventral view. Despite this concavity, the bone surface itself is smooth. There is no evidence of the ridge-like crista oesophagea seen in most Permian dicynodonts, a ventral projection such as in *Placerias* (Camp and Welles, 1956; Cox, 1965), or the midline fossa described in *Kannemeyeria* (Renaut, 2000). Posteriorly, the median pterygoid plate contacts the parabasisphenoid, and the footplate of the epipterygoid rests atop the dorsal surface of the median plate.

Little of the quadrate rami of the pterygoids is preserved (Figs. 6C, D, 8E). They arise from the posterolateral corners of the median pterygoid plate. Broken surfaces in this area in NMT RB42 and UMZC T1340 show that the base of the quadrate ramus was robust and rounded in cross-section. A small portion of the posterior end of the left quadrate ramus of UMZC T1340 is preserved wedged between the quadrate and the paroccipital process. This portion of the bone is mediolaterally flattened and plate-like.

A small (about 9% of the basal length of the skull), diamond-shaped interpterygoid vacuity is preserved in NMT RB42 (Fig. 6C, D). As is typical of dicynodonts, it is bordered anteriorly by the vomer and posteriorly by the median pterygoid plate. The anterior edges, formed by the vomer, extend slightly ventrally, but they do not form a prominent ventral torus around the vacuity such as that in *Dolichuranus* (Damiani et al., 2007).

A small portion of the left epipterygoid footplate is preserved near the transition between the median pterygoid plate and the quadrate ramus of the pterygoid in UMZC T1340, and more complete left and right footplates are present in NMT RB42 (Figs. 7A, B, 9). The posterior half of the footplate is roughly rectangular in shape, whereas the dorsal edge of the anterior half is concave upwards, so that the footplate comes to an anterior point. A small dorsal projection is present near the midpoint of the left epipterygoid footplate in NMT RB42, but it is difficult to say whether this represents the broken remains of the ascending ramus or if it is the dorsal process noted in other dicynodont taxa (Angielczyk, 2002). None of the ascending ramus is preserved in any specimen.

Parts of the fused parasphenoid and basisphenoid (i.e., the parabasisphenoid) are preserved in all three specimens. In ventral view (Figs. 6C, D, 8D, E), the parabasisphenoid meets the pterygoid anteriorly, although a distinct suture is not apparent. Posteriorly, thin laminae of the parabasisphenoid overlap the anterior surfaces of the basioccipital tubera. Each lamina makes an extremely limited contribution to the anterior edge of the

facet surrounding the fenestra ovalis. Paired internal carotid canals are present and located near the midline of the ventral surface of the skull (in contrast to the more lateral and dorsal position seen in some basal dicynodonts; e.g., Angielczyk and Rubidge, 2009, 2013; Angielczyk et al., 2016) (Fig. 8D). The internal carotid canal exits from a single foramen on the dorsal surface of the parabasisphenoid, which is best seen in UMZC T1340. The foramen is oval, with the long axis of the oval running anteroposteriorly.

The cultriform process is best preserved in NMT RB42. There, it is incorporated into a single, plate-like median ossification (Fig. 9), to which the presphenoid and the fused mesethmoid and orbitosphenoid (the anterior plate of Sullivan and Reisz, 2005; see Cluver, 1971, for a detailed discussion of this element) also contribute. Presumably, the parasphenoid primarily contributed to the more posterior and ventral portions of this ossification, but sutures between the elements are not readily visible. Varying degrees of contact and fusion of the anterior plate, presphenoid, and cultriform process have been reported in dicynodontoids (including kannemeyeriiforms; e.g., Huene, 1935; Camp, 1956; Ewer, 1961; Cox, 1968; Cluver, 1971; Renaut, 2000), although contact between the anterior plate and the cultriform process is absent or variable in at least some more basal dicynodonts (e.g., Cox, 1959; Barry, 1968; Sullivan and Reisz, 2005; Angielczyk and Rubidge, 2013; Angielczyk et al., 2016). The ventral edge of the median ossification bisects the dorsal expression of the interpterygoid vacuity and is flanked on either side by rounded openings leading down into the vacuity. A distinct presphenoid is not visible. We assume that it is incorporated into the median ossification and sutures delimiting it are no longer visible.

The anterior plate itself forms the dorsal portion of the median ossification (Fig. 9), but again the exact sutures delimiting it are no longer apparent. Most of the posterior surface of the median ossification forms a thin edge, but just below the level of their contact with the ventral edges of the parietals, the left and right sides diverge to form an open canal that courses anteriorly. The canal opens anteriorly through a pair of bilaterally symmetric foramina located about halfway along the anteroposterior length of the median ossification, and a strong anteroventrally directed ridge extends from the lower corner of the foramen on the lateral surface of the median ossification. Anterior to the foramina, the median ossification thickens slightly, and a weak ridge extends posteroventrally from this thickening. The location and orientation of this ridge suggests that it might mark the original boundary between the cultriform process and the anterior plate. A small oval hole is present near the anterodorsal end of the median ossification, but the uneven edges of the opening and its location along a crack in the median ossification lead us to conclude that it most likely represents damage instead of a real feature. The median ossification forms an essentially complete median septum separating the orbits.

The basioccipital forms the posterior end of the basicranium and extends onto the occipital plate (Figs. 6C, D, 7A–D, 8E–G). The basioccipital tubera are strongly developed and are oriented nearly vertically. They are formed almost exclusively by the basicoccipital, although a thin lamina of the parabasisphenoid laps onto their anterior surfaces. Distinct ridges leading from the parabasisphenoid onto the tubera, such as seen in many basal dicynodonts, are absent. The stapedial facet is semicircular when viewed from below, and it slopes strongly dorsolaterally, such that it opens laterally and ventrally. The fenestra ovalis itself is small compared with the overall size of the tuber, and it is located close to the lateral side of the stapedial facet.

Specimens UMZC T1340 and NMT RB42 differ in the morphology of the intertuberal ridge (Figs. 6C, D, 8E). In UMZC T1340, the anterior portions of the basioccipital tubera are

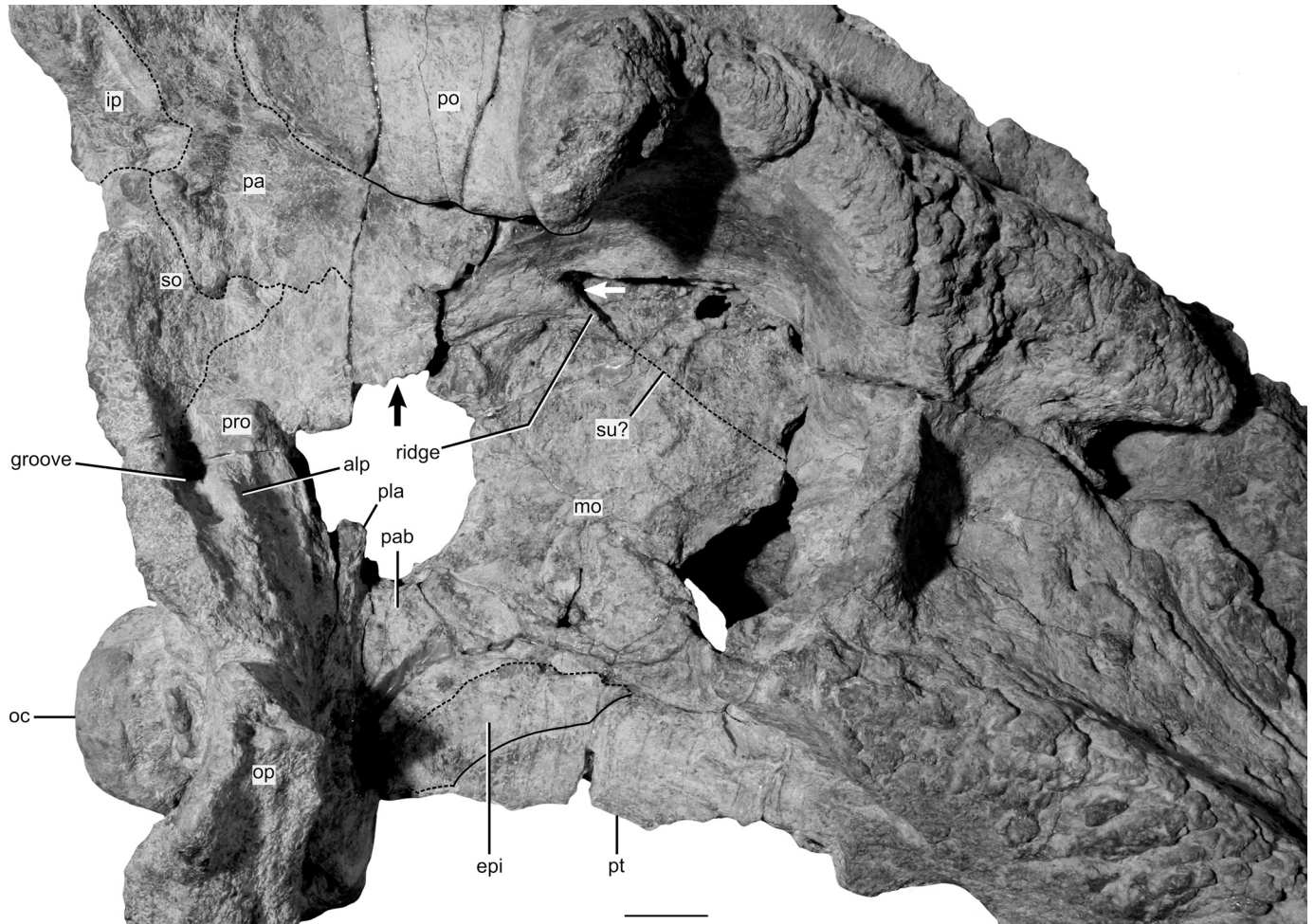


FIGURE 9. Detail of the braincase of *Sangusaurus parringtonii* (NMT RB42) in right lateral view. The black arrow indicates the position of the ventral exit of the pineal tube. The white arrow indicates the position of the foramen leading into the anteroposteriorly aligned canal (see text for details).

Abbreviations: **alp**, alar process; **epi**, epityygoid; **ip**, interparietal; **mo**, median ossification; **oc**, occipital condyle; **op**, opisthotic portion of the periotic; **pa**, parietal; **pab**, parabasisphenoid; **pla**, pila antotica; **po**, postorbital; **pro**, prootic portion of the periotic; **pt**, pterygoid; **so**, supraoccipital; **su?**, ridge marking possible remains of suture between anterior plate and cultriform process. Scale bar equals 2 cm.

separated by a depression, with the intertuberal ridge having the form of a low, rounded ridge running between the medial surfaces of the tubera at about the same level (anteroposteriorly) as the fenestra ovalis. The anterior depression is much less prominent in NMT RB42 (although this might be exaggerated by breakage in the median pterygoid plate), and a tall, thick mass of bone connects the medial surfaces of the tubera for their entire length and roughly half their height. The cause and significance of this variation is uncertain.

Posteriorly, the basioccipital forms the ventral lobe of the three-lobed occipital condyle (Figs. 7C, D, 8G). A central depression is present between the lobes of the condyle, but the sutures between the lobes are fused in both NMT RB42 and UMZC T1340. The basioccipital forms the ventral margin of the jugular foramen, which appears to have been quite small in *S. parringtonii*. In NMT RB42, a thin lamina that projects laterally from the side of the exoccipital portion of the occipital condyle overhangs the jugular foramen, screening it off when the occiput is viewed from behind. Laterally, the basioccipital contacts the paroccipital process of the periotic.

A stapes is not preserved in any of the three specimens of *S. parringtonii*.

The left quadrate-quadratojugal complex is preserved in UMZC T1340 (Fig. 8B, E–G). The quadrate consists of the expanded ventral condyles that articulate with the mandible and a short dorsal process that articulates with the squamosal. The dorsal process is subrectangular and slots into a thin-walled fossa on the squamosal (the fossa is best seen in NMT RB42; Fig. 7G, H). The anterior edge of the dorsal process is thin and appears to be broken. This raises the possibility that an anterior process similar to that reported in *Jachaleria* (Keyser, 1974; Araujo and Gonzaga, 1980) was present, but better-preserved material will be necessary to test this conjecture. The articular surface of the quadrate is similar to those of other dicynodonts in consisting of anteroposteriorly elongate lateral and medial condyles that are separated by a central groove. The lateral and medial condyles are subequal in length (a free-floating piece of bone attached to the lateral condyle by an area of matrix makes it seem somewhat longer than the medial condyle), and the lateral condyle is wider than the medial. The articular surfaces of both condyles are weakly convex, but they are somewhat flatter than is typical in many dicynodonts. Specimen UMZC T1340 shows that the articular condyles of the quadrate are angled anterodorsally when the quadrate is in articulation with the squamosal, such that the

articular surfaces of the condyles primarily face anteriorly instead of ventrally.

The quadratojugal is a triangular plate-like element (Fig. 8F). Its ventral edge is firmly fused to the lateral condyle of the quadrate, but most of the bone is free and rests in a fossa on the squamosal. Primitively in dicynodonts, the exterior surface of the quadratojugal faces primarily laterally. However, in *S. parringtonii*, the quadratojugal has rotated so that its external surface faces anteriorly. A comparable morphology has been described for *Stahleckeria* and *Ischigualastria* (Huene, 1935; Romer and Price, 1944; Cox, 1965; Keyser, 1974), and the quadratojugal of *Stahleckeria* bears a particularly striking resemblance to that of *Sangusaurus* (compare Fig. 8F with Huene, 1935:pl. 6, fig. 1). Near the ventrolateral corner of the squamosal, the margin of the quadratojugal fossa of the squamosal becomes a distinct ventrolaterally trending ridge that braces the dorsolateral edge of the quadratojugal. The relationship between the quadratojugal and the squamosal ridge is clearly seen on the left side of UMZC T1340, and the ridge itself is also well preserved in NMT RB42, although the quadrate-quadratojugal complex is not preserved in the latter specimen. The change in orientation of the quadratojugal relative to the quadrate has caused the quadrate foramen to be reduced to a teardrop-shaped vertical slit that is only visible in anterior view. Like the quadratojugal, the morphology of the quadrate foramen closely resembles that of *Stahleckeria* (Huene, 1935).

The interparietal of *Sangusaurus parringtonii* (Figs. 6A, B, 7C, D, 8C, 9) presents a mixture of similarities to and differences from that of *S. edentatus* (Fig. 3H, I, K). As in *S. edentatus*, the interparietal of *S. parringtonii* contributes to the dorsal surface of the intertemporal bar, where it contacts the parietals anteriorly and laterally. However, the parietal-interparietal suture lacks the distinctive ‘W’ shape seen in *S. edentatus*; the suture is instead ‘U’-shaped (UMZC T1226) to ‘V’-shaped (NMT RB42). The posterior edge of the interparietal also is ‘V’-shaped in *S. parringtonii*, but it lacks the central notch seen in *S. edentatus*. As noted above, the posterior ends of the parietals extend posteriorly past the level of the occipital plate, and the occipital portion of the interparietal slopes anteriorly to accommodate this emargination. The angle between the dorsal and posterior surfaces of the interparietal is much less acute in *S. parringtonii*, though (ca. 70° in NMT RB42 compared with the 25° Cox [1969] reported for *S. edentatus*). The occipital portion of the interparietal is preserved in UMZC T1226 and NMT RB42 (Fig. 7C, D), but sutures are extremely difficult to discern in either specimen. It appears that this part of the bone was roughly trapezoidal in shape (widest dorsally and narrowing ventrally), with contacts with the tabulars along its lateral edges and a contact with the supraoccipital ventrally. As preserved, the surface of the bone is smooth and flat, and there is no evidence of the nuchal crest or pits seen in some dicynodonts. A facet located adjacent to the broken right edge of the occiput in NMT RB42 served to accommodate the tabular.

The tabular is not preserved in UMZC T1340; a small triangular fragment of the left tabular appears to be present in UMZC T1226, but it provides little detail about the element’s morphology. A larger part of the left tabular is preserved in NMT RB42 (Fig. 7C, D). In posterior view, it is superficially plate-like and spans the distance from the dorsal edge of the occiput to the dorsal margin of the supraoccipital. The broken lateral edge of the occiput reveals that the tabular is not simply a thin sheet of bone, but instead has some thickness (e.g., the exposed surface of the tabular is about 11.6 mm thick near its ventral edge). When taken together with the facet present on the exposed right lateral edge of the interparietal, it is clear that the tabular and the interparietal slotted together at their contact. The break between the occiput and the left squamosal, and potentially poor

preservation of sutures on the posterior surface of the left squamosal, makes it unclear how far laterally the tabular extended and to what degree it might have overlapped the squamosal on the posterior surface of the skull. The hint of a discontinuity on the posterior surface of the squamosal, and along its broken medial edge, raises the possibility that the tabular was large and extended far laterally (Fig. 7K–L), similar to the condition in *Stahleckeria* figured by Huene (1935; although note that Romer and Price, 1944, stated they could not discern a tabular in the specimen of *Stahleckeria* that they described). Even if this maximum size of the tabular is assumed, there is no evidence that it contacted the opisthotic.

Parts of the supraoccipital are present in all three specimens of *Sangusaurus parringtonii* (Figs. 7C, D, 8G, 9). The element forms the central portion of the occipital plate above the foramen magnum, and the bone surface in this region is comparatively featureless. The occipital surface of the supraoccipital is concave in NMT RB42, such that a vertical groove extends from the suture with the interparietal to the dorsal margin of the foramen magnum. It is unclear whether this is a real feature or a result of the lateral compression and shearing that NMT RB42 experienced, because a similar groove is not apparent in UMZC T1226 or UMZC T1340, although much less of the supraoccipital is preserved in those specimens. Sutures on the lateral surface of the braincase are obscure, but it appears likely that in NMT RB42, the supraoccipital extended anteriorly to contact the prootic and parietal and to contribute to the posterodorsal walls of the braincase. The ventral suture between the supraoccipital and the exoccipital, and that between the supraoccipital and the paroccipital process, can be traced with a good deal of certainty on the posterior surface of UMZC T1340. The suture is horizontal near the midline of the skull but sweeps upwards more laterally. The posttemporal fenestra is not preserved in any of the specimens, so the degree to which the supraoccipital contributed to its margins is uncertain.

The exoccipitals are completely preserved in NMT RB42 and UMZC T1340 (Figs. 7C, D, 8G), although the sutures surrounding the element are very difficult to distinguish in both specimens. As usual in dicynodonts, the exoccipital contributes to the occipital plate and the occipital condyle. The occipital portion appears to be roughly square. Its medial side forms the lateral margin of the foramen magnum, and the lateral side contacts the paroccipital process of the periotic. Dorsally, the exoccipital shares what appears to be a horizontal but slightly irregular suture with the supraoccipital. The articular facet for the proatlas has the form of a ventrolaterally sloping ledge located just lateral to the foramen magnum (best preserved on the left side of NMT RB42; Fig. 7C, D). A small boss near the ventrolateral tip of the ledge may represent an accessory articular surface for the atlas-axis complex.

Medially, near the entrance of the foramen magnum, a small, round foramen pierces the exoccipital, which likely transmitted the hypoglossal nerve (cranial nerve XII) (e.g., Olson, 1944; Camp and Welles, 1956; Cox, 1959; Surkov and Benton, 2004; Laaß, 2015). A low, rounded ridge forms the anterior margin of this foramen, and slightly anterior to the ridge in UMZC T1340 is what seems to be a small blind fossa, although it is somewhat uncertain whether the fossa is a real feature or an artifact of preparation. The exoccipitals form the two dorsal lobes of the occipital condyle. The sutures between the condylar portions of the exoccipitals and the basioccipital are no longer evident in UMZC T1340 or NMT RB42, but a central depression on the posterior surface of the condyle remains (Figs. 7C, D, 8G). The thin lamina of bone that projects laterally from the occipital condyle, screening the ventral expression of the jugular foramen in posterior view (see description of the basioccipital above), is formed by the exoccipital.

The prootic and opisthotic are fused into a single periotic element that forms the posterior portion of the braincase, encloses the inner ear, and contributes to the occiput (Figs. 7A, D, 8F, G, 9). The prootic portion of the periotic (hereafter prootic) is in close proximity to the ventral exit of the pineal tube and the median ossification formed by the fused cultriform process, presphenoid, mesethmoid, and orbitosphenoid (Figs. 7A, B, 8F, 9). A proportionally greater distance separates these features in more basal dicynodonts, underscoring the anteroposterior shortening of the skull that has occurred in *S. parringtonii*. It is unclear whether a distinct pila antotica was present. In UMZC T1340 only a broken surface in the area from which the pila antotica would be expected to arise is preserved. A short, blunt projection is present in the expected position on the right side of NMT RB42 (Fig. 9). If this accurately reflects the original morphology of the structure, it would contrast strongly with the very narrow, elongate pilae found in most Permian dicynodonts and instead would be more comparable to the reduced pilae found in many Triassic taxa (Surkov and Benton, 2004; note that these authors coded the pila antotica as absent in *Sangusaurus* in their data matrix).

As preserved in NMT RB42, it appears that there was not a distinct notch for the trigeminal nerve (cranial nerve V) posterior to the presumed pila antotica, although breakage in this area may obscure the original morphology. Posterior to the area of the pila antotica in NMT RB42, the lateral surface of the prootic forms a laminar alar process, which overlies a medially directed channel (Fig. 9). Although the alar process does not form as distinct a lamina as in the emydopoids, it is more similar to that morphology than to the mound-like eminence present in cryptodonts and many other dicynodontoids (e.g., Kammerer et al., 2015a; discussed as part of the dorsum sellae there). There is less evidence for a laminar alar process and the underlying groove in UMZC T1340, but the lateral surface of the prootic is more damaged in that specimen. A small foramen for the facial nerve (cranial nerve VII) is present near the ventral margin of the lateral surface of the prootic; Fig. 7A, B). It is at about the same height as the base of the quadrate ramus of the pterygoid, approximately equidistant from the base of the presumed pila antotica dorsally and the facet surrounding the fenestra ovalis ventrally. Dorsally, the prootic contacts the parietal and the supraoccipital (Fig. 9).

The most prominent part of the opisthotic portion of the periotic (hereafter opisthotic) is the robust paroccipital process (Figs. 7C, D, 8G). It resembles the paroccipital processes of other dicynodonts in being dorsoventrally shorter medially, expanding rapidly in height towards its lateral surface. However, its mediolateral width is relatively short, giving it a rather blocky appearance. The lateral surface of the process forms an articular surface that slots into a groove on the medial side of the squamosal. This contact is marked by a vertical ridge on the occipital surface of the skull, as in many dicynodonts, but there is little evidence of a ‘tympanic process’ (sensu Cox, 1959:326). A slightly raised broken surface approximately in the expected position on the left side of UMZC T1340 may represent the base of such a process, but a corresponding feature is not evident in NMT RB42. Medially, the opisthotic contacts the basioccipital and seems to form part of the margin of the jugular foramen, although the small size of the foramen and the poor preservation of sutures make this somewhat uncertain.

The interior of the periotic portion of the braincase is prepared in UMZC T1340 and NMT RB42. The floor of this region of the braincase, formed primarily by the basioccipital, bears a wide, rounded ridge that is flanked by shallow grooves. The ridge is hourglass-shaped when viewed from above, and it continues anteriorly to the level of the pila antotica. There does not seem to be an unossified zone (e.g., Olson, 1944; Cluver, 1971) near

the junction of the parabasisphenoid, basioccipital, and prootic, although there is a slight gap between the bases of the pilae antotica that is backed by the anterior end of the ridge on the dorsal surface of the basioccipital in NMT RB42.

Five foramina are visible on the interior wall of the periotic, although a floccular fossa is absent. The anterior-most foramen is oval and filled with matrix. It is located close to the level of the anterior end of the ridge on the floor of the braincase and somewhat dorsal to the groove that flanks the median ridge. This position is consistent with its being the entrance to the canal that transmits the facial nerve (cranial nerve VII) to the external surface of the periotic (e.g., Olson, 1944; Camp and Welles, 1956; Cox, 1959; Cluver, 1971; Surkov and Benton, 2004; Laaß, 2015). Posterior to the first foramen are two foramina that open into the groove lateral to the midline ridge. Their position close to the midpoint of the wall of the braincase suggests that they are part of the vestibular system. Similar openings in other dicynodonts have been interpreted as ampullary recesses (e.g., Cluver, 1971) or openings for the external semicircular canal (e.g., Camp and Welles, 1956). The fourth foramen is posterior and slightly dorsal to the second and third. Camp and Welles (1956) suggested that a similarly positioned foramen in *Placerias* represented the entrance to a canal to transmit the auditory nerve (cranial nerve VIII), but this nerve is usually reconstructed in a more anterior position, at least in more basal dicynodonts (e.g., Cox, 1959; Fourie, 1993; Surkov and Benton, 2004; Castanhinha et al., 2013; Laaß, 2015). Instead, we consider it more likely that this represents the entrance to the jugular foramen, which also has been considered to transmit the glossopharyngeal, vagus, and spinal accessory nerves (cranial nerves IX, X, and XI). (e.g., Olson, 1944; Camp and Welles, 1956; Cox, 1959; Cluver, 1971; Surkov and Benton, 2004; Laaß, 2015). More extensive preparation would be needed to confirm that the external expression of the jugular foramen is confluent with this internal structure. A seemingly blind fossa and a rounded ridge separate the fourth foramen from the fifth, which pierces the exoccipital. As noted above, we interpret this foramen to have transmitted the hypoglossal nerve (cranial nerve XII).

Mandible

Parts of the mandible are preserved in UMZC T1226 and UMZC T1340. Although neither specimen is complete, together they provide a clear picture of the mandibular morphology of *S. parringtonii* (Fig. 10).

The dentary is the largest element in the mandible, and its symphyseal portion is robustly constructed (Fig. 10D, E, G, H). The symphyses of UMZC T1226 and UMZC T1340 are both broken near the midline, but it seems clear that the dentaries were fused at the symphysis, with the breaks stemming from damage during preservation. The anterior surface of the dentary is flat, and although it bears vascular foramina associated with the presence of the keratinous beak, the bone lacks the extreme rugosity seen on the external surfaces of the premaxilla and maxillae. A vertical median ridge on the anterior surface of the dentary is absent, in contrast to the morphology present in taxa such as *Placerias* (Camp and Welles, 1956). The anterodorsal margin of the symphysis forms a wedge-shaped cutting edge that is slightly raised above the rest of the symphyseal region (best seen in UMZC T1226; Fig. 10A, B). This morphology is similar to that present in taxa such as *Lystrosaurus* or *Kannemeyeria* but differs from the more strongly upturned edge seen in many Permian taxa such as *Oudenodon* or the shovel-shaped symphysis characteristic of emydopoids. At the ventral edge of the symphysis, the dentary contacts the splenial.

On the dorsal surface (Fig. 10D, F, G), a midline groove extends along the length of the dentary symphysis. Lateral to the groove, a dentary table (sensu Angielczyk and Rubidge, 2013) is

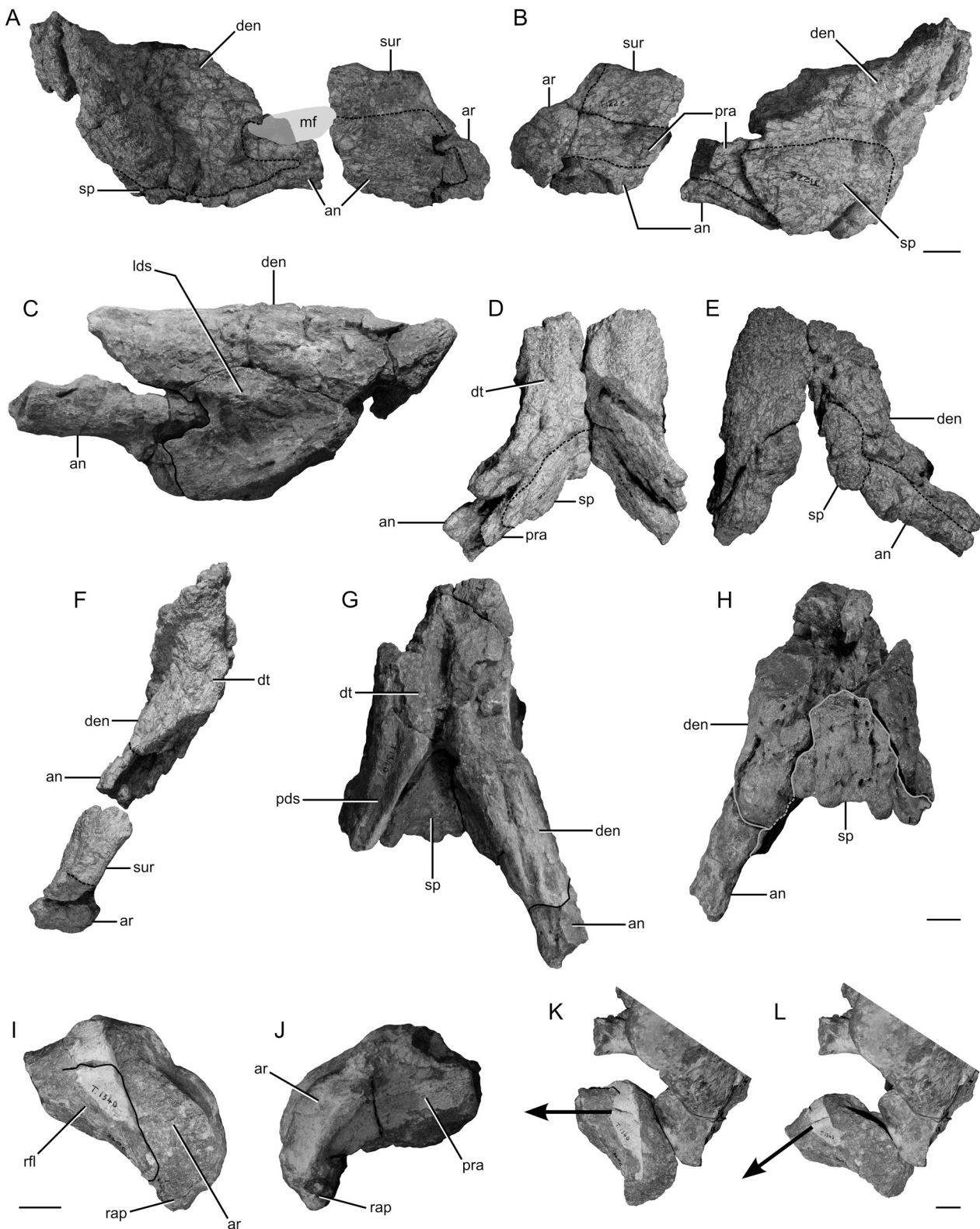


FIGURE 10. Holotype (UMZC T1226) and referred (UMZC T1340) mandibles of *Sangusaurus parringtonii*. Left mandibular ramus of UMZC T1226 in **A**, lateral and **B**, medial views. **C**, right mandibular ramus of UMZC T1340 in lateral view. Symphysis of UMZC T1226 in **D**, dorsal and **E**, ventral views. **F**, left mandibular ramus of UMZC T1226 in dorsal view. Symphysis of UMZC T1340 in **G**, dorsal and **H**, ventral views. Left articular of UMZC T1340 in **I**, lateral and **J**, medial views. Lateral view of articulated left jaw joint of UMZC T1340 in **K**, retracted and **L**, protracted positions. Note that translation of articular relative to quadrate primarily results in a vertical displacement (i.e., orthal motion) of the long axis of the mandible (represented by arrow), as opposed to extensive palinal motion of the mandible. **Abbreviations:** **an**, angular; **den**, dentary; **dt**, dental table; **lds**, lateral dentary shelf; **mf**, mandibular fenestra; **pds**, posterior dental sulcus; **pra**, prearticular; **rap**, retroarticular process; **rfl**, reflected lamina of angular; **sp**, splenial; **sur**, surangular. All scale bars equal 2 cm. Upper scale bar applies to **A-C**. Middle scale bar applies to **D-H**. Lower left scale bar applies to **I-J**. Lower right scale bar applies to **K-L**.

present on each dentary ramus. The dentary table is flat, slopes slightly ventrolaterally, and lacks well-defined lateral and medial walls. Posterior to the dentary table is a narrow, thin-walled posterior dentary sulcus (sensu Angielczyk and Rubidge, 2013; best seen in UMZC T1340). A dentary pad (sensu Cox, 1998), such as that seen in *Stahleckeria* or *Angonisaurus*, is absent. The dentary rami diverge fairly steeply, especially in UMZC T1226, presumably to accommodate the great breadth of the occiput relative to the length of the skull and mandible.

The lateral surface of the dentary is demarcated from the anterior surface by a strong, broadly rounded, posteroventrally curving ridge (Fig. 10A, C). The morphology of the lateral dentary shelf is best preserved in UMZC T1340. Anteriorly, it is a rounded swelling that grades posteriorly into a thin, ventrolaterally sloping shelf that overhangs the mandibular fenestra. Posteriorly, the dentary meets the angular along a sigmoid suture in lateral view, and it forms part of the anterior and dorsal margins of the mandibular fenestra, although neither specimen preserves the fenestra in its entirety. Damage to the symphysis in UMZC T1340 shows that the lateral surface of the dentary is quite thin, despite the overall robust appearance of the anterior end of the jaw. The dentary is dorsoventrally taller than the postdental bones in lateral view, which gives the jaw a distinct 'chin' near the junction between the dentary and angular (most pronounced in UMZC T1340; Fig. 10C), resulting in a profile similar to that of *Kitchinganomodon* (e.g., see Angielczyk et al., 2014:fig. 7.7).

The large splenial is primarily exposed on the ventral and medial surfaces of the mandible (Fig. 10A, B, E, H). As in most dicynodonts, it is a single fused element; there is no sign of a midline suture. The medial portion of the splenial is a robust, triangular block of bone that articulates with the posterior surface of the dentary and forms the posteroventral portion of the symphysis. Its ventral surface is heavily pitted with vascular foramina, indicating that the keratinous beak extended onto it, and its anterior margin lacks the distinct anterior process seen in many Permian dicynodonts. Posteriorly, the splenial bears a pair of plate-like posterior arms that contact the angulars and contribute to the anterior portions of the dentary rami.

The angular forms much of the ventral portion of the mandible, extending from the symphysis to the articular (Fig. 10A–I). Anteriorly, the angular slots between the plate-like portion of the splenial and the thin lateral side of the dentary. This section of the angular is thickened both dorsoventrally and mediolaterally, and together with the robust central portion of the splenial and the dentary symphysis, it contributes to the heavily built anterior portion of the mandible. There is a sharp corner between the anterior part of the angular and the postdental portion, which slightly extends the 'chin' at the posteroventral end of the dentary. The postdental section of the angular is more gracile and forms part of the anterior and ventral margins of the mandibular fenestra. Medial to the fenestra, the angular forms the ventral margin of the Meckelian canal (best seen in UMZC T1226). The posterior portion of the angular contacts the surangular dorsally, the prearticular medially, and the articular posteriorly.

The reflected lamina of the angular is preserved in both UMZC T1226 and UMZC T1340 (Fig. 10A, I). Its lateral surface is smooth and convex, lacking the ornamentation of ridges and grooves found in many more basal dicynodonts. Cruickshank (1986a) noted that the reflected lamina contacted the lateral surface of the articular and included this in his emended diagnosis of the genus *Sangusaurus*. This contact is clearly preserved in UMZC T1340, and it seems likely to have been present in UMZC T1226, although the reflected lamina is more poorly preserved in that specimen. Close approach or contact between the reflected lamina and the articular is a rare feature in dicynodonts, otherwise present only in *Kannemeyeria lophorhinus*, *Stahleckeria*, *Ischigualastia*, and *Moghreberia* (Huene, 1935;

Crozier, 1970; Keyser, 1974; Keyser and Cruickshank, 1979; Dutuit, 1988).

Little of the surangular and prearticular is preserved (Fig. 10A, B, F, J). As is typical of dicynodonts, the surangular forms the dorsal portion of the postdental region of the mandible. In UMZC T1340 there is a channel present in the dentary that would accommodate the anterior portion of the surangular. This channel extends forward into the symphyseal region of the dentary, implying that the surangular had a large anterior section in addition to the exposed postdental portion of the bone, similar to the angular. The fact that the anterior portion of the surangular is not preserved in this specimen, despite relatively minor damage to the dentary, indicates that the surangular and dentary were not strongly fused. The prearticular is a strap-like element present on the medial side of the mandible. It is firmly fused with the articular, and no evidence of a suture between the bones remains.

The morphology of the articular is shown best by UMZC T1340 (Fig. 10I, J). In its basic construction, the articular presents the morphology that typifies dicynodonts, and that proved key to understanding the function of their highly derived feeding system (e.g., Watson, 1912a, 1948; Crompton and Hotton, 1967; King et al., 1989; King, 1994; Angielczyk, 2004). The joint surface consists of elongate, convex lateral and medial condyles that are separated by a midline trochlea, and which grade into a concave articular recess at the anterodorsal end of the articular. The medial articular surface is not completely preserved in UMZC T1340, but based on that specimen and UMZC T1226, it seems clear that the lateral articular surface was the wider of the two. The lateral edge of the lateral articular surface is thickened, and it overhangs the posterior edge of the reflected lamina of the angular. A short, rectangular retroarticular process is present posterior and ventral to the articular surfaces. The articular contacts the angular and surangular anteriorly, and the prearticular contacts its medial surface, although the suture between these bones is no longer visible.

Despite the overall similarity of the articular of *S. parringtonii* to those of other dicynodonts, there are some noteworthy features of its arthology. Specifically, both the main articular surfaces and the articular recess slope strongly posteroventrally and form one more or less continuous surface. This contrasts with the morphology seen in most other dicynodonts, in which the articular recess is more horizontal and somewhat offset from the posteroventrally sloping articular surfaces (e.g., Crompton and Hotton, 1967). The functional implication of this morphology is that although translation of the articular relative to the quadrate is still possible, the result of this translation is a primarily orthal motion of the mandible (Fig. 10K, L) instead of the palinal motion typical of most dicynodonts. A reemphasis on the orthal component of jaw motion also has been suggested for *Lystrosaurus* and *Kannemeyeria* (Crompton and Hotton, 1967; Cluver, 1971; King and Cluver, 1991; Renault, 2001).

Postcrania

Two dorsal vertebrae that include centra and partial neural arches are preserved in NMT RB42 (Fig. 11). In addition, neural spines of two additional vertebrae are preserved in association with these vertebrae (Fig. 11). Although we cannot exactly determine the positions of the vertebrae in the vertebral column, coalescence of the rib facets, and the short, anteroposteriorly narrow transverse processes indicate that they are posterior dorsals (King, 1981a). The general morphology of the vertebrae is very similar to what has been described and figured for other kannemeyeriforms (e.g., Pearson, 1924; Huene, 1935; Camp and Welles, 1956; Sun, 1963; Cox, 1965; Bandyopadhyay, 1988; Vega-Dias and Schultz, 2004; Govender et al., 2008).

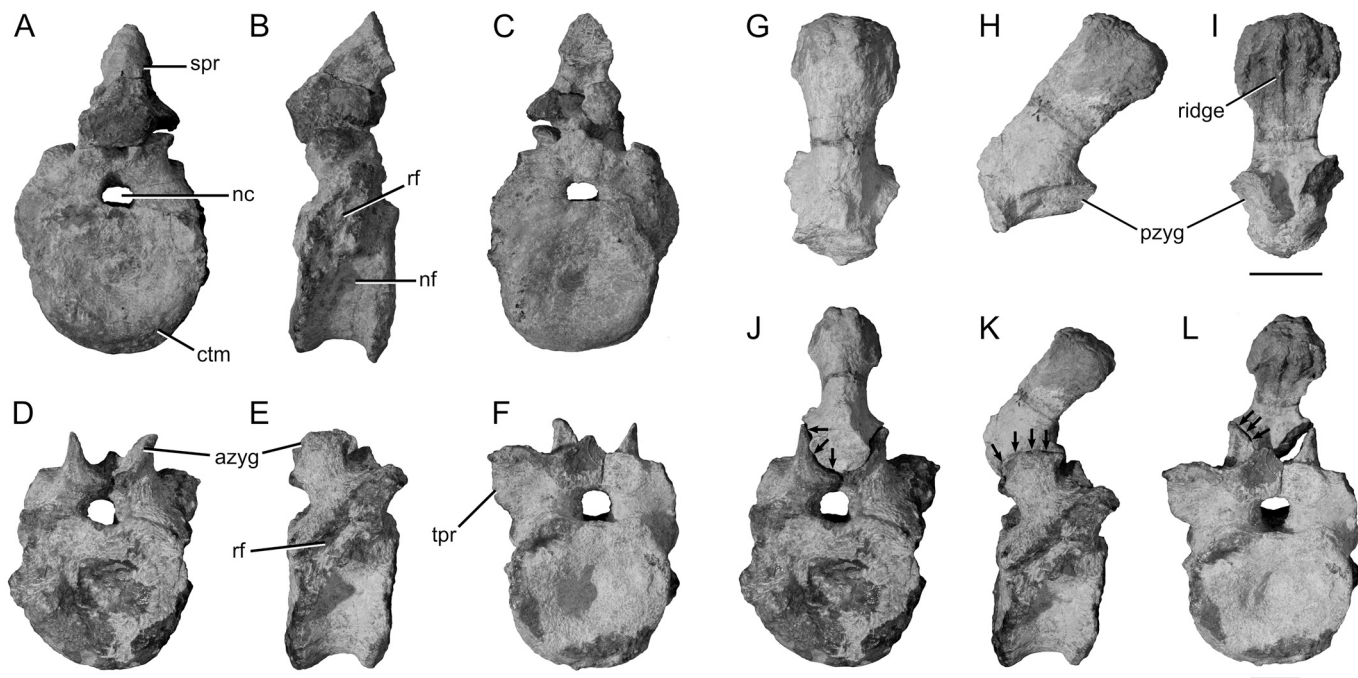


FIGURE 11. Vertebrae of *Sangusaurus parringtonii* (NMT RB42). More anterior dorsal vertebra in **A**, anterior, **B**, left lateral, and **C**, posterior views. More posterior dorsal vertebra in **D**, anterior, **E**, left lateral, and **F**, posterior views. Isolated neural spine in **G**, anterior, **H**, left lateral, and **I**, posterior views. Articulated isolated neural spine and more posterior dorsal vertebra in **J**, anterior, **K**, left lateral, and **L**, posterior views. Arrows highlight the boundary between the anterior zygapophysis (on the dorsal vertebra) and the posterior zygapophysis (on the neural spine). Note the extremely precise fit of these articular surfaces (the right posterior zygapophysis is damaged, explaining the gap between it and the corresponding anterior zygapophysis observed in posterior view). **Abbreviations:** ctm, centrum; nc, neural canal; nf, nutritive foramen; pzyg, posterior zygapophysis; rf, rib facet; spr, spinous process; tpr, transverse process. Scale bars equal 2 cm. Lower scale bar applies to **A–F** and **J–L**; upper scale bar applies to **G–I**.

The centra of both vertebrae are deeply amphicoelous (Fig. 11A, C, D, F) and they are disc-like, being transversely wider than long. The articular surfaces of the centrum are taller and wider than the body, giving the vertebra a waisted appearance in lateral and ventral views. An oval nutritive foramen is present on the lateral surface of the centrum, slightly ventral to the junction with the neural arch and posterior to the ventral margin of the rib facet (Fig. 11B). The suture between the centrum and the neural arch is not obvious, suggesting that NMT RB42 was an adult.

The articular surfaces for the tuberculum and capitulum of the rib have coalesced into a single continuous surface that includes parts of the centrum and neural arch (Fig. 11B, E). The ventral corner of the articular surface projects laterally as a small, rounded to triangular facet. This facet faces dorsolaterally and is buttressed ventrally by a small ridge arising from the lateral margin of the anterior face of the centrum. From there, the articular surface first extends dorsally and then angles posterodorsally, continuing towards the transverse process. This portion of the articular surface is bounded anterodorsally and posteroventrally by raised ridges on the neural arch pedicle, giving it a channel-like appearance. The posterodorsal corner of the articular surface is located on the ventral side of the transverse process. A small subtriangular facet is present here, which faces ventrolaterally.

The pedicles of the neural arch are robust and blocky (Fig. 11A–F). In the better-preserved vertebra, the anterior surface of the pedicle slopes posterodorsally to meet the transverse process, whereas the posterior surface of the pedicle is nearly vertical. The transverse process is small and does not project far beyond the lateral wall of the pedicle. In posterior view, the transverse process is square, with a somewhat thickened dorsal edge. Its ventrolateral corner forms a triangular facet that

contributes to the articular surface for the rib. The spinal canal is subcircular in cross-section.

The prezygapophyses are large, occupying most of the antero-posterior length of the neural arch (Fig. 11D, E). The articular surface of the prezygapophysis is horizontal near the midline, but it curves strongly dorsally to form a near-vertical wall laterally. When the left and right sides are taken together, this morphology causes the prezygapophyses to form a ‘U’-shaped channel into which the postzygapophyses slide. Given the size of the prezygapophyses, the neural spine has the appearance of projecting from the posterior surface of the neural arch.

The preserved neural spines are short and are angled posterodorsally (Fig. 11B, G–I). The dorsal end of the spine is expanded, rugose, and triangular, with the apex of the triangle oriented anteriorly. A pair of low ridges extend up the posterior surface of the neural spine, and they are flanked laterally by shallow grooves. The postzygapophyses arise from the base of the neural spine. The articular surface of each postzygapophysis is subtriangular to oval, gently concave, and faces ventrolaterally. The dorsal rim of the articular surface overhangs the rest of the facet and is buttressed by low ridges arising from the lateral and posterior surfaces of the neural spine. There is an extremely precise fit between the pre- and postzygapophyses of the preserved vertebrae (Fig. 11J–L), which allows some dorsoventral flexion of the vertebral column but strictly prohibits any lateral bending.

Most information about the morphology of the sacrum comes from the right innominate of NMT RB42. There were at least six sacral vertebrae, and two lines of evidence suggest that seven sacrals were present (Fig. 12B, G). First, the remains of six clear sacral ribs are present on the medial surface of the right ilium in NMT RB42, as well as a small piece of bone articulated with the posterior end of the ilium that seems to represent part of a small

seventh sacral rib. Second, the three well-preserved sacral centra represent the fourth, fifth, and six sacrals. These vertebrae are solidly fused together, and the sixth centrum appears to have the anterior portion of an additional, poorly preserved vertebra

fused to it. The position of this potential seventh sacral is such that if its sacral rib slanted posteriorly at an angle similar to that seen in the preceding vertebrae, it would articulate with the ilium where the apparent remains of the seventh sacral are located.

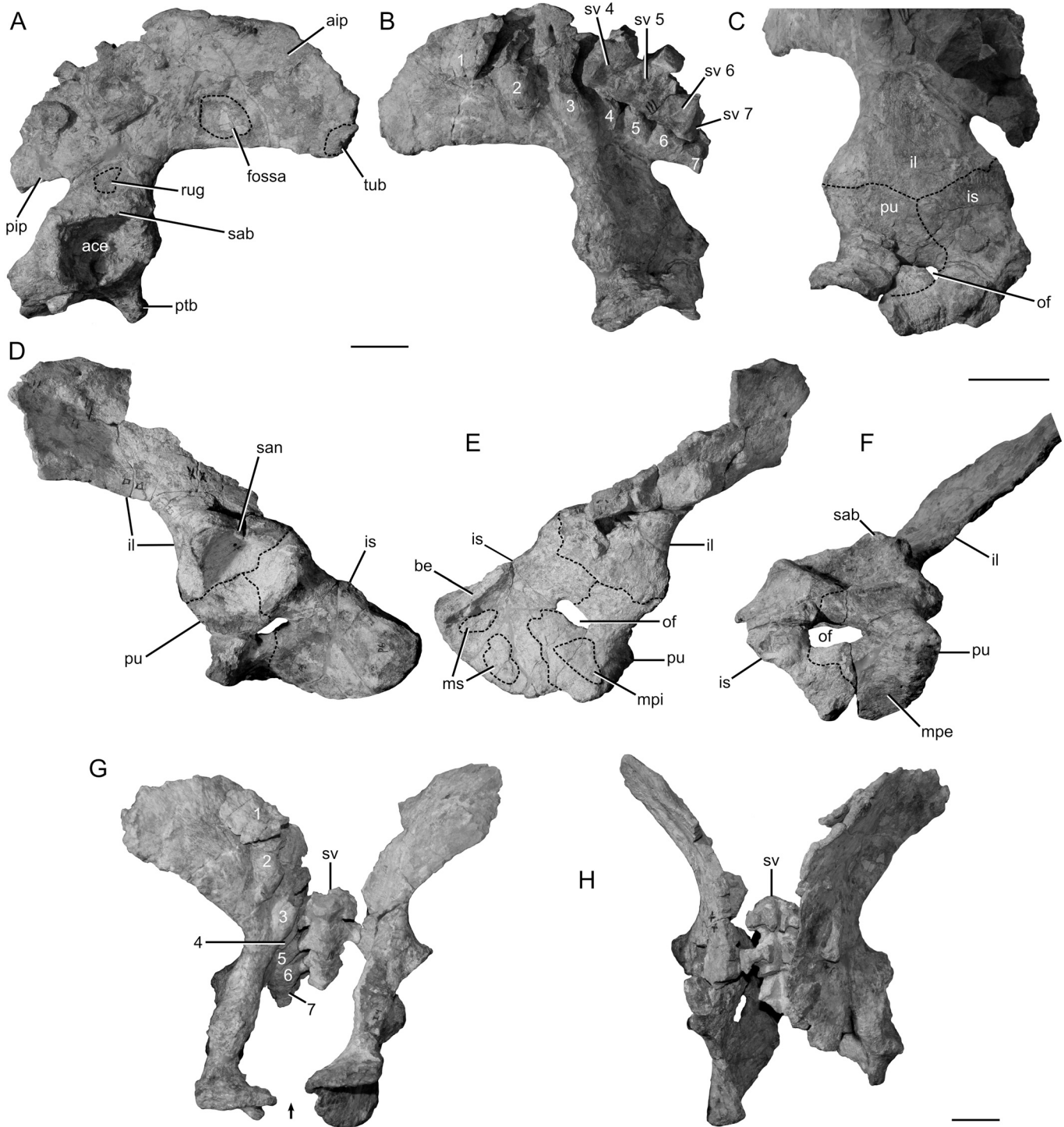


FIGURE 12. Pelvis of *Sangusaurus parringtonii* (NMT RB42). Right pelvis in **A**, lateral, and **B**, medial views. **C**, detail of right pelvis in medial view to show sutures between ilium, ischium, and pubis. Left pelvis in **D**, lateral and **E**, medial views. **F**, right pelvis in ventral view to show details of ischium and pubis. **G**, articulated pelvis in anteroventral view. Arrow highlights the lack of contact between the puboischiadic plates along the ventral midline. **H**, articulated pelvis in dorsal view. Note lateral splay of the ilia. Abbreviations: **ace**, acetabulum; **aip**, anterior iliac process; **be**, broken edge; **il**, ilium; **is**, ischium; **mpe**, likely origin of *M. puboischiofemoralis externus*; **mpi**, likely origin of *M. puboischiofemoralis internus*; **of**, obturator foramen; **ms**, unidentified muscle scar; **pip**, posterior iliac process; **ptb**, pubic tubercle; **pu**, pubis; **rug**, rugosity; **sab**, supraacetabular buttress; **san**, supraacetabular notch; **sv**, sacral vertebra; **tub**, tubercle. Scale bars equal 6 cm. Upper left scale bar applies to **A–B** and **D–E**; upper right scale bar applies to **C** and **F**; lower right scale bar applies to **G–H**.

There is a general trend for an increase in the number of sacral vertebrae in later-occurring, derived dicynodonts (Ray, 2006), and kannemeyeriiform dicynodonts vary in the number of sacral vertebrae. However, seven sacrals is an unusually high number. For comparison, five sacrals have been reported in *Shansiodon* (Yeh, 1959), *Sinokannemeyeria* (Sun, 1963), *Ischigualastia* (Cox, 1965), and *Jachaleria* (Araújo and Gonzaga, 1980; Vega-Dias and Schultz 2004); five to six are present in *Wadiasaurus* (Bandyopadhyay, 1988) and *Parakannemeyeria* (Sun, 1963; K.D.A., pers. observ. of PIN 2422/1); and six are present in *Kannemeyeria* (Pearson, 1924; Cruickshank, 1975), *Tetragonias* (K.D.A., pers. observ. of UMZC T754; also see Cruickshank, 1967), *Dinodontosaurus* (Morato, 2006; although see Cox, 1965), and *Angonisaurus* (K.D.A., pers. observ. of NHMUK PV R9732). Huene (1935) reported eight sacrals in *Stahleckeria*, and our observations of GPIT/RE/8001 suggest that at least six to seven sacrals were present in that taxon.

Compared with the proportions of the posterior dorsal vertebrae, the centra of the preserved sacrals are anteroposteriorly longer and dorsoventrally shorter, giving them a more spool-shaped appearance (Fig. 12B, G). The centra are firmly fused together, and the edges of the central faces do not flare beyond the vertebrae to the degree seen in the posterior dorsals, giving the sacrals a less waisted appearance. The contact between the vertebra and sacral rib extends from about the level of the prezygapophyses dorsally onto the dorsal half of the centrum (Fig. 12G, H). At least for the preserved posterior sacrals, the sacral ribs only articulate with a single vertebra. The neural canal is small and more oval than those of the posterior dorsals (Fig. 12H).

The lateral ends of the first three sacral ribs are preserved in articulation with the medial side of the right ilium, complete right sacral ribs are preserved for sacrals 4–6, and what appears to be the lateral end of a seventh sacral rib is articulated with the posterior end of the right ilium (Fig. 12B, G). Parts of the distal ends of sacral ribs 4–6 are present on the medial surface of the left ilium, but they are more poorly preserved than those of the right side. The end of the first sacral rib is spatulate and roughly square. The dorsal and ventral edges of the lateral end flare past the edges of the shaft, such that the rib narrows proximally. The lateral ends of the next five (and possibly six) sacral vertebrae (i.e., sacrals 2–6 or 7) are chevron-shaped and less flattened than that of the first sacral rib, although the degree to which the chevron shape is developed is greater in the more anterior ribs. The ventral edges of all of these ribs flare well past their shafts, and they are rounded in sacrals 2–4 but squared-off in sacrals 5–6. In contrast, only the dorsal edge of the end of sacral rib 2 flares dorsally past the shaft. The sacral ribs also show a gradient in their angulation relative to the centra. Sacral ribs 1–3 are angled anteriorly, such that the edge of the distal end flares anteriorly past the shaft. Sacral rib 4 extends laterally from the vertebra, and its anterior and posterior ends are not strongly flared. Sacral ribs 5 and 6 (and possibly 7) are angled posteriorly, with their lateral edges flaring posteriorly past the shaft. The medial ends of the preserved fourth, fifth, and sixth sacral ribs are anteroposteriorly flattened closest to the vertebrae (this likely represents part of the fused transverse processes), but become more rounded in cross-section near mid-shaft before flaring outwards and flattening at their lateral ends. A weak, posteriorly directed groove is present at about mid-height on the posteromedial surface of the sixth and probable seventh sacral ribs, giving the posterior edges of these ribs a bilobed appearance in posterior view.

Although neither the right or left side is perfectly preserved, the pelvis of NMT RB42 gives a very complete picture of the overall pelvic morphology of *S. parringtonii*. The right ilium is nearly complete; the acetabular portion of the left ilium also is well preserved, but the left iliac blade is damaged dorsally and posteriorly (Fig. 12A, B, D, E). The ilium consists of a fan-

shaped blade that articulates with the sacrum, a narrower neck, and the dorsal portion of the acetabulum. The iliac blade can be divided into an anteroposteriorly elongate anterior iliac process and a much smaller posterior iliac process. The disparity in the sizes of the processes is reflected in the lengths of their ventral edges: the ventral length of the anterior iliac process is about 53% of the total length of the iliac blade, whereas the ventral length of the posterior iliac process is ca. 17% of the total length. The anterior iliac process gently curves ventrally, and beginning at the level of the third sacral rib, its anterior end also splays laterally. In contrast, the triangular posterior iliac process angles slightly dorsally when the sacrum is oriented horizontally, and it does not curve laterally or medially. Kammerer et al. (2013) reviewed the iliac blade shapes of kannemeyeriiforms, and comparison with their observations shows that the blade of *S. parringtonii* is similar to those of *Kannemeyeria* or *Angonisaurus*, not sharply curved as in *Stahleckeria* or broadly rounded as in *Jachaleria* or *Ischigualastia*.

The dorsal edge of the iliac blade is smoothly convex (Fig. 12A, B) and does not bear the notches present in *Lystrosaurus* (e.g., Watson, 1912b; Ray, 2006). The blade itself is quite thin, although its dorsal edge is somewhat thickened at the level of the first sacral rib, presumably because this rib attaches very close to the dorsal margin of the blade. There is also a rugose, rounded tubercle at the anteroventral corner of the anterior iliac process. A number of authors have reconstructed the origin of *M. iliotibialis* near the anterior end of the iliac blade (King, 1981a, 1985; Li, 1983; DeFauw, 1986; Walter, 1986; Ray and Chinsamy, 2003; Morato, 2006; Ray, 2006) and have suggested that the origin of *M. puboischiofemoralis internus* was located in this region. The hypothesized attachments for these muscles are on the lateral surface of the ilium instead of its anterior edge, however, and typically there is not a comparable tubercle present on the anterior margin. The presence of the tubercle may indicate that the attachment of the muscle may have shifted anteriorly in *S. parringtonii*. Alternatively, the tubercle might represent an attachment for the iliopubic ligament (DeFauw, 1986).

The lateral surface of the iliac blade is relatively flat posteriorly, becoming gently concave more anteriorly. Two circular nutritive foramina are present near the dorsal margin of the blade, at the level of the first and third sacral ribs. A shallow fossa is present above the ventral margin of the anterior iliac process, close to where it meets the neck of the ilium. The somewhat rough preservation of the bone surface on the lateral surface of the blade makes it difficult to delineate specific muscle scars. Most of the lateral surface was likely occupied by *M. iliofemoralis*, with *M. iliofibularis* originating on the posterior iliac process (King, 1981a, 1985; Li, 1983; DeFauw, 1986; Walter, 1986; Ray and Chinsamy, 2003; Morato, 2006; Ray, 2006). The majority of the medial surface of the iliac blade is covered by the sacral ribs, but the anterior fifth of the blade was free of the sacrum. This area may include one of the areas of origin of *M. puboischiofemoralis internus* and/or the attachment for the iliopubic ligament (DeFauw, 1986; Ray and Chinsamy, 2003; Ray, 2006). An oval nutritive foramen is located above the third sacral rib.

The neck of the ilium forms a short, robust pillar between the iliac blade and the acetabulum (Fig. 12A–E). It is roughly triangular in cross-section, with the anterior end being wider than the posterior end, and it transitions from being mediolaterally flattened where it meets the iliac blade to transversely expanded just above the acetabulum. Breakage on the left ilium of NMT RB42 shows that the anterior portion of the neck is solid bone, whereas the posterior portion of the neck houses an open cavity that extends ventrally deep to the exterior surface of the acetabulum. A slightly raised, striated rugosity is present near the center of the lateral surface of the neck. Previous workers generally

have not reconstructed a distinct muscle attachment on this area in dicynodonts, although in some cases parts of the attachment of *M. iliofemoralis* are reconstructed as having extended onto this area (e.g., DeFauw, 1986). Li's (1983) reconstruction differs from most others in placing the origin of *M. iliotibialis* on the lateral surface of the neck of the ilium.

The ventral margin of the lateral surface of the neck sweeps laterally to form the overhanging supraacetabular buttress (Fig. 12A, F). This buttress is most pronounced anteriorly and is separated from the posterior portion of the dorsal acetabular margin by a shallow supraacetabular notch (Fig. 12D). The acetabulum itself is roughly hemispherical, with the anterior portion of the supraacetabular buttress forming an oval to subtriangular overhang. The ilium meets the puboischiadic plate near the center of the acetabulum. Although the ilium is fused to the puboischiadic plate, remains of the sutures are visible, with the ilium-pubis suture angling anterodorsally and the ilium-ischium suture angling posterodorsally (Fig. 12D). A degree of flexibility between the ilium and the puboischiadic plate has been suggested in some dicynodonts (Cox, 1959; Cruickshank, 1967; King, 1981a), but the fusion of these elements would preclude such flexibility in *S. parringtonii*. It is also noteworthy that the ilium and puboischiadic plate are aligned roughly vertically, in contrast to the stronger medial inflection of the puboischiadic plate suggested by Fröbisch (2006) for *Tetraponias*.

The pubis is complexly shaped and forms the anterior half of the ventral portion of the acetabulum and slightly less than half of the puboischiadic plate (Fig. 12A–F). It is fused to the ilium and ischium, but remains of the sutures between these elements can still be made out. In lateral view, the pubis is triangular and forms a short process (the pubic tubercle) that projects anteroventrally. The lateral surface of the tubercle is striated, and a small projection is present just above the tip of the pubis. This area typically is reconstructed as representing the origin of *M. ambiens* in dicynodonts (DeFauw, 1986; Walter, 1986; Ray and Chinsamy, 2003; Morato, 2006; Ray, 2006). The pubic margin of the acetabulum is slightly raised, but it does not form a strong rim or buttress.

At its anterior tip, the pubis sweeps medially and then posteriorly to form the anterior portion of the puboischiadic plate (Fig. 12C, F, G). The curvature of the pubis causes the anterior portion of the puboischiadic plate to project strongly medially, and for the surfaces of the plate to face anterodorsally and posteroventrally. The posteroventrally facing surface of the plate is strongly striated and likely represents part of the attachment for *M. puboischiofemoralis externus* (King, 1981a, 1981b; DeFauw, 1986; Ray, 2006). The pubic portion of the puboischiadic plate is thickest at its anterolateral tip, becoming progressively thinner until it meets the ischium. The anterior and anteromedial edges of the puboischiadic plate are highly rugose and bear numerous circular pits on their surfaces. Two explanations for this pitting are (1) that it represents an area for muscle or ligament attachment (e.g., it represents part of the origination of *M. ambiens* or an attachment for the iliopubic and/or puboischiadic ligaments; DeFauw, 1986), or (2) that it was covered in cartilage, possibly as part of a cartilaginous pubic symphysis. Of these two options, we favor the latter because the ornamentation of the bone, especially the circular pits, closely resembles that found on cartilage-covered joint surfaces in the long bones of dicynodonts (e.g., see the description of the humerus below).

The left and right puboischiadic plates in dicynodonts are not thought to have met at a bony symphysis along the ventral midline (see Cox, 1959, and Fröbisch, 2006, for reviews). When the left and right halves of the pelvis of NMT RB42 are rearticulated with the sacrum (Fig. 12G, H), the anterior (pubic) portions of the puboischiadic plates approach each other relatively closely (they are separated by about 4.5 cm, compared with 36.5 cm for

the length of the complete right iliac blade and an inner antero-posterior acetabular length of about 9 cm) but they do not contact. Interestingly, the most rugose and pitted portions of the edge of the pubis face anteriorly when rearticulated instead of medially, which may indicate that part of the cartilaginous symphysis (if present) projected anteriorly from the puboischiadic plate. Posteriorly, the pubis surrounds the anterior half of the oval obturator foramen. A raised, subtriangular area just below the obturator foramen on the medial surface of the left pubis, near its junction with the ischium, likely represents the origin of *M. puboischiofemoralis internus* (e.g., King, 1981a; DeFauw, 1986; Morato, 2006).

The left ischium of NMT RB42 (Fig. 12D, E) is more complete than the right, and our description focuses on this element. The dorsal portion of the ischium is robust and forms the posterior half of the ventral portion of the acetabulum. Its lateral surface sweeps laterally to form a more strongly defined rim of the acetabulum than is the case for the pubis. It also surrounds the posterior half of the obturator foramen. Moving posteriorly, the ischium rapidly flattens to form the fan-shaped posterior section of the puboischiadic plate. This area of the ischium is much less strongly curved than the pubis and forms a flat plate than faces ventrolaterally. The plate is quite thin, and its ventral edge is smooth. There is no evidence of a bony connection between the ischia, nor is there strong evidence for a cartilaginous connection (Fig. 12G, H). At its posterodorsal corner, the edge of the ischium becomes markedly thicker. Based on the presence of a broken edge on the medial surface of the bone, it is clear that the puboischiadic plate had a medially inflected section that arose from this thickened corner, similar to the morphology that has been figured for a number of other kannemeyeriiforms (e.g., Pearson, 1924; Huene, 1935; Sun, 1963; Cox, 1965, 1969; Bandyopadhyay, 1988; Vega-Dias and Schultz, 2004). However, the medially inflected portion of the ischium is not preserved on either side of NMT RB42, so we are uncertain of its exact size or shape.

Although the lateral surface of the plate likely served as the attachment area for several muscles (e.g., *M. puboischiofemoralis externus*, *M. adductor femoris*, *M. puboischiotibialis*; King, 1981a; Li, 1983; DeFauw, 1986; Walter, 1986; Morato, 2006; Ray, 2006), distinct muscle scars are not readily apparent. Two potential muscle scars are visible on the medial surface of the ischium (Fig. 12E). One is an oval area that has a somewhat lumpy bone texture and is slightly raised above the surface of the surrounding bone. This scar is located just above the ventral edge of the puboischiadic plate. The second is an area located just below the beginning of the (now broken) medially inflected portion of the ischium, posterodorsal to the previous scar. Its texture is somewhat lumpy as well, and it is also marked by a thin, posteroventrally trending ridge. *M. iliofibularis*, *M. ischiotrochantericus*, *M. flexor tibialis externus*, and *M. flexor tibialis internus* have been reconstructed as attaching on this general area of the ischium (King, 1981a, 1981b, 1985; Li, 1983; DeFauw, 1986; Ray and Chinsamy, 2003; Morato, 2006; Ray, 2006), but the exact configuration of these muscles varies from author to author, making an exact identification of the scars difficult.

The posterior half of the distal end of the left humerus is preserved in NMT RB42 (Fig. 13A–C). Given its fragmentary nature, only a few details of the anatomy of the element can be described. The preserved dorsal and ventral surfaces of the bone are relatively flat, although the distal end of the strip of bone that encloses the entepicondylar foramen arises from a somewhat rounded swelling on the ventral surface. The entepicondyle is more dorsoventrally flattened and sweeps posteriorly more strongly than is the case in most kannemeyeriiforms. Its shape in dorsal and ventral views most closely resembles that of some specimens of *Placerias hesternus* (e.g., UCMP A269/25361, UCMP A269/32460), although it is less dorsoventrally flattened in those specimens.

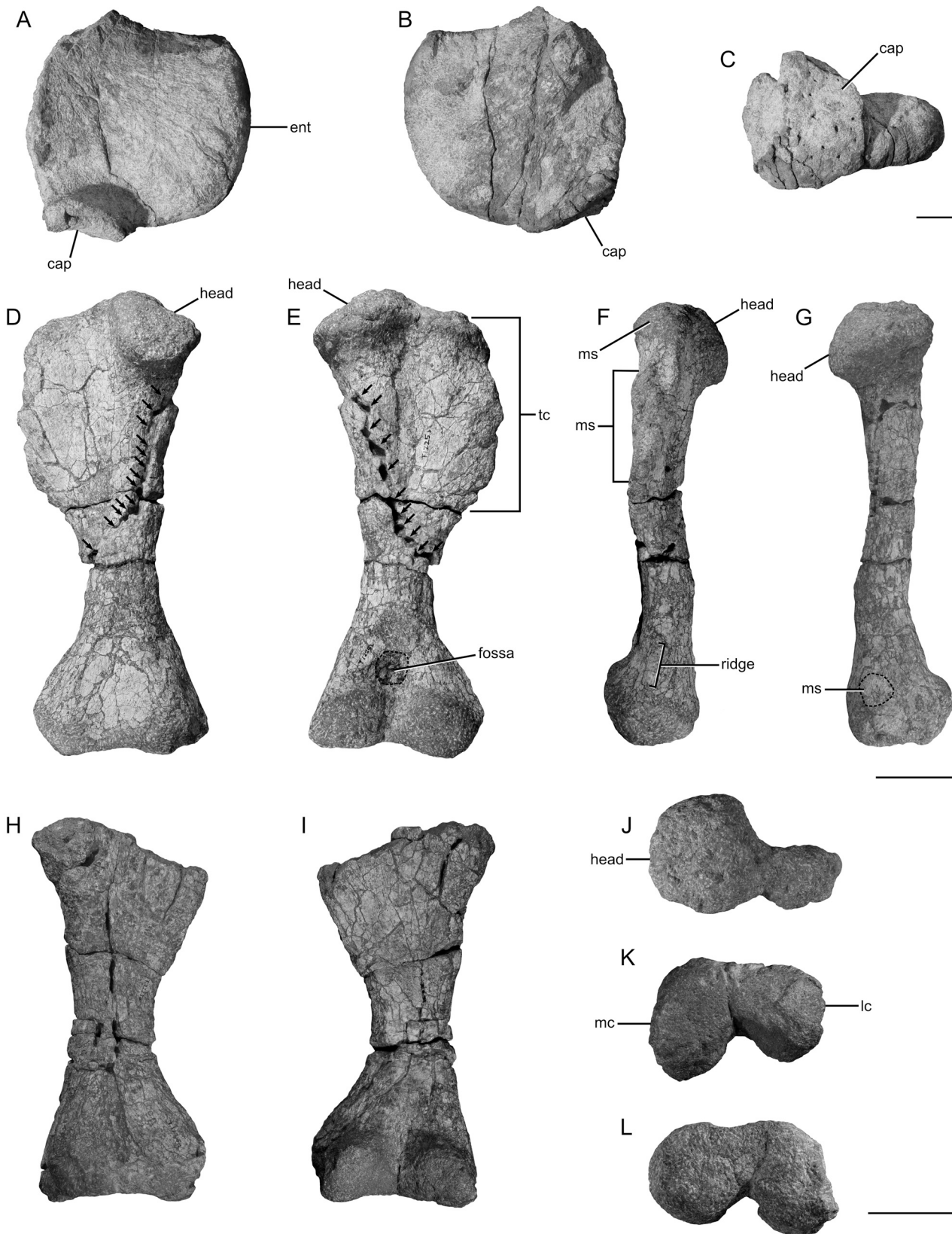


FIGURE 13. Humerus (NMT RB42) and femora (UMZC T1225) of *Sangusaurus parringtonii*. Left humerus in **A**, dorsal, **B**, ventral, and **C**, distal views. Right femur in **D**, anterior, **E**, posterior, **F**, lateral, and **G**, medial views. Arrows indicate bite marks that are the holotype of the ichnofossil *Mandaodonites coxi* Cruickshank, 1986b. Left femur in **H**, anterior and **I**, posterior views. **J**, right femur in proximal view. **K**, left and **L**, right femora in distal view. **Abbreviations:** **cap**, capitulum; **lc**, lateral condyle; **mc**, medial condyle; **ms**, muscle scar; **tc**, trochanteric crest. Scale bars equal 2 cm (**A–C**) and 6 cm (**D–L**). Upper scale bar applies to **A–C**, middle scale bar applies to **D–I**, and lower scale bar applies to **J–L**.

Perhaps the most distinctive feature of the preserved portion of the humerus is the capitulum. Typically in dicynodonts, the capitulum is saddle-shaped, with a small exposure on the dorsal surface of the distal humerus and a larger exposure on the ventral surface. In contrast, the capitulum of *S. parringtonii* is much flatter and faces almost exclusively distally, with no parts of the articular surface extending onto the dorsal or ventral surfaces of the humerus (Fig. 13A–C). On the dorsal surface, the capitulum is strongly set off from the rest of the distal end of the bone by a shallow groove and its own thickened, strongly flared edge. The ventral surface of the capitulum is more continuous with the rest of the bone, although it still is strongly flared, with a distinct edge demarcating the articular surface. The articular surface bears a number of prominent round pits, which indicates the likely presence of a thick cartilaginous cap in life.

A complete right femur and a left femur that is missing its proximal end (both UMZC T1225) were collected by Nowack in association with the holotype of *S. parringtonii* (Fig. 13D–L). The right femur has a series of tooth marks that extend from just below the femoral head to the mid-shaft region (most prominent on the posterior surface), which Cruickshank (1986b) described as the holotype of the ichnofossil *Mandaodonites coxi* (Fig. 13D, E). His description includes drawings of the anterior and posterior surfaces of the right femur, but he focused on the bite marks and did not describe the femora. Likewise, Cruickshank (1986a) noted that the holotypic skull was associated with postcranial material, but he did not specify what that material constituted. Our description focuses on the right femur; the left closely resembles it in all salient features. Both femora experienced extensive cracking and mild crushing during preservation, and the articular surfaces bear tool marks from preparation. Cruickshank's (1986b) description of the bite marks is quite detailed, and we will not consider them further here.

As is typical for most dicynodonts, the general morphology of the femur is much more consistent with an upright posture than is the case for the forelimb. The head of the femur is subcircular, convex anteroposteriorly, and flattened mediolaterally (Fig. 13D–G, J). This gives it a somewhat flattened appearance that resembles that figured for *Ischigualastia* by Cox (1965), instead of the more spherical femoral heads of taxa such as *Placerias*, *Parakannemeyeria dolichocephala*, or *Stahleckeria* (Huene, 1935; Camp and Welles, 1956; Sun, 1963; Kammerer et al., 2013; Kammerer et al., 2018). The head protrudes only slightly above the rest of the proximal surface of the femur, mostly as a result of the rest of the proximal end sloping ventrolaterally away from the head. It is offset on the anteroposterior axis of the bone such that it overhangs the anterior surface more strongly than the posterior surface. The articular surface of the head faces dorsomedially. Many authors reconstruct an attachment for *M. puboischiofemoralis internus* on the medial surface of the femur just distal to the femoral head (King, 1981a, 1981b; Li, 1983; DeFauw, 1986; Walter, 1986; Ray and Chinsamy, 2003; Morato 2006; Ray, 2006). A distinct muscle scar in this area is not apparent in UMZC T1225, but the bone has undergone extensive postmortem cracking in this area, potentially obscuring the presence of a scar. Lateral to the head, the proximal end of the femur narrows before widening again at the lateral corner. The proximal end of the insertion of *M. puboischiofemoralis externus* likely began near the waist of the proximal edge and extended distally onto the posterior surface of the femur (King, 1981a, 1981b, 1985; Walter, 1986; Ray and Chinsamy, 2003; Morato 2006, Ray, 2006). Li's (1983) and DeFauw's (1986) reconstructions of the insertion of this muscle differ from those of most other authors because they hypothesized that the attachment was limited to the posterior surface of the femur.

The trochanteric crest is prominent, parallels the long axis of the femur, and has a relatively straight lateral edge in anterior view (Fig. 13D–F). Two well-developed muscle scars are present

on the crest. The first of these occupies the lateral corner of the proximal end of the femur and it is oriented obliquely, such that its long axis trends from anterolateral to posteromedial. The anterior edge of the scar is nearly flush with the anterior surface of the diaphysis, but its posterior edge overhangs the posterior surface of the diaphysis. Like the humeral head, the surface of this scar bears many small tool marks from preparation. *M. ischiotrochantericus* and a portion of *M. iliofemoralis* are most commonly reconstructed as attaching in this area (King, 1981a, 1981b, 1985; Li, 1983; DeFauw, 1986; Walter, 1986; Ray and Chinsamy, 2003; Morato, 2006; Ray, 2006), although Morato (2006) also included an insertion for *M. caudifemoralis* on the equivalent of the posterior surface of this scar in *Dinodontosaurus*. Unfortunately, the tool marks covering much of this area make it impossible to differentiate distinct attachments for these muscles. The second muscle scar is located more distally on the trochanteric crest, and it is separated from the first by a shallow fossa in which the bone texture is smooth. The bone in this region has undergone some crushing, but the fossa seems to be a real feature even when this is taken into account. The second muscle scar has the form of a rugosity extending down the lateral surface of the trochanteric crest. It is weakly curved, trending from posterodorsal to anteroventral. The trochanteric crest of dicynodonts has been reconstructed as representing the insertion site of *M. iliofemoralis* (King, 1981a, 1981b, 1985; Li, 1983; DeFauw, 1986; Walter, 1986; Ray and Chinsamy, 2003; Morato, 2006; Ray, 2006), with most authors hypothesizing the differentiation of this muscle into two to three bodies. In addition to the possibility of part of *M. iliofemoralis* attaching to the more proximal scar, the fact that the more distal scar can be divided into a more rounded proximal portion and more ridge-like distal portion may reflect differentiation of the muscle as well.

The mid-shaft region of the diaphysis is narrow compared with the expanded proximal and distal ends of the femur and is oval in cross-section (Fig. 13D, E, H, I). The bone in this region of both femora has undergone extensive postmortem cracking, which obscures surface details. The femur shows a weak sigmoid curvature in lateral view, although this might be exaggerated slightly by crushing and breakage in the mid-shaft region.

The distal end of the femur is transversely expanded (Fig. 13D–I). In anterior view, the lateral condyle is more flared than the medial condyle, but overall the distal end is roughly symmetrical. The medial surface of the distal end is more or less flat, although there is a rounded, slightly raised muscle scar at the anterodistal corner of the surface. DeFauw (1986) proposed reconstructing the origin of *M. flexor digitorum communis* from the medial surface of the femur, although in a somewhat more posterior position than the location of this scar. King (1981a) proposed an attachment for the medial ligament to the tibia in a similar position in *Dicynodon huenei* (*D. trigocephalus* in that paper; see Kammerer et al., 2011), although she described the surface features of the bone as a rugose, striated band as opposed to the scar observed in NMT RB42. The lateral surface bears a weak, rounded ridge along its approximate midline. It arises near the level where the distal end starts to flare laterally, and it extends to the edge of the articular surface, curving slightly posterodistally. The ridge likely represents the origin of *M. extensor digitorum longus* (King, 1981a; DeFauw, 1986; Walter, 1986; Morato, 2006). The anterior surface of the distal end is relatively flat and lacks the smooth semilunar surface described in *Dicynodontoides* (King, 1985). A distinct fossa is present on the posterior surface between the articular condyles. It is suboval in shape, with the proximal end being slightly wider than the distal end. Similar structures in other dicynodonts are typically considered to represent the origin of *M. gastrocnemius* (King, 1981a, 1981b; DeFauw, 1986; Walter, 1986; Ray and Chinsamy, 2003;

Ray, 2006), usually with the assumption that it had not yet divided into two heads.

The articular surfaces of the lateral and medial condyles are contiguous, and they present the same surface texture and tool marks visible on the femoral head (Fig. 13K, L). The anterior edge of the articular surface is flush with the anterior surface of the femur, but the posterior portion of the articular surface encroaches on the posterior surface of the bone. In distal view, the lateral condyle is subhemispherical in shape. The medial condyle is less convex and anteroposteriorly longer, but mediolaterally narrower.

PHYLOGENETIC ANALYSIS

Methods

As noted above, *Sangusaurus* has been included in several previous phylogenetic analyses (Maisch, 2001; Surkov and Benton, 2004; Kammerer et al., 2011, 2013, 2015b; Castaninha et al., 2013; Angielczyk and Cox, 2015; Cox and Angielczyk, 2015; Angielczyk et al., 2016; Boos et al., 2016). The codings used in these analyses relied almost exclusively on the specimens of *S. parringtonii* housed at the UMZC, although a limited amount of data (primarily codings for the pelvis) from NMT RB42 were included in analyses based on the data set of Kammerer et al. (2011) (i.e., Castaninha et al., 2013; Kammerer et al., 2013, 2015b; Angielczyk and Cox, 2015; Cox and Angielczyk, 2015; Angielczyk et al., 2016; Boos et al., 2016). Our detailed redescription of *Sangusaurus*, especially considering new information available in NMT RB42, revealed some characters that were coded incorrectly in previous analyses, as well as a number of characters that could be coded for the first time. These new observations facilitate a reappraisal of the phylogenetic relationships of *Sangusaurus*, which is important considering the persistent disagreement found in the literature about the placement of the taxon within Kannemeyeriiformes. Because of the highly fragmentary nature of the only specimen of *S. edentatus*, we did not attempt to include that species in our analysis. Instead, our coding is specifically for *S. parringtonii* and incorporates observations from all known specimens of the species.

Our data set is based on that of Angielczyk and Kammerer (2018), which in turn is a modified version of the data set presented in Cox and Angielczyk (2015) and Angielczyk et al. (2016). Angielczyk and Kammerer (2018) modified and recoded several characters found in previous versions of their data set, and a complete description of those changes can be found in that paper. We generated a new coding for *S. parringtonii*, which is substantially more complete than in previous iterations of the data set (22% missing data for discrete-state characters and 39% missing data for continuous characters for *S. parringtonii* in the current data set compared with 41% and 67%, respectively, in the data set of Cox and Angielczyk, 2015). We also added a small number of new measurements to the data set underlying the continuous character codings and removed two duplicate measurements, which caused minor changes to the codings for *Cistecephalus*, *Colobodectes*, *Dicynodon huenei*, *Dicynodontoides*, *Diictodon*, *Lystrosaurus curvatus*, *Odontocyclops*, *Oudenodon*, *Pristerodon*, *Rhinodicynodon*, *Stahleckeria*, *Tetragonias*, and *Tropidostoma*. A complete list of characters, a copy of the data matrix, and data used for coding the continuous characters are available in Supplemental Data.

The final data set included 100 operational taxonomic units (OTUs) and 194 characters. One hundred seventy-one of these characters were discrete binary or multistate characters. Of these, seven characters were ordered (see character list in Supplemental Data) and 164 were treated as unordered. All discrete-state characters were weighted equally. The remaining 23 characters were continuous. We treated the continuous characters as additive using the method of Goloboff et al. (2006) and

used mean values as the codings for the OTUs except in cases when only a single measurement was available for an OTU. Unknown and inapplicable discrete-state and continuous characters were coded as “?” (Strong and Lipscomb, 2000).

We analyzed the data set using TNT 1.1 (October 2010 version) (Goloboff et al., 2008), and two search strategies were employed. The first search used the new technology methods of TNT. We employed a driven search with the initial search level set at 65, which was checked every three hits. The initial number of addition sequence replicates was 500, and the search was required to find the trees of shortest length 20 times. The analysis started with default settings for sectorial searching, tree drifting, parsimony ratchet, and tree fusing. In the second analysis, we used the traditional search method of tree bisection reconnection (TBR) branch swapping with 10,000 replicates and 10 trees held per replicate. *Biarmosuchus* served as the outgroup to root the most parsimonious cladograms from both analyses.

We utilized symmetric resampling (Goloboff et al., 2003), jackknife analysis (Mueller and Ayala, 1982; Farris et al., 1996), and decay analysis (Bremer, 1988, 1994) to measure support for the most parsimonious cladograms. The symmetric resampling results are based on 10,000 replicates; each replicate included a new technology search with default settings for tree drifting, parsimony ratchet, and tree fusing and 10 random addition sequence replicates. Absolute frequency values were used to summarize the results (Kopuchian and Ramírez, 2010). Recent research (e.g., Kopuchian and Ramírez, 2010; Simmons and Freudenstein, 2011) suggests that jackknife-based resampling approaches produce fewer spurious groups than bootstrap-based methods, so we also conducted a jackknife analysis as an additional measure of clade support. We utilized 10,000 resampling replicates, with a 36% probability of character removal, and the same search parameters as for the symmetric resampling analysis. The decay analysis results are based on a sample of 954,314 suboptimal cladograms with lengths up to six steps longer than the most parsimonious cladograms. Following the recommendations of Goloboff et al. (2008), the suboptimal trees were generated through a series of traditional searches in which the length of suboptimal cladograms retained, as well as the number of suboptimal cladograms, were incrementally increased. The resulting cladograms were filtered to remove duplicates before the decay analysis, so the 954,314 cladograms in the sample are all unique. Finally, a 50% majority-rule consensus of the 954,314 cladograms was calculated to gain insight into how frequently the clades recovered in the most parsimonious cladograms are represented in suboptimal trees.

As noted above, hypotheses regarding the relationships of *Sangusaurus* have varied, although analyses based on the data matrix of Kammerer et al. (2011) have consistently recovered it as a stahleckeriid. To compare the results of our phylogenetic analysis with prior hypotheses, we conducted a series of seven constrained analyses (see Supplemental Data for the topologies of the constraint trees). Two of the constraint trees are based on the cladograms resulting from the computerized cladistic analyses of Maisch (2001) and Surkov and Benton (2004). The third and fourth constraint trees are based on the classifications and hand-drawn cladograms of King (1988) and Cox (1998). The final three constraint trees are based on the non-cladistic classifications of Cox (1965; as modified by Cox [1969], with the inclusion of *Zambiasaurus* in Stahleckeriidae and *Sangusaurus* in Kannemeyeriidae), Keyser and Cruickshank (1979), and Cox and Li (1983). Together, the constrained topologies of these analyses cover both specific hypotheses of relationships for *Sangusaurus* that have been put forward in the past and provide insight into how the taxon might have fit into previous classifications in which it was considered to be incertae sedis (i.e., Cox and Li, 1983; King, 1988). We ran the constrained tree searches using the same starting parameters as the primary new technology

search described above. For the Cox (1965/1969), Keyser and Cruickshank (1979), Cox and Li (1983), King (1988), and Cox (1998) analyses, taxa that were considered incertae sedis or that were not included as distinct OTUs were treated as ‘floaters’ (*Angonisaurus*, *Dolichuranus*, *Eubrachiosaurus*, *Jachaleria*, *Kannemeyeria lophorhinus*, *Moghreberia*, *Rabidosaurus*, *Rechnisaurus*, *Rhadiodromus*, *Rhinodictynodon*, *Shaanbeikannemeyeria*, *Uralokannemeyeria*, *Vinceria*, *Wadiasaurus*, and *Xiyukannemeyeria* for Cox, 1965/1969; *Angonisaurus*, *Eubrachiosaurus*, *Moghreberia*, and *Xiyukannemeyeria* for Keyser and Crucikshank, 1979; *Rhadiodromus*, *Rechnisaurus*, *Sangusaurus*, and *Xiyukannemeyeria* for Cox and Li, 1983; *Eubrachiosaurus*, *Jachaleria*, *Rechnisaurus*, *Sangusaurus*, and *Xiyukannemeyeria* for King, 1988; *Dolichuranus*, *Eubrachiosaurus*, *Moghreberia*, *Rhadiodromus*, *Shaanbeikannemeyeria*, and *Xiyukannemeyeria* for Cox, 1998).

Results

A single most parsimonious cladogram was recovered by both the new technology and traditional searches (length = 1105.904 steps, consistency index [CI] = 0.247, retention index [RI] = 0.719). Topological results are shown in Figure 14. The topology shows a mixture of similarities to and differences from other recent analyses of anomodont phylogeny. For example, among non-dicynodont anomodonts, *Venyukovioidea* occupies a more rootward position and *Anomocephaloidea* a more derived position than in the analyses of Angielczyk et al. (2016) and Boos et al. (2016). The topology for non-bidental dicynodonts is more similar to that of Angielczyk et al. (2016) and Boos et al. (2016) than Cox and Angielczyk (2015) in the separation of ptyaecephalids and emydopoids, and it particularly resembles the tree of Boos et al. (2016) in its paraphyly of *Cryptodontia*, although the arrangement of taxa within this grade is somewhat different. The most important differences in the context of the current study involve the topology of Kannemeyeriiformes. Prior analyses with various versions of the Kammerer et al. (2011) data set recovered a rough three-fold division of Kannemeyeriiformes, with a monophyletic *Shansiodontidae* being the sister group of the rest of the clade and a paraphyletic assemblage of ‘kannemeyeriids’ on the stem leading to *Stahleckeriidae* (e.g., Castanhinha et al., 2013; Kammerer et al., 2013, 2015b; Cox and Angielczyk, 2015; Angielczyk et al., 2016). In the present analysis, the ‘core shansiodontids’ *Rhinodictynodon*, *Shansiodon*, *Vinceria*, and *Tetragonias* form a grade at the base of Kannemeyeriiformes, with the rest of the group divided into kannemeyeriid and stahleckeriid subclades.

Within this framework, *Sangusaurus parringtonii* is reconstructed as a stahleckeriid, specifically the sister taxon of *Stahleckeria* itself. Two discrete-state synapomorphies support the sister-group relationship between *Sangusaurus* and *Stahleckeria*: postorbitals extend the entire length of the temporal bar (discrete-state character 52, state 0); and intertuberal ridge present (discrete-state character 103, state 1). It is also supported by the relative position of the pineal foramen on the skull roof (continuous character 6), although missing data for this character within Stahleckeriidae makes its value somewhat uncertain. The clade Stahleckeriidae (sensu Kammerer et al., 2013) is supported by five discrete-state synapomorphies: ventral edge of the caniniform process or dorsal edge of the erupted tusk anterior to the anterior orbital margin (discrete-state character 32, state 0); interparietal makes a large contribution to the intertemporal skull roof (discrete-state character 57, state 2); pronounced pila antotica absent and trigeminal notch is a horizontal hollow in the anterior edge of the periotic (discrete-state character 95, state 1); angular with anterolateral trough for the dentary present (discrete-state character 134, state 1); and anterior edge of

scapula extended laterally to form a strong crest (discrete-state character 145, state 1). Missing data for characters 95 and 134 among the stahleckeriids makes the value of these synapomorphies uncertain. The larger clade *Stahleckeriidae* + *Angonisaurus* + *Dinodontosaurus* is supported by three discrete-state synapomorphies: ventral surface of the median pterygoid plate smooth and flat (discrete-state character 92, state 1); number of sacral vertebrae six or more (discrete-state character 142, state 3); and insertion of *M. latissimus dorsi* at rugose tuberosity on the posteroventral surface of humerus (discrete-state character 152, state 0). The value of character 92 as a synapomorphy is somewhat uncertain due to missing data and variation within the clade, and reversals occur within some stahleckeriid species for the other two characters. Three continuous characters also support this clade: length of the interpterygoid vacuity relative to basal length of skull (continuous character 10); ratio of minimum width of the scapula to maximum width of the dorsal end of the scapula (continuous character 17); and ratio of anterior iliac process length to acetabulum diameter (continuous character 21). Missing data and variation within the clade make the true value of these characters as diagnostic features uncertain, however.

The results of the symmetric resampling, jackknife, and decay analyses indicate that the most parsimonious cladogram is weakly supported (Fig. 14; Supplemental Data), a widespread problem in phylogenetic analyses of anomodonts (e.g., see Cox and Angielczyk, 2015, and Angielczyk et al., 2016, for recent examples). Regarding the relationships of *Sangusaurus*, it is important to note that its sister-group relationship with *Stahleckeria*, the monophyly of *Stahleckeriidae*, and the monophyly of the clade including *Stahleckeriidae*, *Dinodontosaurus*, and *Angonisaurus* all receive poor branch support even compared with other nodes in the current phylogeny. Nevertheless, the most parsimonious cladograms from the constrained analyses ranged from 12.106 to 31.882 steps longer than the preferred cladogram from the primary analysis (see Supplemental Data for the cladograms resulting from the constrained analyses), indicating that the alternative hypotheses of kannemeyeriiform relationships fit the current data set comparatively poorly. It is also telling that in the constrained analyses in which the position of *Sangusaurus* was allowed to float (i.e., the constrained analyses based on Cox and Li, 1983, and King, 1988), it was recovered within clades essentially equivalent to the Stahleckeriidae of the current analysis.

FUNCTIONAL ANALYSIS OF THE FEEDING SYSTEM OF *SANGUSAURUS PARRINGTONII*

Methods

The skull and mandible of *Sangusaurus* are highly distinctive (Fig. 15), and many of their features (large, deep snout; short temporal bar; tall, broad occiput; posteroventrally sloping articular surface of the articular) have implications for the positioning of the jaw adductor musculature and the range of motion of the mandible. To investigate the function of the feeding system, we conducted a lever mechanics analysis and calculated the mechanical advantage of *S. parringtonii* and three other dicynodonts that have more typical skull morphologies.

Because there is no complete skull with associated mandible known for *S. parringtonii*, our analysis is based on information from three specimens. We used NMT RB42 for the skull because it is the most complete and undistorted skull that is known. The mandible we used is a composite reconstruction based on UMZC T1226 and UMZC T1340, which we scaled to the appropriate size for NMT RB42. Neither of these mandibles is complete, but together they provide a good overview of the jaw morphology of *S. parringtonii*. Our first comparative specimen is

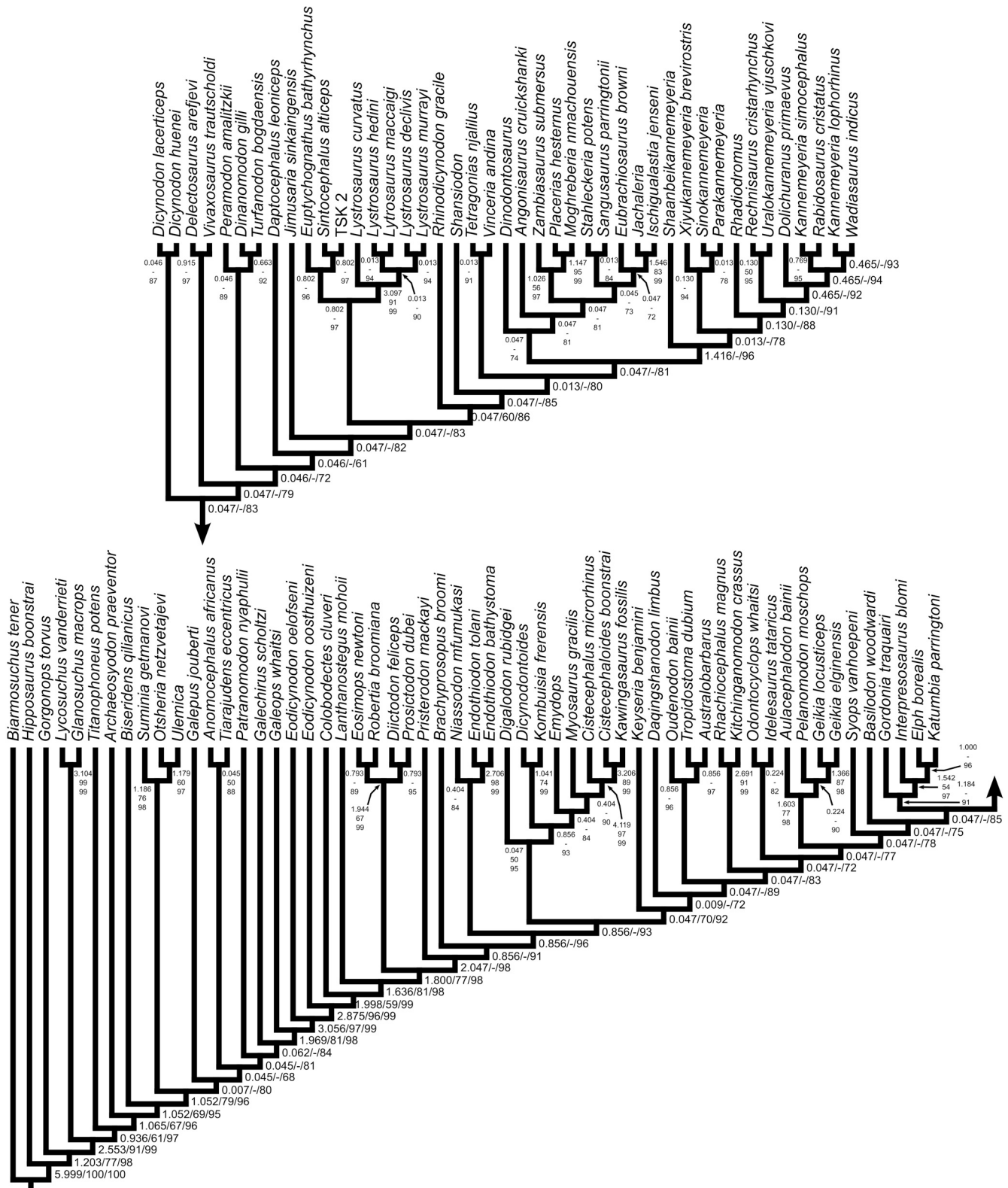


FIGURE 14. Most parsimonious cladogram from the phylogenetic analysis. Scores: 1105.904 steps, consistency index = 0.247, retention index = 0.719. Numbers at nodes represent decay index (left/top), symmetric resampling (middle), and the percentage of the 954,314 suboptimal trees in which the node is resolved (right/bottom). Results of the jackknife analysis are similar to those of the symmetric resampling analysis and are presented in Supplementary Data.

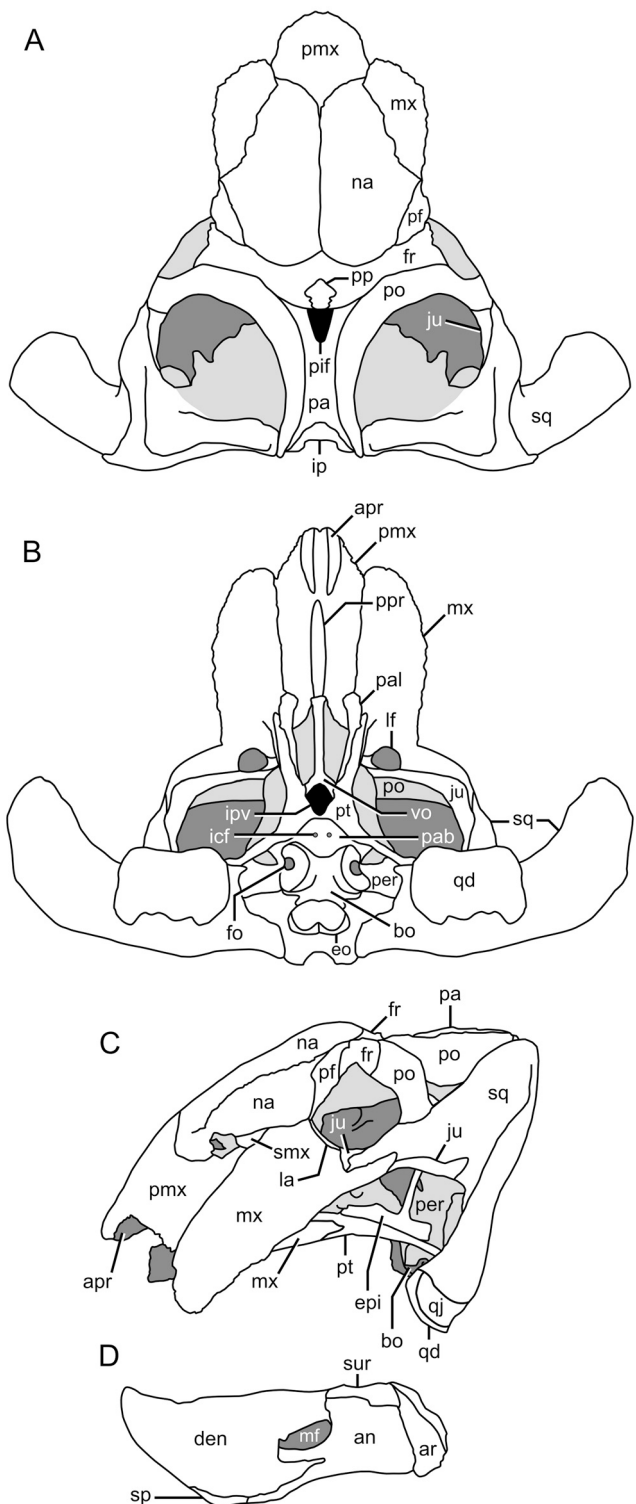


FIGURE 15. Reconstructions of the skull and mandible of *Sangusaurus parringtonii*. Skull in **A**, dorsal; **B**, ventral, and **C**, left lateral views. Mandible in **D**, left lateral view. **Abbreviations:** **an**, angular; **apr**, anterior palatal ridge; **ar**, articular; **bo**, basioccipital; **den**, dentary; **eo**, exoccipital; **epi**, epipterygoid; **fo**, fenestra ovalis; **fr**, frontal; **icf**, internal carotid foramen; **ip**, interparietal; **ipv**, interpterygoid vacuity; **ju**, jugal; **la**, lacrimal; **lf**, labial fossa; **mf**, mandibular fenestra; **mx**, maxilla; **na**, nasal; **pa**, parietal; **pab**, parabasisphenoid; **pal**, palatine; **per**, periotic; **pf**, prefrontal; **pif**, pineal foramen; **pmx**, premaxilla; **po**, postorbital; **pp**, preparietal; **ppr**, posterior palatal ridge; **pt**, pterygoid; **qd**, quadrate; **qj**, quadratojugal; **smx**, septomaxilla; **sp**, splenial; **sq**, squamosal; **sur** surangular; **vo**, vomer.

BP/1/3927, a specimen of *Dapocephalus leoniceps* that consists of a very well-preserved skull and mandible that was described in detail by Ewer (1961). We chose to use *D. leoniceps* in the analysis because it is a large, basal dicynodontoid (e.g., Kammerer et al., 2011; Castanhinha et al., 2013; Cox and Angielczyk, 2015) and as such is a reasonable model of the ancestral morphotype from which kannemeyeriforms evolved. The second comparative specimen is SAM-PK-3017. This specimen is the holotype of *Kannemeyeria erithrea* Haughton, 1915, which is now recognized as a junior synonym of *K. simocephalus* (Cruickshank, 1970; King, 1988; Renaut, 2000), and consists of a nearly undeformed skull and mandible. *Kannemeyeria* is a good example of a generalized kannemeyeriform, and it shows some modifications to the skull and mandible that suggest that its feeding system emphasized a more orthogonal movement of the jaw than is the case for most Permian dicynodonts (Renaut, 2000, 2001). The third comparative specimen is GPIT/RE/7107, an articulated skull that is the lectotype of *Stahleckeria potens* (see Maisch, 2001), which is inferred to be the sister taxon of *Sangusaurus*. *Stahleckeria* shows some similarities to *Sangusaurus* in its overall skull morphology, such as a proportionally long snout and short temporal region, a broad occipital plate, and relatively vertical squamosal fossa, although its morphology is not taken to the extremes seen in *Sangusaurus* (e.g., the snout is not telescoped and the lateral margin of the squamosal does not curve anteriorly as strongly). Specimen GPIT/RE/7107 was mounted with a mandible that includes a relatively complete dentary, but the postdental bones are mostly reconstructed. The reconstruction is closely based on the more complete mandible figured by Huene (1935) (part of the mounted skeleton GPIT/RE/7106), and the proportions of the mandible seem to be approximately correct for the skull, so we used it in our functional analysis of *Stahleckeria*.

Our quantitative analysis focused on the lines of action and lever arm mechanics, as has been performed for various fossil vertebrates (e.g., Ostrom, 1964; Crompton and Hotton, 1967; DeMar and Barghusen, 1972; Tanoue et al., 2009; Sakamoto, 2010; Mallon and Anderson, 2015; Nabavizadeh, 2016). We performed these analyses on two muscles: *M. adductor mandibulae externus medialis* (mAMEM) and *M. adductor mandibulae externus lateralis* (mAMEL). Using lateral views of the skull and mandible that had been scaled to the same size and superimposed such that the jaw was positioned in a closed-mouth orientation, we mapped the origins and insertions of mAMEM and mAMEL with Photoshop, based on muscle scarring and attachment sites that had been proposed in the literature (Watson, 1948; Crompton and Hotton, 1967; Cluver, 1975; Barghusen, 1976; King, 1981a; King et al., 1989; Ray, 2000; Renaut, 2001; Maisch, 2003). We then calculated the centroid of the origins and insertions of both mAMEM and mAMEL using ImageJ, which were added to the images with the mapped attachment areas. We quantified muscular lines of action as the angle of the connection between the origin and insertion centroids of each muscle. Following that step, we used lever arm mechanical advantage methodologies to analyze the mechanical advantage (MA) of mAMEM and mAMEL, as well as the resultant angle of both muscle vectors combined. The distance from the jaw joint to the perpendicular intersection of the muscle vector analyzed measures the input lever, or moment arm. The distance from the jaw joint to the bite point (i.e., distal tip of the beak) measures the output lever. Because there are no data for physiological cross-sectional area of the muscles in the fossil record, we simplified the muscle body size to a unit of 1 for both muscles, creating a simple input/output lever equation to find MA, or relative bite force, across the four species.

In addition to considering the function of the jaw muscles, we also calculated the occipital indices of Surkov and Benton (2008). These indices reflect the relative effectiveness of the

lateral and dorsal portions of the neck musculature and have been inferred to provide insight into the preferred plane of head movement and feeding level of dicynodont species. Only NMT RB42 is complete enough for the required measurements to be taken, and our analysis focuses on this specimen. We were able to measure skull height (H) and skull length along the palatal midline (L_{cr}) directly from the specimen. We estimated width across the squamosals (W_{sq}) in two steps. First, we rearticulated the left squamosal and measured the distance from its lateral edge to the midpoint of the occipital condyle. Then we multiplied the resulting value by 2 to obtain the total width of the occiput.

Results

Our quantitative results show that *Sangusaurus parringtonii* possesses lower adductor angles ($mAMEM = 56.31^\circ$; $mAMEL = 43.37^\circ$) (Fig. 16) than its sister species *Stahleckeria potens* ($mAMEM = 72.32^\circ$; $mAMEL = 47.90^\circ$), and higher adductor angles than *Kannemeyeria simocephalus* ($mAMEM = 51.48^\circ$; $mAMEL = 33.45^\circ$). *Dapocephalus leoniceps* possesses a comparatively higher $mAMEM$ angle ($= 68.32^\circ$) and a lower $mAMEL$ angle ($= 41.38^\circ$).

In *Sangusaurus parringtonii*, the MA of both $mAMEM$ ($= 0.286$) and $mAMEL$ ($= 0.351$) (Fig. 16) were mid-range compared with the lower values in *Kannemeyeria simocephalus* ($mAMEM = 0.223$; $mAMEL = 0.218$) and higher values in *Dapocephalus leoniceps* ($mAMEM = 0.369$; $mAMEL = 0.368$). *Stahleckeria potens* possesses a slightly lower $mAMEM$ MA ($= 0.270$) and a substantially lower $mAMEL$ MA ($= 0.230$) compared with *Sangusaurus parringtonii*. However, the values for these two taxa are more similar to each other than either taxon is to *Kannemeyeria* or *Dapocephalus*.

The skull height (H) of NMT RB42 is 205.7 mm, and its length along the palatal midline (L_{cr}) is 334.0 mm. We estimated the width across the squamosals (W_{sq}) as 512.0 mm. Based on these values, the dorsal index (I_{dor}) is 0.616 and the lateral index (I_{lat}) is 0.767. These values result in an occipital index (OI) of 0.151.

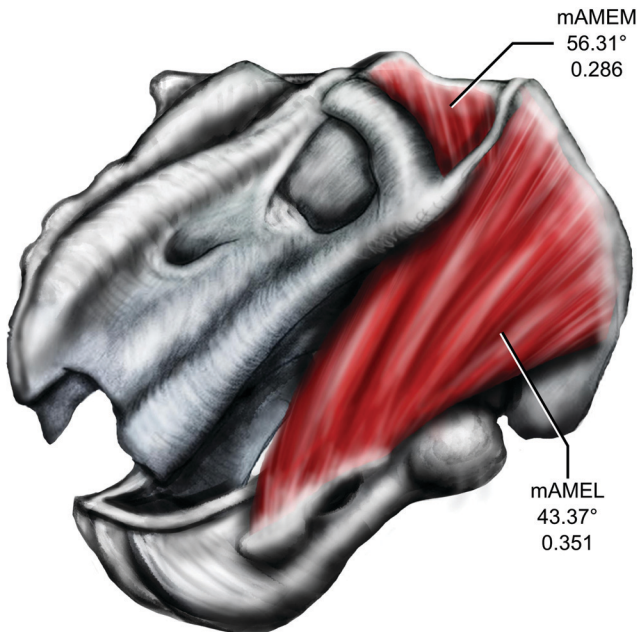


FIGURE 16. Reconstruction of the two major jaw adductor muscles of *Sangusaurus parringtonii*. Upper number is the adductor angle for the muscle in question; lower number is the mechanical advantage (MA). Abbreviations: **mAMEL**, M. adductor mandibulae externus lateralis; **mAMEM**, M. adductor mandibulae externus medialis.

DISCUSSION

Taxonomy of *Sangusaurus*

Sangusaurus has a comparatively simple taxonomic history for a dicynodont. Only two species have been described, and there have not been revisions of those species or attempts to synonymize the genus with other kannemeyeriform taxa. However, three taxonomic questions require attention: (1) is there adequate evidence to refer the species *parringtonii* Cruickshank, 1986a, to the genus *Sangusaurus*; (2) do *S. edentatus* and *S. parringtonii* represent distinct species; and (3) what is the significance of variation observed within the known sample of *S. parringtonii*?

The only known specimen of *S. edentatus* is very fragmentary, and it does not preserve the portions of the skull and mandible that include the most striking diagnostic characters in the specimens of *S. parringtonii*. Taken individually, none of the characters that unite *S. edentatus* and *S. parringtonii* is unique to the genus *Sangusaurus*. However, the combination of characters shared between *S. edentatus* and *S. parringtonii* seems to be unique among kannemeyeriforms, arguing that there is a sound basis for uniting the species within the same genus. Perhaps the most compelling diagnostic character for *Sangusaurus* is the postpineal boss (Figs. 3H, 6A, B). A somewhat similar boss was reported in *Rechnisaurus* (Roy-Chowdhury, 1970; Bandyopadhyay, 1989), but there the boss is wider than in either species of *Sangusaurus*, taking up nearly the entire width of the dorsal surface of the intertemporal bar (flat areas of the parietals flank the boss in *Sangusaurus*), and it arises at the posterior edge of the pineal foramen (the boss in *Sangusaurus* arises a short distance behind the foramen). Other kannemeyeriforms lack a comparable boss. Based on these observations, we consider it most conservative to retain *S. edentatus* and *S. parringtonii* in the genus *Sangusaurus*, but we acknowledge that the support for this arrangement ideally should be stronger.

Given the close proximity of the Ruhuhu Basin and the northern Luangwa Basin now and in the Triassic, it is surprising to have a different species of a single large dicynodont genus in each basin. This is particularly the case considering the more cosmopolitan distribution of roughly contemporaneous southern Gondwanan dicynodonts such as *Stahleckeria potens* (Huene, 1935; Abdala et al., 2013), *Kannemeyeria simocephalus* (Cruickshank, 1965, 1970; Renaut, 2000), *K. lophorhinus* (Crozier, 1970; Keyser, 1973; Keyser and Cruickshank, 1979; Renaut, 2000; Renaut et al., 2003), and potentially *Angonisaurus cruickshanki* (Cox and Li, 1983; Hancox et al., 2013; Sidor et al., 2014) and *Dolichuranus primaevus* (Keyser, 1973; Kammerer et al., 2018; Smith et al., 2018). The small sample size available for *Sangusaurus* (a total of four specimens) makes an assessment of interspecific variation challenging. Nevertheless, there do appear to be some consistent differences between the Tanzanian and Zambian specimens. The most obvious of these differences is the very strong development of the lateral caniniform buttress in all three Tanzanian specimens (Figs. 6, 7A, B, 8A, B) and the absence of this feature in the Zambian specimen (Fig. 3E–G). The parietal portion of the intertemporal bar also is proportionally narrower in the two Tanzanian specimens that preserve it (Fig. 7A, B, 8C), despite the specimens being deformed differently (dorsalventral compression in UMZC T1226, lateral compression/shear in NMT RB42), and the shape of the parietal-interparietal suture varies between the Tanzanian and Zambian specimens (Figs. 3H, 7A, B, 8C). Some of the unusual characters of *S. parringtonii*, such as the extremely prominent crest on the snout and telescoping of the skull, also may be autapomorphies of the species, but the holotype of *S. edentatus* is not preserved in a manner that allows these characters to be assessed. Even though the number of comparisons that can be made between the Tanzanian and Zambian specimens is limited, we think it is

justified to retain both *S. edentatus* and *S. parringtonii* as distinct species at this time because the specimens from each basin are diagnosably different.

It is important to reiterate that both of these areas of uncertainty stem from the very incomplete nature of the holotype of *S. edentatus*. The available specimens of *S. parringtonii* show clearly that it is a unique morphotype among dicynodonts (Figs. 1, 15), and there is no reason to doubt its validity. It may be possible to extend aspects of this distinctive morphology to the genus *Sangusaurus* as a whole, or to show that *S. parringtonii* actually is a synonym of *S. edentatus*, or even that *S. edentatus* Cox, 1969, and *S. parringtonii* Cruickshank, 1986a, are not closely related and could be assigned to different genera. The key to answering these questions will be the discovery of better-preserved material of *S. edentatus* in Zambia that can be more fully compared with the specimens of *S. parringtonii*.

Finally, despite the fact that all three skulls of *S. parringtonii* are close to the same size and apparently represent adult individuals, some differences among the specimens are apparent. When UMZC T1226 and NMT RB42 are compared, for example, the former specimen has a less prominent nasal crest, narrower exposure of the parietals on the dorsal surface of the intertemporal bar, and it lacks a postpineal boss (Figs. 6A, B, 7A, B, 8A, C). Likewise, the ventral margin of the mandibular ramus has a more gently curving profile in UMZC T1226 than in UMZC T1340, which has a more distinct ‘chin’ (Fig. 10A, C). Most of these differences concern ornamental features, and although some might have been affected by preservation (e.g., the dorsal surface of the snout is more poorly preserved in UMZC T1226 than NMT RB42), others almost certainly are real (e.g., the dentaries of UMZC T1226 and UMZC T1340 have well-preserved ventral margins). Intraspecific variation in skull ornamentation in dicynodonts previously has been hypothesized to stem from sexual differences (e.g., Tollman et al., 1980; Sullivan et al., 2003; Kammerer et al., 2015a), so it is tempting to speculate that it may be indicative of sexual dimorphism in *S. parringtonii* as well. Given our experience collecting dicynodonts in the Manda Beds, and working with museum specimens from the unit, we are uncertain whether there will ever be enough material of *S. parringtonii* to quantitatively test whether the species was sexually dimorphic. The discovery of even a small number of additional specimens might be enough to test whether some of the patterns of variation we observed in the known skulls are consistent (e.g., whether a less prominent snout ridge is always associated with the absence of a postpineal boss and/or a ‘chin’ on the mandibular ramus), though, so it is important to keep this possibility in mind should more individuals come to light.

Phylogenetic Relationships of *Sangusaurus*

The position of *Sangusaurus* within the classification and phylogeny of kannemeyeriiform dicynodonts has remained poorly constrained, largely on account of the highly incomplete nature of the holotype of *S. edentatus* and the very limited amount of information available in the literature about *S. parringtonii*. Since the analysis of Kammerer et al. (2011), all phylogenetic analyses that included *Sangusaurus* have been permutations of that data set. Those analyses have been consistent in placing *Sangusaurus* within Stahleckeriidae, although its exact position within the clade is somewhat variable. The codings for *Sangusaurus* in the various versions of the Kammerer et al. (2011) data set were based nearly entirely on observations of UMZC T1226 and UMZC T1340, although pelvis characters were coded based on NMT RB42. The current analysis expands upon this work by including a completely revised coding based on all available material for *S. parringtonii* (NMT RB42, UMZC T1225, UMZC T1226, and UMZC T1340), including parts of these specimens

that were not considered previously. The results of the analysis including this new coding corroborate the hypothesis that *Sangusaurus* is a stahleckeriid and suggest that it is the sister taxon of *Stahleckeria*. Branch support for both of these results is weak (Fig. 14), but five discrete-state synapomorphies provide evidence of the former relationship and two support the latter (see above). This topology also is notably more parsimonious in the context of the current data set than the alternative placements of *Sangusaurus* that we examined. The stahleckeriid status of *Sangusaurus* echoes Cooper’s (1980) placement of the genus in that family (based primarily on its lack of tusks), but it differs from most other papers that have attempted to address its relationships. Therefore, some consideration of the data supporting the alternative hypotheses is necessary.

Cox (1969) was the first to discuss the relationships of *Sangusaurus*, and he did this in the context of his broader work on the morphology, taxonomy, and phylogeny of Triassic dicynodonts (Cox, 1965). The division of kannemeyeriiforms into two subgroups, the Stahleckeriidae and Kannemeyeriidae, in Cox (1965) primarily was based on the idea that kannemeyeriids had relatively narrow snouts, longer temporal openings, posterodorsally angled intertemporal bars, and relatively tall occiputs, whereas stahleckeriids had wider snouts, shorter temporal openings, and wider occiputs. In this framework, Cox (1969) concluded that *S. edentatus* was a kannemeyeriid because the snout seemed relatively narrow and the anteroventral slope of the occipital surface of the interparietal led him to believe that the intertemporal bar was angled posterodorsally. He also noted that *S. edentatus* appeared to have a median ridge on the snout, like many other kannemeyeriids in his classification, and that the structure of the intertemporal bar was similar to *Ischigualastia*, which he also considered a kannemeyeriid. In the time since Cox’s (1969) paper, the importance and interpretation of many of these characters have been challenged. For example, older reports tended to exaggerate the width of the snout in *Stahleckeria*, a midline ridge on the snout is present in *Stahleckeria*, and the structure of the temporal bar of *Ischigualastia* (particularly the large contribution of the interparietal to the skull roof) has been recognized as being more similar to that of *Stahleckeria* than to those of taxa such as *Kannemeyeria* (e.g., Keyser and Cruickshank, 1979; Maisch, 2001). Specimens of *Sangusaurus parringtonii* also reveal new information about the morphology of *Sangusaurus* that likely would have affected Cox’s (1969) interpretation of the taxon’s relationships. Specifically, the occiput is very wide, similar to *Stahleckeria*, and the anterior slope of the occipital portion of the interparietal reflects the fact that the posterior end of the intertemporal bar extends posteriorly past the level of the occipital plate, not posterodorsal angulation of the intertemporal bar. Despite these problems, most subsequent treatments of *Sangusaurus* persisted in assuming a close relationship between *Sangusaurus* and the kannemeyeriids (*sensu* Cox, 1965), usually with little discussion of the characters supporting this assignment (Roy-Chowdhury, 1970; Keyser and Cruickshank, 1979; Keyser and Brink in Brink, 1982; Cox, 1991, 1998).

In his description of *Sangusaurus parringtonii*, Cruickshank (1986a) also posited that *Sangusaurus* was a kannemeyeriid, and his reasoning was based on similarities (presence of postpineal boss, groove on the dorsal surface of the intertemporal bar, close approach or contact of the reflected lamina of the angular and the lateral surface of the articular) to the taxon he referred to as *Kannemeyeria cristarhynchus*. This is problematic because Cruickshank’s (1986a) concept of *K. cristarhynchus* has since been shown to be a chimera consisting of material belonging to *Rechnisaurus cristarhynchus* from India and *K. lophorhinus* from southern Africa (Bandyopadhyay, 1989; Renaut, 2000; Renaut et al., 2003). *Rechnisaurus* does possess a postpineal boss, but its morphology differs from that of *Sangusaurus* (see above). Furthermore, if the cranial anatomy of *S. parringtonii* is typical of

the genus as a whole, a number of other features differentiate it from *Rechnisaurus*, including a different morphology of the snout ridge, presence of a boss anterior to the pineal foramen, telescoped skull, and more horizontal intertemporal bar. The reflected lamina of the angular does closely approach the articular in *K. lophorhinus* (a mandible is not known in *Rechnisaurus*), but this character state also is present in stahleckeriids such as *Stahleckeria* (Huene, 1935) and *Ischigualastia* (Keyser, 1974). Similarly, the skull of *Sangusaurus* minimally differs from that of *K. lophorhinus* in the presence of a postpineal boss and the larger contribution of the interparietal to the dorsal surface of the skull roof, and many other characters would differentiate the taxa if the morphology of *S. parringtonii* is representative of the genus as whole. Because of these issues, we do not find Cruickshank's (1986a) argument for the kannemeyeriid status of *Sangusaurus* to be convincing.

Maisch (2001) presented the first computerized cladistic analysis of kannemeyeriiform phylogeny, and his topology differed in important ways from most previous treatments of the group. *Sangusaurus* was recovered as the sister taxon of *Rechnisaurus* within a clade (Dinodontosauridae) consisting of a mixture of taxa from Cox's (1965) Kannemeyeriidae and Stahleckeriidae, as well as taxa that had not yet been described at the time of Cox's paper. Important in the context of previous classifications, *Kannemeyeria*, *Stahleckeria*, and *Ischigualastia* all fell in clades outside of Dinodontosauridae. The characters supporting Dinodontosauridae in Maisch's (2001) analysis include short postorbital skull length, temporal fenestrae less than one-third the length of the skull, snout longer than the postorbital portion of the skull, caniniform process large, and occipital width equal to or greater than the length of the skull. Characters supporting a close relationship with *Rechnisaurus* (i.e., Rechnisaurinae of Maisch, 2001) include strongly developed snout ridge and wide exposure of the caniniform processes lateral to the skull roof in dorsal view. Although we agree with many of the basic observations incorporated into Maisch's (2001) data matrix, we have greater confidence in the results of our analysis for four reasons. First, several of the characters listed above have similar or identical counterparts in our matrix, but our data matrix also incorporates a large number of additional characters not considered by Maisch (2001), including some that are recovered as synapomorphies of Stahleckeriidae, including *Sangusaurus* (e.g., tip of caniniform process anterior to anterior orbital margin; reduction of the pila antotica). Second, given the difference in the morphology of the snout ridge in *Sangusaurus* and *Rechnisaurus* (see above), we are skeptical as to whether it represents a homologous character state in these taxa. Third, Maisch's (2001) topology requires several seemingly significant characters (e.g., absence of tusks, large contribution of the interparietal to the skull roof, close approach of the reflected lamina and the articular, the distinctive shape of the quadrate and its articulation with the squamosal) to have evolved independently in *Sangusaurus* and *Stahleckeria*, and his cladogram is notably less parsimonious in the context of our data set (22.051 steps longer than our most parsimonious cladogram). Finally, although the low branch support for our most parsimonious cladogram means that we cannot completely reject Maisch's (2001) topology, we do note that the position of *Sangusaurus* within Stahleckeriidae has been a consistent result in all analyses of derivatives of the Kammerer et al. (2011) data set, despite variation among these analyses in other aspects of the inferred relationships of Kannemeyeriiformes.

Surkov and Benton (2004) suggested a close relationship between *Sangusaurus*, *Uralokannemeyeria*, *kannemeyeria*, and *Rechnisaurus*. One synapomorphy in their data set supports this topology, a reversal to a single foramen for the entrance of the

internal carotids into the sella turcica. According to their codings, *Sangusaurus* differs in this character from the other putative stahleckeriids and their close relatives that are included in the data set (i.e., *Stahleckeria*, *Placerias*, *Angonisaurus*). However, they also recorded the presence of the derived state (paired foramina for the internal carotids) in taxa that we recover as part of Kannemeyeriidae (*Rhadiodromus*, *Uralokannemeyeria*) or at the base of Kannemeyeriiformes (*Shansiodon*). This raises questions about the phylogenetic utility of the character, and assessment of this character in a wider range of dicynodonts will be necessary to address the issue.

At a broader scale of the relationships of all kannemeyeriiforms, our analysis differs from previous permutations of the Kammerer et al. (2011) data set in recovering a non-monophyletic 'core' Shansiodontidae (i.e., *Shansiodon*, *Tetragonias*, *Vinceria*, *Rhinodicynodon*), a monophyletic Kannemeyeriidae, and the placement of *Dinodontosaurus* and *Angonisaurus* on the stem leading to Stahleckeriidae. The synapomorphies supporting the latter relationship were noted above in our description of the results of the phylogenetic analysis. However, the character support for the other changes warrants discussion as well.

Although a monophyletic Shansiodontidae has been a consistent feature of previous versions of the Kammerer et al. (2011) data set, it typically had low branch support statistics and was supported by a small number of discrete-state synapomorphies. For example, in the analysis of Cox and Angielczyk (2015), the clade was diagnosed by two discrete-state synapomorphies: five sacral vertebrae (character 124, state 2 of that data set) and femoral head offset dorsally from the proximal end of the femur (character 147, state 1 of that data set). In the current data set, five sacral vertebrae likely represents the primitive condition for Kannemeyeriiformes as a whole, although it is unclear whether it is a synapomorphy for the clade because missing data for *Rhinodicynodon* and several non-kannemeyeriiform dicynodontoids results in ambiguous ancestral state reconstructions around this node. An offset femoral head is reconstructed as a kannemeyeriiform synapomorphy, with reversals in *Dinodontosaurus* and Kannemeyeriidae. Branch support is still low, though, and the most parsimonious cladograms that include a monophyletic 'core' Shansiodontidae are only 1.303 steps longer than our overall most parsimonious cladograms (see Supplemental Data for constraint tree used in this analysis and the most parsimonious cladogram resulting from it). Because of these facts, we consider the question of shansiodontid monophyly to be in need of further investigation.

Kannemeyeriidae sensu lato formed a paraphyletic grade between Shansiodontidae and Stahleckeriidae in all analyses of previous versions of the Kammerer et al. (2011) data set except Angielczyk and Cox (2015), although support values along the backbone of the grade were low. In the current version of the data set, the branch subtending Kannemeyeriidae (here *Shaanbeikannemeyeria*, *Wadiasaurus*, and all descendants of their most recent common ancestor) is one of the most strongly supported within Kannemeyeriiformes (although support is still low in a global sense), and it is diagnosed by four discrete-state synapomorphies: ventral edge of the caniniform process anterior to anterior orbital margin (character 32, state 0); temporal portion of skull roof angled dorsally (character 44, state 1); postorbitals extend the entire length of the intertemporal bar (character 52, state 0); and basioccipital tubera elongate, nearly quadrangular, with tubera extremely close together (character 101, state 2). Assuming this topology is correct, it implies an important biogeographic dichotomy in Triassic dicynodont evolution, with kannemeyeriids being a predominantly Laurasian radiation and stahleckeriids and their closest relatives being a primarily Gondwanan clade. Based on generally accepted terrestrial biostratigraphic correlations for the Triassic (e.g., Lucas, 2010), stahleckeriids were relatively slow to disperse out of Gondwana,

with only Late Triassic representatives such as *Placerias* or *Eubrachiosaurus* in Laurasia (e.g., Kammerer et al., 2018). Kannemeyeriids, on the other hand, quickly dispersed into the southern continents, with taxa such as *Kannemeyeria* and *Dolichuranus* reaching southern Africa by early in the Middle Triassic.

Functional Morphology of the Feeding System

Numerous studies have explored the feeding mechanism of dicynodonts, which is characterized by a highly derived craniomandibular anatomy adapted for a strictly herbivorous diet (Watson, 1948; Crompton and Hotton, 1967; Cluver, 1970, 1975; Barghusen, 1976; King, 1981a; King et al., 1989; Cox, 1998; Ray, 2000; Renaut, 2001; Maisch, 2003; Jasinoski et al., 2009; Cox and Angielczyk, 2015). Rostrally extending jaw adductor musculature and a sloped, rostrocaudally sliding quadrate-articular joint allow for the strong palinal (i.e., caudally directed) feeding stroke characteristic of a majority of dicynodont taxa (Crompton and Hotton, 1967). Among extinct vertebrates, palinal feeding is also especially prevalent in various ornithischian dinosaur clades and is suggested to have been a key foundational adaptation for their successful herbivorous lifestyles (Mallon and Anderson, 2014; Nabavizadeh and Weishampel, 2016). The preceding Permo-Triassic radiation of palinal feeding dicynodont taxa seems to have achieved similar success (although Angielczyk, 2004, questioned whether the palinal feeding system was the sole feature underlying their radiation). Interestingly, a secondary transition to a primarily orthal feeding mechanism has been suggested in the predominantly Triassic lystrosaurids and kannemeyeriiforms (Crompton and Hotton, 1967; Cluver, 1971; King and Cluver, 1991; Renaut, 2001). Because *Sangusaurus* is a stahleckeriid kannemeyeriiform, we expect to see adaptations for a secondarily more orthal feeding mechanism in this taxon as well, and these adaptations are explored below.

The distinctively large, dorsoventrally deep snout and tall, transversely broadened occiput of *S. parringtonii* suggest relatively powerful bite strength compared with most other dicynodont taxa. Rugosities on the external surface of the premaxilla, the maxilla, and the dentary, created by attachment of the keratinous rhamphothecal sheath, are extremely prominent and deep, suggesting the likelihood of large forces from feeding causing remodeling of the bone beneath the rhamphotheca. Cutting ridges are present running longitudinally along the inner margins of the beak and on the secondary palate, which also were covered by the keratinous rhamphotheca and used for shearing vegetation in a primarily orthal feeding stroke, with slight palinal movement.

The mandible also is visibly built to resist powerful bite forces. The rostral extent of the dentary is dorsoventrally deepened at the symphysis (particularly in UMZC T1340), for higher mesial force resistance in orthal feeding, and prominent rugosities showing rhamphothecal attachment are further indicators of this. The articular surface of the articular slopes strongly caudoventrally, which is also indicative of a primarily orthal feeding motion, because translation of the articular relative to the quadrate results in the mandible moving dorsally during occlusion. The oral margin along the longitudinal dorsal rim of the dentary is transversely expanded bilaterally and would have been exaggerated by the keratinous sheath. The transversely broadened oral margin suggests possible dissipation of force in a transverse component of feeding as well.

Transverse feeding motions occasionally have been proposed in dicynodonts (Watson, 1948; Cluver, 1974b; Keyser, 1975; Ray, 2000; Cox and Angielczyk, 2015). These suggestions often were based on inferred movements at the quadrate-articular joint, but the presence of a kinetic joint between the dentary and postdental bones, allowing potential flexibility around a dorsoventral axis for transverse motion, also has been proposed (Cox and

Angielczyk, 2015). Likewise, even though it is usually portrayed as a change associated with the evolution of palinal jaw movement (e.g., King et al., 1989), the reduction of the transverse flange of the pterygoid in dicynodonts also would have removed a prominent bony stop preventing transverse jaw movements that was present in most other nonmammalian synapsids. Although we do not have preserved wear data from a keratinous sheath or tusk wear facets, it is necessary to consider the possibility of transverse feeding in light of the highly distinctive cranial anatomy of *S. parringtonii*.

In lateral view, the temporal bar is rostrocaudally shorter relative to the snout compared with the other dicynodont taxa we considered in the analysis of jaw mechanics, restricting the caudal expansion of mAMEM origination along its lateral aspect. The muscle also likely attached to the medial surface of the zygomatic arch (i.e., medial to the lateral adductor fossa of the squamosal), and the temporal fenestra is large and subcircular in shape, providing a large space for adductor muscle attachment. The mAMEM extends rostroventrally to attach along the dorsal margin of the surangular. This insertion point creates a larger adductor vector angle for mAMEM and results in a more vertical contraction of the muscle that would have aided in orthal feeding.

One of the most striking characteristics of the skull of *Sangusaurus* is the highly exaggerated laterally flaring adductor fossa on the squamosal for the lateral origin of mAMEL muscle fibers, with the muscle then extending rostroventrally to insert on the lateral dentary shelf. Typically, the dicynodont adductor fossa extends caudally without significant lateral projection, resulting in a muscular arrangement optimized for a directly caudally oriented palinal motion. The adductor fossa of *Sangusaurus* is strongly verticalized and uniquely expanded laterally, which reorients the adductor vector to pull the mandible in both an orthal as well as a lateral (transverse) motion. A slight palinal component is also likely, due to the minimally caudodorsal orientation of muscle fibers in lateral view; however, this is less important in *Sangusaurus* than in more typical dicynodonts that strongly emphasize a palinal jaw movement.

As mentioned above, the MA values for both mAMEM and mAMEL in *Sangusaurus* were mid-range and most closely resembled those calculated for its sister taxon *Stahleckeria*, as opposed to the lower values in *Kannemeyeria* and higher values of *Daptocephalus*. Interestingly, although *Kannemeyeria* and the stahleckeriids we examined appear to have emphasized an orthal movement of the mandible, they achieved this goal in different ways. For example, *Sangusaurus* has higher adductor angles, which lower MA values, whereas *Kannemeyeria* has rostrally displaced insertions of mAMEL that substantially lower MA values as well. Even though *Stahleckeria* has somewhat different overall adductor muscle angles, its MA values are similar to those of *Sangusaurus*. This similarity is not surprising given the close relationship of these taxa, but the more transversely widened occiput in *Sangusaurus* suggests a change in feeding motion to a more transverse power stroke compared with *Stahleckeria*.

The M. pterygoideus (mPT) in dicynodonts is commonly suggested to largely aid in orthal feeding (Crompton and Hotton, 1967), and this is the case in *Sangusaurus*. The mPT originates along the lateral aspect of the characteristic 'X'-shaped pterygoids. Its muscle body has been hypothesized to insert on the medial surface of the posterior portion of the mandible and/or to extend ventrally to wrap ventrolaterally around the angular and attach caudal to the reflected lamina or on the lateral surface of the reflected lamina (e.g., Crompton and Hotton, 1967; Barghusen, 1976; King et al., 1989). Because the postorbital region of the cranium is rostrocaudally shortened and the postdental elements are shortened relative to the length of the dentary, the resulting vector angle of mPT would have been relatively vertical and well suited for a primarily orthal power stroke. The slightly rostral

orientation of muscle fibers would have also contributed to the return of the jaw to normal position before the next power stroke. Lastly, *M. depressor mandibulae* (mDM) is the primary muscle acting in opening the jaw, pulling the retroarticular process dorsally when contracted caudal to the mandible.

Taking all of these characteristics of the *Sangusaurus* skull into account, we propose a feeding mechanism consisting of a primarily orthal power stroke of the oral cavity, with slight palinal motion in tandem, followed by transverse motion of the dentary aided by a lateral pulling vector of the dorsolaterally oriented mAMEL. This form of feeding is unique among most dicynodont taxa and could represent a novel means for dicynodonts to exploit altered vegetation following the Permo-Triassic extinction.

Among the Triassic dicynodonts included in Surkov and Benton's (2008) data set, the occipital index value for NMT RB42 (0.151) is closest to *Kannemeyeria* (0.13), *Rhadiodromus* (0.12), and *Angonisaurus* (0.123) but is less than the value for *Stahleckeria* (0.26). Our calculated value for *Sangusaurus* indicates that it was an intermediate-level feeder in Surkov and Benton's (2008) classification of Triassic dicynodonts, and that lateral movements of the head were more important in feeding than vertical movements. The somewhat higher occipital index for *Stahleckeria* implies that it fed at a lower level with greater emphasis on lateral movements than *Sangusaurus*. This divergence parallels the difference observed in the adductor angle and mechanical advantage results for the two taxa and suggests that minor differences in ecology existed between them despite their apparently close phylogenetic relationship.

Biostratigraphic Significance of *Sangusaurus*

Despite being a relatively obscure taxon, *Sangusaurus* has been used in two ways in Triassic terrestrial biostratigraphy in southern and eastern Africa. First, beginning with the initial description of *S. edentatus* (Cox, 1969), its presence in the upper Ntawere Formation along with *Zambiasaurus* has been used to argue that this part of the formation preserves a fauna that is temporally separated from that of the lower Ntawere Formation (characterized by the presence of *Kannemeyeria lophorhinus* and '*Kannemeyeria latirostris*'). Second, the discovery of *Sangusaurus* in the Ruhuhu Basin led to its being used as an index fossil to correlate the Manda Beds with the upper Ntawere Formation (Cruickshank, 1986a; Cox, 1991; Battail, 1993; Abdala and Sa-Teixeira, 2004; Fröbisch, 2009; Angielczyk et al., 2014; Peacock et al., 2018).

The idea that the presence of *Sangusaurus* indicates rocks postdating the stratigraphic range of *Kannemeyeria* (i.e., roughly equivalent to subzone B of the *Cynognathus* Assemblage Zone in the main Karoo Basin) probably is correct. Not only does *Sangusaurus* occur in strata above those that have produced *Kannemeyeria* in the Luangwa Basin, but this is also the case in the Ruhuhu Basin. *Sangusaurus parringtonii* occurs in the mid-to-upper Lifua Member of the Manda Beds. This places it well above the reported occurrence of *Kannemeyeria* in the underlying Kingori Sandstone Member (Cruickshank, 1965), and also above a recently discovered fossiliferous horizon in the lower Lifua Member that includes the dicynodont *Dolichuranus* (Kammerer et al., 2018; Nesbitt et al., 2017; Smith et al., 2018), a taxon that co-occurs with *K. lophorhinus* in the Upper Omingonde Formation of Namibia (e.g., Keyser, 1973; Fröbisch, 2009). Generally, both the upper Ntawere and mid-to-upper Lifua Member have been considered to be Anisian to early Ladinian in age (e.g., Lucas, 1998, 2010; Abdala et al., 2005, 2013). This hypothesis may be incorrect, however, given recent radiometric dates for South American rock units previously thought to be Middle Triassic on the basis of tetrapod biostratigraphy (Ottone et al., 2014; Marsicano et al., 2016), and we caution against the assumption that the presence of *Sangusaurus* indicates an Anisian or

Ladinian age until the absolute ages of the Ntawere Formation and the Lifua Member are better constrained. The use of *Sangusaurus* as an index fossil to correlate the Lifua Member and the Ntawere Formation also is somewhat questionable on account of the very fragmentary nature of *S. edentatus*. Discovery of better-preserved material of *S. edentatus*, allowing confirmation that the genus *Sangusaurus* as currently composed is valid, will be needed to confirm its biostratigraphic utility.

ACKNOWLEDGMENTS

We thank C. Saanane (University of Dar es Salaam) and A. Taibajuka, L. Nampunju, and M. Salehe (Department of Antiquities, Ministry of Natural Resources and Tourism) for assistance in arranging and carrying out field work in the Ruhuhu Basin. M. Abdalla, S. Nesbitt, C. Sidor, W. Simpson, R. Smith, J.-S. Steyer, M. Stocker, N. Tabor, and L. Tsuji also made numerous contributions to the field work and subsequent research. Field work in Tanzania was supported by National Geographic Society grants 7787-05 (to C. Sidor), 8962-11 (to C. Sidor), and 9606-14 (to S. Nesbitt), with additional support from NSF DBI-0306158 (to K. D.A.), NSF EAR-1337291 (to K.D.A.), NSF EAR-1337569 (to C. Sidor), and The Grainger Foundation (to K.D.A.). C. van Beek prepared NMT RB42. M. Donnelly drafted the drawings in Figures 1, 6, 7, and 15. C. Mateke (ZLS) and M. Lowe and the late Ray Symonds (both UMZC) provided access to specimens of *Sangusaurus*. C. Vega, R. Irmis, and an anonymous reviewer provided helpful suggestions that improved the manuscript. We dedicate this paper to the memory of Arthur R. I. Cruickshank (1932–2011), in recognition of his work on the Triassic dicynodonts of the Ruhuhu Basin. Arthur began a more detailed description of *Sangusaurus parringtonii* with one of us (P.J.H.), but the manuscript was never completed. We hope he would approve of the current contribution.

LITERATURE CITED

- Abdala, F., and A. M. Sa-Teixeira. 2004. A traversodontid cynodont of African affinity in the South American Triassic. *Palaeontologia africana* 40:11–22.
- Abdala, F., P. J. Hancox, and J. Neveling. 2005. Cynodonts from the uppermost Burgersdorp Formation, South Africa, and their bearing on the biostratigraphy and correlation of the Triassic *Cynognathus* Assemblage Zone. *Journal of Vertebrate Paleontology* 25:192–199.
- Abdala, F., C. A. Marsicano, R. M. H. Smith, and R. Swart. 2013. Strengthening western Gondwanan correlations: a Brazilian dicynodont (Synapsida, Anomodontia) in the Middle Triassic of Namibia. *Gondwana Research* 23:1151–1162.
- Angielczyk, K. D. 2002. Redescription, phylogenetic position, and stratigraphic significance of the dicynodont genus *Odontocyclops* (Synapsida: Anomodontia). *Journal of Paleontology* 76:1047–1059.
- Angielczyk, K. D. 2004. Phylogenetic evidence for and implications of a dual origin of propaliny in anomodont therapsids (Synapsida). *Paleobiology* 30:268–296.
- Angielczyk, K. D., and C. B. Cox. 2015. Distinctive emydopoid dicynodont (Therapsida, Anomodontia) mandibles from the Permian Ruhuhu and Usili formations (Songea Group), Ruhuhu Basin, Tanzania. *Journal of Vertebrate Paleontology*. doi: 10.1080/02724634.2015.1008699.
- Angielczyk, K. D., and C. F. Kammerer. 2017. The cranial morphology, phylogenetic position, and biogeography of the upper Permian dicynodont *Compsodon helmoedi* van Hoepen (Therapsida, Anomodontia). *Papers in Palaeontology* 3:513–545.
- Angielczyk, K. D., and A. A. Kurkin. 2003. Phylogenetic analysis of Russian Permian dicynodonts (Therapsida: Anomodontia): implications for Permian biostratigraphy and Pangaean biogeography. *Zoological Journal of the Linnean Society* 139:157–212.
- Angielczyk, K. D., and B. S. Rubidge. 2009. The Permian dicynodont *Colobodectes cluveri* (Therapsida, Anomodontia), with notes on its ontogeny and stratigraphic range in the Karoo Basin, South Africa. *Journal of Vertebrate Paleontology* 29:1162–1173.

- Angielczyk, K. D., and B. S. Rubidge. 2013. Skeletal morphology, phylogenetic relationships, and stratigraphic range of *Eosimops newtoni* Broom, 1921, a ptyctodontid dicynodont (Therapsida, Anomodontia) from the middle Permian of South Africa. *Journal of Systematic Palaeontology* 11:191–231.
- Angielczyk, K. D., B. S. Rubidge, M. O. Day, and F. Lin. 2016. A reevaluation of *Brachyoprosopus broomi* and *Chelyodontops altidentalis*, dicynodonts (Therapsida, Anomodontia) from the middle Permian *Tapinocephalus* Assemblage Zone of the Karoo Basin, South Africa. *Journal of Vertebrate Paleontology*. doi: 10.1080/02724634.2016.1078342.
- Angielczyk, K. D., J.-S. Steyer, C. A. Sidor, R. M. H. Smith, R. L. Whatley, and S. Tolan. 2014. Permian and Triassic dicynodonts (Therapsida: Anomodontia) faunas of the Luangwa Basin, Zambia: taxonomic update and implications for dicynodont biogeography and biostratigraphy; pp. 93–138 in C. F. Kammerer, K. D. Angielczyk, and J. Fröbisch (eds.), Early Evolutionary History of the Synapsida. Springer, Dordrecht, The Netherlands.
- Araújo, D. C., and Gonzaga, T. D. 1980. Uma nova espécie de *Jachaleria* (Therapsida, Dicynodontia) do Triássico do Brasil; pp. 159–174 in Actas Del Congreso Argentino de Paleontología y Bioestratigrafía y Primer Congreso Latinoamericano de Paleontología Tomo I.
- Bandyopadhyay, S. 1988. A kannemeyeriid dicynodont from the Middle Triassic Yerrapalli Formation. *Philosophical Transactions of the Royal Society of London Series B* 320:185–233.
- Bandyopadhyay, S. 1989. The mammal-like reptile *Rechnisaurus* from the Triassic of India. *Palaeontology* 32:305–312.
- Barbolini, N., M. K. Bamford, and S. Tolan. 2016. Permo-Triassic palynology and palaeobotany of Zambia: a review. *Palaeontologia africana* 50:18–30.
- Barghusen, H. R. 1976. Notes on the adductor jaw musculature of *Venjukovia*, a primitive anomodont therapsid from the Permian of the U.S.S.R. *Annals of the South African Museum* 69:249–260.
- Battail, B. 1993. On the biostratigraphy of Triassic therapsid-bearing formations; pp. 31–35 in S. G. Lucas, and M. Morales (eds.), The Non-marine Triassic. New Mexico Museum of Natural History and Science Bulletin 3.
- Boos, A. D. S., C. F. Kammerer, C. L. Schultz, M. B. Soares, and A. L. R. Ilha. 2016. A new dicynodont (Therapsida: Anomodontia) from the Permian of southern Brazil and its implications for bidental origins. *PLoS ONE* 11:e0155000. doi: 10.1371/journal.pone.0155000.
- Bremer, K. 1988. The limits of amino acid sequence data in angiosperm phylogenetic reconstruction. *Evolution* 42:795–803.
- Bremer, K. 1994. Branch support and tree stability. *Cladistics* 10:295–304.
- Brink, A. S. 1982. Illustrated bibliographical catalogue of the Synapsida. Geological Survey of South Africa Handbook 10.
- Broom, R. 1905. On the use of the term Anomodontia. *Albany Museum Records* 1:266–269.
- Camp, C. L. 1956. Triassic dicynodont reptiles. Part II. Triassic dicynodonts compared. *Memoirs of the University of California* 13:305–341.
- Camp, C. L., and S. P. Welles. 1956. Triassic dicynodont reptiles. Part I. The North American genus *Placerias*. *Memoirs of the University of California* 13:255–304.
- Castanhinha, R., R. Araújo, L. C. Júnior, K. D. Angielczyk, G. G. Martins, R. M. S. Martins, C. Chaouiya, F. Backmann, and F. Wilde. 2013. Bringing dicynodonts back to life: paleobiology and anatomy of a new emydopoid genus from the Upper Permian of Mozambique. *PLoS ONE* 8:e80974. doi: 10.1371/journal.pone.0080974.
- Cluver, M. A. 1970. The palate and mandible in some specimens of *Dicynodon testudirostris* Broom and Haughton (Reptilia, Therapsida). *Annals of the South African Museum* 56:133–153.
- Cluver, M. A. 1971. The cranial morphology of the dicynodont genus *Lystrosaurus*. *Annals of the South African Museum* 56:155–274.
- Cluver, M. A. 1974a. The cranial morphology of the Lower Triassic dicynodont *Myosaurus gracilis*. *Annals of the South African Museum* 66:35–54.
- Cluver, M. A. 1974b. The skull and mandible of a new cistecephalid dicynodont. *Annals of the South African Museum* 64:137–155.
- Cluver, M. A. 1975. A new dicynodont reptile from the *Tapinocephalus* Zone (Karoo System, Beaufort Series) of South Africa, with evidence of the jaw adductor musculature. *Annals of the South African Museum* 67:7–23.
- Cluver, M. A., and G. M. King. 1983. A reassessment of the relationships of Permian Dicynodontia (Reptilia, Therapsida) and a new classification of dicynodonts. *Annals of the South African Museum* 91:191–273.
- Cooper, M. R. 1980. “The origins and classifications of Triassic dicynodonts” by A. W. Keyser, and A. R. I. Cruickshank. Discussion. *Transactions of the Geological Society of South Africa* 83:107–110.
- Cox, C. B. 1959. On the anatomy of a new dicynodont genus with evidence of the position of the tympanum. *Proceedings of the Zoological Society of London* 132:321–367.
- Cox, C. B. 1965. New Triassic dicynodonts from South America, their origins and relationships. *Philosophical Transactions of the royal Society Series B* 248:457–514.
- Cox, C. B. 1968. The Chañares (Argentina) Triassic reptile fauna. IV. The dicynodont fauna. *Breviora* 295:1–27.
- Cox, C. B. 1969. Two new dicynodonts from the Triassic Ntawere Formation, Zambia. *Bulletin of the British Museum (Natural History), Geology* 17:255–294.
- Cox, C. B. 1991. The Pangaea dicynodont *Rechnisaurus* and the comparative biostratigraphy of Triassic dicynodont faunas. *Palaeontology* 34:767–784.
- Cox, C. B. 1998. The jaw function and adaptive radiation of the dicynodont mammal-like reptiles of the Karoo Basin of South Africa. *Zoological Journal of the Linnean Society* 122:349–384.
- Cox, C. B., and K. D. Angielczyk. 2015. A new endothiodont dicynodont (Therapsida, Anomodontia) from the Permian Ruhuhu Formation (Songea Group) of Tanzania and its feeding system. *Journal of Vertebrate Paleontology*. doi: 10.1080/02724634.2014.935388.
- Cox, C. B., and J.-L. Li. 1983. A new genus of Triassic dicynodont from East Africa and its classification. *Palaeontology* 26:389–406.
- Crompton, A. W., and N. Hotton, III. 1967. Functional morphology of the masticatory apparatus of two dicynodonts (Reptilia, Therapsida). *Postilla* 109:1–51.
- Crozier, E. A. 1970. Preliminary report on two Triassic dicynodonts from Zambia. *Palaeontologia africana* 13:39–45.
- Cruickshank, A. R. I. 1965. On a specimen of the anomodont reptile *Kannemeyeria latifrons* (Broom) from the Manda Formation of Tanganyika, Tanzania. *Proceedings of the Linnean Society of London* 176:149–157.
- Cruickshank, A. R. I. 1967. A new dicynodont genus from the Manda Formation of Tanzania (Tanganyika). *Journal of Zoology* 153:163–208.
- Cruickshank, A. R. I. 1970. Taxonomy of the Triassic anomodont genus *Kannemeyeria*. *Palaeontologia africana* 13:47–55.
- Cruickshank, A. R. I. 1975. The skeleton of the Triassic anomodont *Kannemeyeria wilsoni* Broom. *Palaeontologia africana* 18:137–142.
- Cruickshank, A. R. I. 1986a. Biostratigraphy and classification of a new Triassic dicynodont from east Africa. *Modern Geology* 10:121–131.
- Cruickshank, A. R. I. 1986b. Archosaur predation on an east African Middle Triassic dicynodont. *Palaeontology* 29:415–422.
- Damiani, R., C. Vasconcelos, A. Renaut, J. Hancox, and A. Yates. 2007. *Dolichuranus primaevus* (Therapsida, Anomodontia) from the Middle Triassic of Namibia and its phylogenetic relationships. *Palaeontology* 50:1531–1546.
- DeFauw, S. L. 1986. The appendicular skeleton of African dicynodonts. Unpublished Ph.D. dissertation. Wayne State University, Detroit, Michigan, 284 pp.
- DeMar, R., and H. R. Barghusen. 1972. Mechanics and the evolution of the synapsid jaw. *Evolution* 26:622–637.
- Drysdall, A. R., and J. W. Kitching. 1963. A re-examination of the Karoo succession and fossil localities of part of the upper Luangwa Valley. *Geological Survey of Northern Rhodesia Memoir* 1:1–62.
- Dutuit, J.-M. 1988. Ostéologie crânienne et ses enseignements, apports géologique et paléocologique, de *Moghareberia nnachouensis*, Dicynodonte (Reptilia, Therapsida) du Trias supérieur marocain. *Bulletin du Muséum national d'Histoire naturelle Section C (Sciences de la Terre, Paléontologie, Géologie, Minéralogie)*, 4^e série 10:227–285.
- Ewer, R. F. 1961. The anatomy of the anomodont *Daptocephalus leoniceps* (Owen). *Proceedings of the Zoological Society of London* 136:375–402.
- Farris, J. S., V. A. Albert, M. Källersjö, D. Lipscomb, and A. G. Kluge. 1996. Parsimony jackknifing outperforms neighbor-joining. *Cladistics* 12:99–124.
- Fröbisch, J. 2006. Locomotion in derived dicynodonts (Synapsida, Anomodontia): a functional analysis of the pelvic girdle and hind limb of *Tetragonias njalilus*. *Canadian Journal of Earth Sciences* 43:1297–1308.

- Fröbisch, J. 2009. Composition and similarity of global anomodont-bearing tetrapod faunas. *Earth-Science Reviews* 95:119–157.
- Fourie, H. 1993. A detailed description of the internal structure of the skull of *Emydops* (Therapsida: Dicynodontia). *Palaeontologia africana* 30:103–111.
- Goloboff, P. A., J. S. Farris, and K. C. Nixon. 2008. TNT, a free program for phylogenetic analysis. *Cladistics* 24:774–786.
- Goloboff, P. A., C. I. Mattoni, and A. S. Quinteros. 2006. Continuous characters analyzed as such. *Cladistics* 22:589–601.
- Goloboff, P. A., J. S. Farris, M. Källersjö, B. Oxelman, M. J. Ramírez, and C. A. Szumik. 2003. Improvements to resampling measures of group support. *Cladistics* 19:324–332.
- Govender, R., P. J. Hancock, and A. M. Yates. 2008. Re-evaluation of the postcranial skeleton of the Triassic dicynodont *Kannemeyeria simocephalus* from the *Cynognathus* Assemblage Zone (Subzone B) of South Africa. *Palaeontologia africana* 43:19–37.
- Hancock, P. J., K. D. Angielczyk, and B. S. Rubidge. 2013. *Angonisaurus* and *Shansiodon*, dicynodonts (Therapsida, Anomodontia) from subzone C of the *Cynognathus* Assemblage Zone (Middle Triassic) of South Africa. *Journal of Vertebrate Paleontology* 33:655–676.
- Huene, F. von. 1935. Die fossilen Reptilien des Südamerikanischen Gondwanalandes. Ergebnisse der Sauriergrabungen in Südbrasilien 1928–29:1. *Ordnung Anomodontia*. C. H. Beck'sche Verlagsbuchhandlung, Munich, Germany, 92 pp.
- Jain, S. L. 1996. Aspects of vertebrate fossils from Pranhita-Godavari Valley with emphasis on dinosaur discoveries. *Journal of the Palaeontological Society of India* 41:1–16.
- Jain, S. L., and T. Roy-Chowdhury. 1987. Fossil vertebrates from the Pranhita-Godavari Valley (India) and their stratigraphic correlation; pp. 219–228 in J. W. Collinson, D. H. Elliot, S. M. Haban, and G. D. McKenzie (eds.), *Gondwana Six: Stratigraphy, Sedimentology, and Paleontology*. Geophysical Monograph Series 41.
- Jasinoski, S. C., E. J. Rayfield, and A. Chinsamy. 2009. Comparative feeding biomechanics of *Lystrosaurus* and the generalized dicynodont *Oudenodon*. *Anatomical Record* 292:862–874.
- Kaaya, C. Z. 1992. Depositional environment of Late Permian Karoo beds in the Ruhuhu Basin and Mikumi area of Tanzania. *Geologisches Institut der Universität zu Köln Sonderveröffentlichungen* 83:1–126.
- Kammerer, C. F., K. D. Angielczyk, and J. Fröbisch. 2011. A Comprehensive Taxonomic Revision of *Dicynodon* (Therapsida, Anomodontia) and Its Implications for Dicynodont Phylogeny, Biogeography, and Biostratigraphy. *Society of Vertebrate Paleontology Memoir* 11. *Journal of Vertebrate Paleontology* 31(6, Supplement 1), 158 pp.
- Kammerer, C. F., J. Fröbisch, and K. D. Angielczyk. 2013. On the validity and phylogenetic position of *Eubrachiosaurus browni*, a kannemeyeriiform dicynodont (Anomodontia) from Triassic North America. *PLoS ONE* 8:e64203. doi: 10.1371/journal.pone.0064203.
- Kammerer, C. F., K. D. Angielczyk, and J. Fröbisch. 2015a. Redescription of the geikiid *Pelanomodon* (Therapsida, Dicynodontia), with a reconsideration of '*Propelanomodon*'. *Journal of Vertebrate Paleontology*. doi: 10.1080/02724634.2015.1030408.
- Kammerer, C. F., K. D. Angielczyk, and J. Fröbisch. 2015b. Redescription of *Digalodon rubidgei* from the Late Permian of South Africa. *Fossil Record* 18:43–55.
- Kammerer, C. F., K. D. Angielczyk, and S. J. Nesbitt. 2018. Novel hind limb morphology in a kannemeyeriiform dicynodont from the Manda Beds (Songea Group, Ruhuhu Basin) of Tanzania; pp. 178–188 in C. A. Sidor, and S. J. Nesbitt (eds.), *Vertebrate and Climatic Evolution in the Triassic Rift Basins of Tanzania and Zambia*. *Society of Vertebrate Paleontology Memoir* 17. *Journal of Vertebrate Paleontology* 37(6, Supplement).
- Keyser, A. W. 1973. A new Triassic vertebrate fauna from South West Africa. *Palaeontologia africana* 16:1–15.
- Keyser, A. W. 1974. Evolutionary trends in Triassic Dicynodontia. *Palaeontologia africana* 17:69–85.
- Keyser, A. W. 1975. A re-evaluation of the cranial morphology and systematics of some tuskless anomodonts. *Memoirs of the Geological Survey of South Africa* 67:1–110.
- Keyser, A. W., and A. R. I. Cruickshank. 1979. The origins and classification of Triassic dicynodonts. *Transactions of the Geological Society of South Africa* 82:81–108.
- King, G. M. 1981a. The functional anatomy of a Permian dicynodont. *Philosophical transactions of the Royal Society of London Series B* 291:243–322.
- King, G. M. 1981b. The postcranial skeleton of *Robertia broomiana*, an early dicynodont (Reptilia, Therapsida) from the South African Karoo. *Annals of the South African Museum* 84:203–231.
- King, G. M. 1985. The postcranial skeleton of *Kingoria nowacki* (von Huene) (Therapsida: Dicynodontia). *Zoological Journal of the Linnean Society* 84:263–289.
- King, G. M. 1988. Anomodontia. *Handbuch der Paläoherpetologie*, 17C. Gustav Fischer Verlag, Stuttgart, Germany, 174 pp.
- King, G. M. 1994. The early anomodont *Venjukovia* and the evolution of the anomodont skull. *Journal of Zoology* 232:651–673.
- King, G. M., and M. A. Cluver. 1991. The aquatic *Lystrosaurus*: an alternative lifestyle. *Historical Biology* 4:323–342.
- King, G. M., B. W. Oelofsen, and B. S. Rubidge. 1989. The evolution of the dicynodont feeding system. *Zoological Journal of the Linnean Society* 96:185–211.
- Kopuchian, C., and M. J. Ramírez. 2010. Behaviour of resampling methods under different weighting schemes, measures, and variable resampling strengths. *Cladistics* 26:86–97.
- Laaß, M. 2015. Virtual reconstruction of the cranial endocast of *Pristerodon mackayi* (therapsida, Anomodontia). *Journal of Morphology* 276:1089–1099.
- Lehman, J.-P. 1961. Dicynodontia; pp. 287–351 in J.-P. Piveteau (ed.), *Traité de Paléontologie*, VI. Mammifères, Volume 1: Origine Reptilienne Évolution. Masson et Cie, Paris.
- Li, Y. 1983. Restoration of pelvic muscles in *Lystrosaurus*. *Vertebrata PalAsiatica* 21:328–340.
- Lucas, S. G. 1998. Global Triassic tetrapod biostratigraphy and biochronology. *Palaeogeography, Palaeoclimatology, Palaeoecology* 143:347–384.
- Lucas, S. G. 2010. The Triassic timescale based on nonmarine tetrapod biostratigraphy and biochronology; pp. 447–507 in S. G. Lucas (ed.), *The Triassic Timescale*. Geological Society, London Special Publication 334.
- Maisch, M. W. 2001. Observation on Karoo and Gondwana vertebrates. Part I: a new skull-reconstruction of *Stahleckeria potens* von Huene, 1935 (Dicynodontia, Middle Triassic) and a reconstruction of kannemeyeriiform phylogeny. *Neues Jahrbuch für Geologie und Paläontologie, Abhandlungen* 220:127–152.
- Maisch, M. W. 2003. Lower jaw morphology and jaw adductor musculature of the giant Permian dicynodont *Rhachiocephalus* Seeley, 1898 (Therapsida) from the Late Permian of Tanzania. *Geologica et Palaeontologica* 37:89–106.
- Maisch, M. W. 2005. Observations on Karoo and Gondwana vertebrates. Part 6. A new rhachiocephalid dicynodont (Therapsida) from the Upper Permian of the Ruhuhu Basin (Tanzania). *Neues Jahrbuch für Geologie und Paläontologie, Abhandlungen* 237:313–355.
- Mallon, J. C., and J. S. Anderson. 2014. The functional and palaeoecological implications of tooth morphology and wear for the megaherbivorous dinosaurs from the Dinosaur Park Formation (upper Campanian) of Alberta, Canada. *PLoS ONE* 9:e98605. doi: 10.1371/journal.pone.0098605.
- Mallon, J. C., and J. S. Anderson. 2015. Jaw mechanics and evolutionary palaeoecology of the megaherbivorous dinosaurs from the Dinosaur Park Formation (Upper Campanian) of Alberta, Canada. *Journal of Vertebrate Paleontology*. doi: 10.1080/02724634.2014.904323.
- Markwort, S. 1991. Sedimentation und Diagenese der untertriadischen Karoo Schichten des Ruhuhu Beckens, SW Tanzania. *Geologisches Institut, Universität Köln, Sonderveröffentlichungen* 80:1–118.
- Marsicano, C. A., R. B. Irmis, A. C. Mancuso, R. Mundil, and F. Chemale. 2016. The precise temporal calibration of dinosaur origins. *Proceedings of the National Academy of Sciences of the United States of America* 113:509–513.
- Moldowan, P. D., R. J. Brooks, and J. D. Litzgus. 2015. Turtles with “teeth”: beak morphology of Testudines with a focus on the tomiodonts of painted turtles (*Chrysemys* spp.). *Zoomorphology*. doi: 10.1007/s00435-015-0288-1.
- Morato, L. 2006. *Dinodontosaurus* (Synapsida, Dicynodontia): reconstituições morfológicas e aspectos biomecânicos. Unpublished M.Sc. thesis, Universidade Federal do Rio Grande do Sul, Porto Alegre, Brazil, 158 pp.

- Mueller, L. D., and F. J. Ayala. 1982. Estimation and interpretation of genetic distance in empirical studies. *Genetical Research* 40:127–137.
- Nabavizadeh, A. 2016. Evolutionary trends in the jaw adductor mechanics of ornithischian dinosaurs. *The Anatomical Record* 299:271–294.
- Nabavizadeh, A., and D. B. Weishampel. 2016. The predentary bone and its significance in the evolution of feeding mechanisms in ornithischian dinosaurs. *The Anatomical Record* 299:1358–1388.
- Nesbitt, S. J., R. J. Butler, M. D. Ezcurra, P. M. Barrett, M. R. Stocker, K. D. Angielczyk, R. M. H. Smith, C. A. Sidor, G. Niedzwiedzki, A. G. Sennikov, and A. J. Charig. 2017. The earliest bird-line archosaurs and the assembly of the dinosaur body plan. *Nature*. doi: 10.1038/nature22037.
- Nowack, E. 1937. Zur Kenntnis der Karruformation im Ruhuhu-Graben (D.O.A.). *Neues Jahrbuch für Mineralogie, Geologie, und Paläontologie*, Abteilung B 78:380–412.
- Olson, E. C. 1944. Origin of mammals based upon cranial morphology of the therapsid suborders. *Geological Society of America Special Papers* 55:1–136.
- Ostrom, J. H. 1964. A functional analysis of jaw mechanics in the dinosaur *Triceratops*. *Postilla* 88:1–35.
- Ottone, E. G., M. Monti, C. A. Marsicano, M. S. de la Fuente, M. Naipauer, R. Armstrong, and A. C. Mancuso. 2014. A new Late Triassic age for the Puesto Viejo Group (San Rafael depocenter, Argentina): SHRIMP U-Pb zircon dating and biostratigraphic correlations across southern Gondwana. *Journal of South American Earth Sciences* 56:186–199.
- Owen, R. 1860. On the orders of fossil and recent Reptilia, and their distribution in time; pp. 153–166 in Report of the Twenty-Ninth Meeting of the British Association for the Advancement of Science, 1859.
- Pearson, H. S. 1924. A dicynodont reptile reconstructed. *Proceedings of the Zoological Society of London* 1924:827–855.
- Peecook, B. R., J.-S. Steyer, N. J. Tabor, and R. M. H. Smith. 2018. Updated geology and vertebrate paleontology of the Triassic Ntawere Formation of northeastern Zambia, with special emphasis on the archosauromorphs; pp. 8–38 in C. A. Sidor and S. J. Nesbitt (eds.), Vertebrate and climatic evolution in the Triassic rift basins of Tanzania and Zambia. Society of Vertebrate Paleontology Memoir 17. *Journal of Vertebrate Paleontology* 37 (6, supplement).
- Ray, S. 2000. Endothiodont dicynodonts from the Late Permian Kun-daram Formation, India. *Palaeontology* 43:375–404.
- Ray, S. 2006. Functional and evolutionary aspects of the postcranial anatomy of dicynodonts (Synapsida, Therapsida). *Palaeontology* 49:1263–1286.
- Ray, S., and A. Chinsamy. 2003. Functional aspects of the postcranial anatomy of the Permian dicynodont *Diictodon* and their ecological implications. *Palaeontology* 46:151–183.
- Renaut, A. J. 2000. A re-evaluation of the cranial morphology of the Triassic dicynodont *Kannemeyeria*. Unpublished Ph.D. dissertation, University of the Witwatersrand, Johannesburg, South Africa, 191 pp.
- Renaut, A. J. 2001. Dicynodont jaw mechanisms reconsidered: the *Kannemeyeria* (Anomodontia Therapsida) masticatory cycle. *Asociación Paleontológica Argentina Publicación Especial* 7:167–170.
- Renaut, A. J., R. J. Damiani, A. M. Yates, and P. J. Hancox. 2003. A taxonomic note concerning a dicynodont (Synapsida: Anomodontia) from the Middle Triassic of East Africa. *Palaeontologia africana* 39:93–94.
- Romer, A. S., and L. I. Price. 1944. *Stahleckeria lenzii*, a giant Triassic Brazilian dicynodont. *Bulletin of the Museum of Comparative Zoology* 93:465–491.
- Roy-Chowdhury, T. 1970. Two new dicynodonts from the Triassic Yerra-palli Formation of central India. *Palaeontology* 13:132–144.
- Sakamoto, M. 2010. Jaw biomechanics and the evolution of biting performance in theropod dinosaurs. *Proceedings of the Royal Society of London B, Biological Sciences* 277:3327–3333.
- Sidor, C. A., R. M. H. Smith, A. K. Huttenlocker, and B. R. Peecook. 2014. New Middle Triassic tetrapods from the Upper Fremouw Formation of Antarctica and their depositional setting. *Journal of Vertebrate Paleontology* 34:793–801.
- Simmons, M. P., and J. V. Freudenstein. 2011. Spurious 99% bootstrap and jackknife support for unsupported clades. *Molecular Phylogenetics and Evolution* 61:177–191.
- Smith, R. M. H., C. A. Sidor, K. D. Angielczyk, S. J. Nesbitt, and N. J. Tabor. 2018. Taphonomy and paleoenvironments of Middle Triassic bone accumulations in the Lifua Member of the Manda Beds, Sonagea Group (Ruhuhu Basin), Tanzania; pp. 65–79 in C. A. Sidor and S. J. Nesbitt (eds.), *Vertebrate and Climatic Evolution in the Triassic Rift Basins of Tanzania and Zambia*. Society of Vertebrate Paleontology Memoir 17. *Journal of Vertebrate Paleontology* 37(6, Supplement).
- Stockley, G. M. 1932. The geology of the Ruhuhu coalfields, Tanganyika Territory. *Quarterly Journal of the Geological Society of London* 88:610–622.
- Stockley, G. M., and F. Oates. 1931. Report on geology of the Ruhuhu Coalfields. *Bulletin of the Geological Survey of Tanganyika* 2:1–68.
- Strong, E. E., and D. Lipscomb. 2000. Character coding and inapplicable data. *Cladistics* 15:363–371.
- Sullivan, C., and R. R. Reisz. 2005. Cranial anatomy and taxonomy of the late Permian dicynodont *Diictodon*. *Annals of Carnegie Museum* 74:45–75.
- Sullivan, C. A., R. R. Reisz, and R. M. H. Smith. 2003. The Permian mammal-like herbivore *Diictodon*, the oldest known example of sexually dimorphic armament. *Proceedings of the Royal Society of London B, Biological Sciences* 270:173–178.
- Sun, A.-L. 1963. The Chinese kannemeyerids. *Palaeontologica Sinica, New Series C* 17:1–109.
- Surkov, M. V., and M. J. Benton. 2004. The basicranium of dicynodonts (Synapsida) and its use in phylogenetic analysis. *Palaeontology* 47:619–638.
- Surkov, M. V., and M. J. Benton. 2008. Head kinematics and feeding adaptations of the Permian and Triassic dicynodonts. *Journal of Vertebrate Paleontology* 28:1120–1129.
- Tanoue, K., B. S. Grandstaff, H. You, and P. Dodson. 2009. Jaw mechanics in basal Ceratopsia (Ornithischia, Dinosauria). *The Anatomical Record* 292:1352–1369.
- Tollman, S. M., F. E. Grine, and B. D. Hahn. 1980. Ontogeny and sexual dimorphism in *Aulacephalodon* (Reptilia, Anomodontia). *Annals of the South African Museum* 81:159–186.
- Vega-Dias, C., and C. L. Schultz. 2004. Postcranial material of *Jachaleria candelariensis* Araújo and Gonzaga 1980 (Therapsida, Dicynodontia), Upper Triassic of Rio Grande do Sul, Brazil. *PaleoBios* 24:7–31.
- Vega-Dias, C., M. W. Maisch, and C. L. Schultz. 2004. A new phylogenetic analysis of Triassic dicynodonts (Therapsida) and the systematic position of *Jachaleria candelariensis* from the Upper Triassic of Brazil. *Neues Jahrbuch für Geologie und Paläontologie, Abhandlungen* 231:145–166.
- Walter, L. R. 1986. The limb posture of kannemeyerid dicynodonts: functional and ecological considerations; pp. 89–97 in K. Padian (ed.), *The Beginning of the Age of Dinosaurs*. Cambridge University Press, Cambridge, U.K.
- Watson, D. M. S. 1912a. On some reptilian lower jaws. *Annals and Magazine of Natural History Series 8* 10:573–587.
- Watson, D. M. S. 1912b. The skeleton of *Lystrosaurus*. *Albany Museum Records* 2:287–295.
- Watson, D. M. S. 1948. *Dicynodon* and its allies. *Proceedings of the Zoological Society of London* 118:823–877.
- Yeh, H.-K. 1959. New dicynodont from *Sino-kannemeyeria*-fauna from Shansi. *Vertebrata PalAsiatica* 3:187–204.

Submitted November 24, 2016; revisions received May 1, 2017;
accepted September 30, 2017.
Memoirs editor: Randall Irmis.